Connectomic Analysis of a Peptidergic Circuit in *Drosophila*

Dissertation

zur Erlangung des

Doktorgrades (Dr. rer. nat.)

der Mathematisch-Naturwissenschaftlichen Fakultät

der Rheinischen Friedrich-Wilhelms-Universität Bonn

vorgelegt von

Philipp Schlegel

aus Frankfurt a.M.

BONN 2016

Angefertigt mit Genehmigung der Mathematisch-Naturwissenschaftlichen Fakultät
der Rheinischen Friedrich-Wilhelms-Universität Bonn.

1. Gutachter:	Prof. Dr. Michael J. Pankratz
2. Gutachter:	PD Dr. Reinhard Bauer
Tag der Promotion:	20. Juli 2017
Erscheinungsjahr:	2017

“An expert is a person who has made all the mistakes that can be made in a very narrow field." - **Nils Bohr**

ZUSAMMENFASSUNG

Die homologen Neuropeptide NeuromedinU (NMU) und Hugin haben ähnliche Effekte auf Nahrungsaufnahme und physische Aktivität in Säugetieren bzw. *Drosophila*. Über die neuralen Netzwerke, in denen das jeweilige Neuropeptid eine Rolle spielt, ist wenig bekannt. In dieser Arbeit wurde die Konnektivität von Hugin-produzierenden Neuronen in larvalen *Drosophila* auf Ebene von Synapsen und Peptid-Rezeptor Verbindungen untersucht.

Das damit generierte *Hugin Konnektom* zeigt, dass Hugin Neurone in unabhängige Subnetzwerke organisiert sind, von denen jedes einen einzigartigen Satz von prä- und postsynaptischen Partnern hat. Eines dieser Subnetzwerke verbindet das chemosensorische mit dem neuroendokrinen System und stellt damit möglicherweise die neuronale Grundlage für den Effekt von Hugin Neuronen auf die Nahrungsaufnahme dar. Diese Verbindung zwischen hugin und dem endokrinen System basiert auf paralleler synaptischer Transmission mittels Acetylcholin und Peptid-Rezeptor Verbindung. Beide Arten von Transmission werden für den Effekt von Hugin Neuronen auf die Nahrungsaufnahme benötigt.

Unter den Zielen von Hugin Neuronen sind neuroendokrine Zellen im Pars Intercerebralis, dem *Drosophila*-Homolog des Hypothalamus, die Insulin-ähnliche Peptide, diuretisches Hormon 44 und Dromyosuppressin produzieren. Diese chemische Konnektivität ähnelt der von NMU in Säugetieren und ist damit ein Hinweis auf eine starke Konservierung zwischen Hugin und NMU nicht nur auf funktioneller Ebene, sondern auch auf Ebene der Konnektivität.

Abstract

The homologous neuropeptides neuromedinU (NMU) and hugin have similar effects on food intake and physical activity in mammals and *Drosophila*, respectively. Little is known about the neuronal networks that employ either neuropeptide. This study maps the connectivity of hugin-producing neurons in the *Drosophila* larva on both synaptic and peptide-receptor level.

This *hugin connectome* reveals that hugin neurons are organized into independent subnetworks, each with its own sets of pre- and postsynaptic partners. One of these subnetworks connects the chemosensory with the neuroendocrine system and thereby possibly provides the neural substrate for the effect of hugin neurons on feeding behavior. Strikingly, the connection between hugin and endocrine neurons is based on parallel synaptic transmission using acetylcholine as synaptic small molecule transmitter and a peptide-receptor connection. Both types of transmission are required for the effect of hugin neurons on feeding behavior.

Among the targets of hugin neurons are neuroendocrine cells of the *pars intercerebralis*, the *Drosophila* homolog of the hypothalamus, that produce insulin-like peptides, diuretic hormone 44 and Dromyosuppressin. This chemical connectivity is very similar to how NMU operates in mammals, indicating a strong conservation between hugin and NMU, not only on the functional but also on a connectivity level.

Dedication

This work would not have been possible without the help and support of numerous people. First, I would like to thank my family. Especially my parents and grandparents, without whom I would not be here today - not just in the very biological sense but also due to their unwavering and unconditional support for which I will be forever grateful: my mom for always offering safe haven and a meal, my dad for all his solicited and unsolicited advice, and my brother for being my brother in every sense of the word.

I am much obliged to Prof. Michael Pankratz for his constant enthusiasm for the work we have been doing and, most of all, for sending me across the globe to interact with other scientists. Thank you for making me experience this exciting aspect of science by giving me the chance to meet people and visit places that I would not have otherwise.

Big thanks go out to my fellow colleagues: first and foremost to Andreas, Sebastian and Anton for their support, their collegiality and, most importantly, their friendship over the many years we've now known each other. Tania, Sarah and Ingo for being key to keeping the place running smoothly. And of course the whole Pankratz lab for your help, the cheerful atmosphere and your friendship.

Last but not least I would like to thank my most favorite comrades-in-arms. Thank you Lucia, Lorenz, Felix, Nina and Philippa for all the good times in and out of the lab.

Table of Contents

List of Tables

List of Figures

CHAPTER 1

INTRODUCTION

1.1 Towards understanding the brain

The human brain remains one of the few organs that modern science still struggles to fully comprehend. On a basic level, the elementary principles of neuronal networks have long been studied. This understanding is to a large extent based on research in purportedly simple organisms, i.e. the generation of stereotyped behaviors in the crabs or the molecular processes of learning and memory in the sea slug *Aplysia* [Marder and Bucher, 2001; Kandel, 2001]. While such fundamental principles appear to be applicable to neuronal networks across species, the central nervous systems of higher animals, including that of humans, are orders of magnitudes more complex. To date, the most comprehensive map of an entire nervous system is that of the roundworm *Caenorhabditis elegans* [White et al., 1986; Varshney et al., 2011; Jarrell et al., 2012]. This map, a so-called "connectome", covers the anatomical connections between all 302 neurons of the nervous system of *C. elegans*. In contrast, the human brain comprises about 100.000.000.000 neurons and even smaller brains of other vertebrates which are commonly used for medical research (e.g. mice or zebrafish) still feature millions of neurons. This complexity in numbers as well as in behavior is one of the reasons why in the past scientists have instead used a variety of simpler organisms to study the basic principles of neuronal networks.

These days, human neurological and psychiatric disorders, such as Alzheimer's disease, Parkinson's disease, or depression, pose increasing financial and social problems for modern society. Therefore considerable effort is made to push research towards a better understanding of neuronal networks in general and the human brain in particular. In 2014, the United States, led by president Barack Obama, started a multi-million dollar program called the BRAIN (**B**rain **R**esearch through **A**dvancing **I**nnovative **N**eurotechnologies) Initiative aimed at "revolutionizing

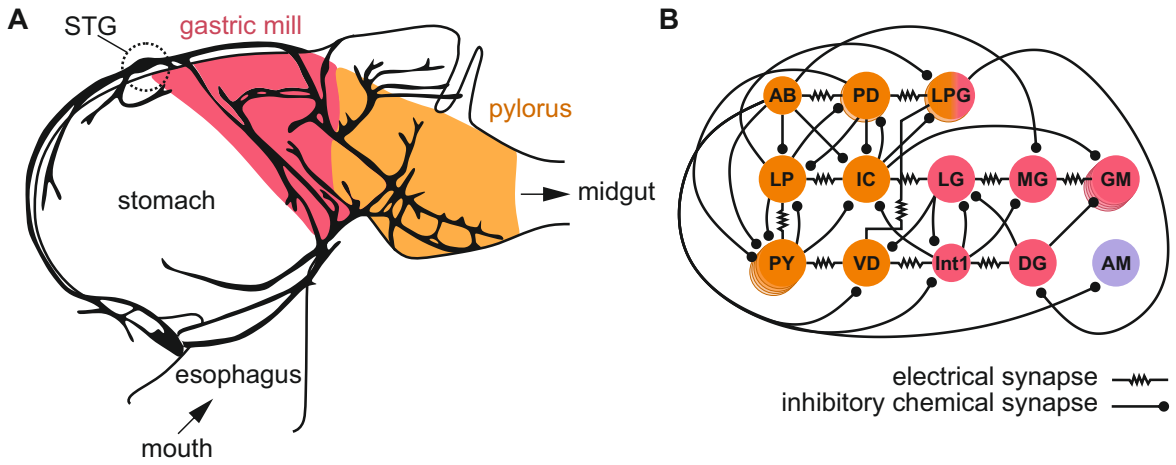

FIGURE 1.1. Neural circuits of the crustacean stomatogastric ganglion (STG). **A**, Schematic of the crustacean stomach. Ingested food is cut and ground by teeth of the gastric mill (red) and then moved towards the midgut by peristaltic movements of the pylorus (orange). Central pattern generators (CPGs) of the STG produce the motor rhythms responsible for those movements. **B**, Neurons of the STG that form the two interlinked CPGs driving gastric (red) and pyloric (orange) movements have been completely mapped. Figure reproduced from Marder and Bucher [2007]; Mulloney [1987].

our understanding of the human brain[1]". Likewise, the European Union has been running a ten-year program called the Human Brain Project to fund international research in neuroscience and computation science since 2013. This financial, political and public attention is indicative of the renewed importance of neurobiology research. After the sequencing of the human genome in 2003, one of the next major milestones for scientific research will be understanding the brain.

1.2 Connectomes

The term *connectome* is derived from *genome* and was first introduced by Sporns et al. [2005]. A connectome comprises information on the entirety of neurons and their connectivity within a given neural network, e.g. the human brain. Even though this term came into existence only 11 years ago, scientist have been studying connectivity between neurons for over 100 years [Levine, 2007].

At its core, connectomic research tries to understand how ensembles of neurons integrate and process incoming (e.g. sensory) information and produce an appropriate output (e.g. motor patterns) that eventually translates into behavior. The following section will give a brief overview of the research on neuronal networks in different organisms and how *Drosophila* contributes to these ongoing efforts.

[1]BRAIN Initiative, official project description, http://www.braininitiative.nih.gov

1.2.1 Small nervous systems

"In order to understand the fundamental organizational principles of neural circuits, it is essential that we compare them."
- Paul Katz, 2013

One of the fascinating properties of nervous systems is their ability to function in plethora of different environments and life styles while operating on the same basic principles. The above quote from renowned neuroscientist Paul Katz points out why research should not rely on only a single but rather a range of different model system [Katz et al., 2013]. Many of the fundamental principles of neuronal function were first discovered in invertebrate model systems and subsequently confirmed in more complex organisms. This ranges from small scale like intracellular processes, to large scale such as the interaction of neurons within a network.

For example, the concept of electrical excitability and propagation of action potentials was first discovered in cephalopods in the early 20th century [for extensive review see Keynes, 1989]. At that time, available tools and techniques required the preparations to be rather large and well accessible. Therefore Hodgkin and Huxley [1939] used a 500μm diameter squid giant axon for the first intracellular recording of an action potential.

Another prominent example for invertebrate research are the cellular processes of learning and the formation of memory. In 2000, the Nobel Prize was awarded to Eric Kandel for his work on habituation, sensitization and classical conditioning in the sea slug *Aplysia* [Kandel, 2001]. Using its gill withdrawal reflex as model system, Kandel and others were the first to establish that learning results from changes in the strength of synaptic connections between connected cells. Crucial for this discovery was exact knowledge of all the neurons involved and their connectivity. With only 6 motor, 24 sensory and less than 10 interneurons the circuit underlying the gill withdrawal reflex is rather simple but nevertheless had a major impact on our understanding of neuronal processes.

Many other invertebrate preparations had similar impacts on the field. One of the best studied neural circuits are those responsible for the generation of the foregut movements in crustaceans. Here, two networks interact to efficiently process ingested food (Fig. 1.1A). The pyloric network opens and closes the pylorus and acts as a valve controlling transport of food into the midgut. The gastric network controls the gastric mill, a system of teeth that grinds food particles. Both networks are interconnected to coordinate foregut movements.

The neurons forming these networks reside in the stomatogastric ganglion (STG) and are capable of producing the motor patterns that drive the gut movements without any input from the outside. When physically removed from the animal and placed in a saline solution, the STG continues to produce "fictive" motor patterns that resemble those in vivo. As such these circuits represent prime examples of so-called central pattern generators (CPGs). The number of neurons within the STG is relatively small and varies between 25 and 32 depending on the species. Their small number and large size allowed the use of electrophysiological techniques to establish a map

of the connections between those neurons (Fig. 1.1B). Simplified, the system consists of intrinsic oscillators that, by virtue of their electrical and inhibitory chemical coupling to each other, force sub units of the network to be active in distinct phases and therefore ensure the coordinated movement of all the muscles involved [Mulloney and Selverston, 1974; Hartline, 1979]. In reality, the activity within the network is much more complex and the gastric mill network specifically is able to generate a range of different types of motor patterns e.g. in response to different types of food [Heinzel, 1988a]. In addition to these intrinsic properties, there is a plethora of descending synaptic inputs from other parts of the stomatogastric nervous system (STNS) and neuromodulatory substances such as dopamine or proctolin that can dramatically alter the role of neurons within the network [Heinzel, 1988b].

Research on the STNS has greatly contributed to our understanding of the generation of rhythmic motor patterns which are the basis of almost all repetitive behavior such as walking, breathing and eating [see Marder and Bucher, 2007, for an extensive review]. Other famous examples of neurobiological research in invertebrates include walking in stick insects, flight in locusts and tail flipping in lobster [see Clarac and Pearlstein, 2007; Marder and Bucher, 2001, for overview]. The common denominator of these systems is that they represent only selected aspects of the animals' behavioral repertoire and involve only a small part of the nervous system.

As techniques developed, larger and more complex nervous system became accessible. The first nervous system to be fully mapped was that of the nematode *Caenorhabditis elegans*. Albertson and Thomson [1976], White et al. [1976] and White et al. [1986] provided a comprehensive anatomical description of all muscles, neurons, chemical synapses and gap junctions of the hermaphrodite worm based on electron microscopy (EM) sections of an entire animal. This wiring diagram was since updated and now encompasses 302 neurons that form 6393 chemical synapses, 890 gap junctions and 1410 neuromuscular junctions (Fig. 1.2) [Varshney et al., 2011]. This data on *C. elegans* connectivity has been processed and made freely available to help scientists in their research[2].

The initial work on *C. elegans* by White et al. [1986] provided researcher with a wealth of data and founded the yet-to-be-named field of connectomics. Unsurprisingly, it took scientists decades to understand even small pieces of the wiring diagram and many aspects are still under ongoing investigations. In some cases interpretation of the circuitry was comparatively easy. For example, Chalfie and Sulston [1981] had shown that touch cells in the head and tail were required for avoidance of light touch. The connectome revealed that indeed touch cells are wired to the circuits for forward and backward locomotion, respectively. Other, more complicated aspects still remain under investigation [Emmons, 2015]. Even today the original dataset is continuously extended by the addition of new information. The identification of all the neurotransmitters used by distinct neuron classes has yet to be completed. In 2015, Pereira et al. added a complete map of cholinergic transmission to existing maps of GABAergic, glutamatergic and aminergic neurons

[2] e.g. www.wormatlas.org

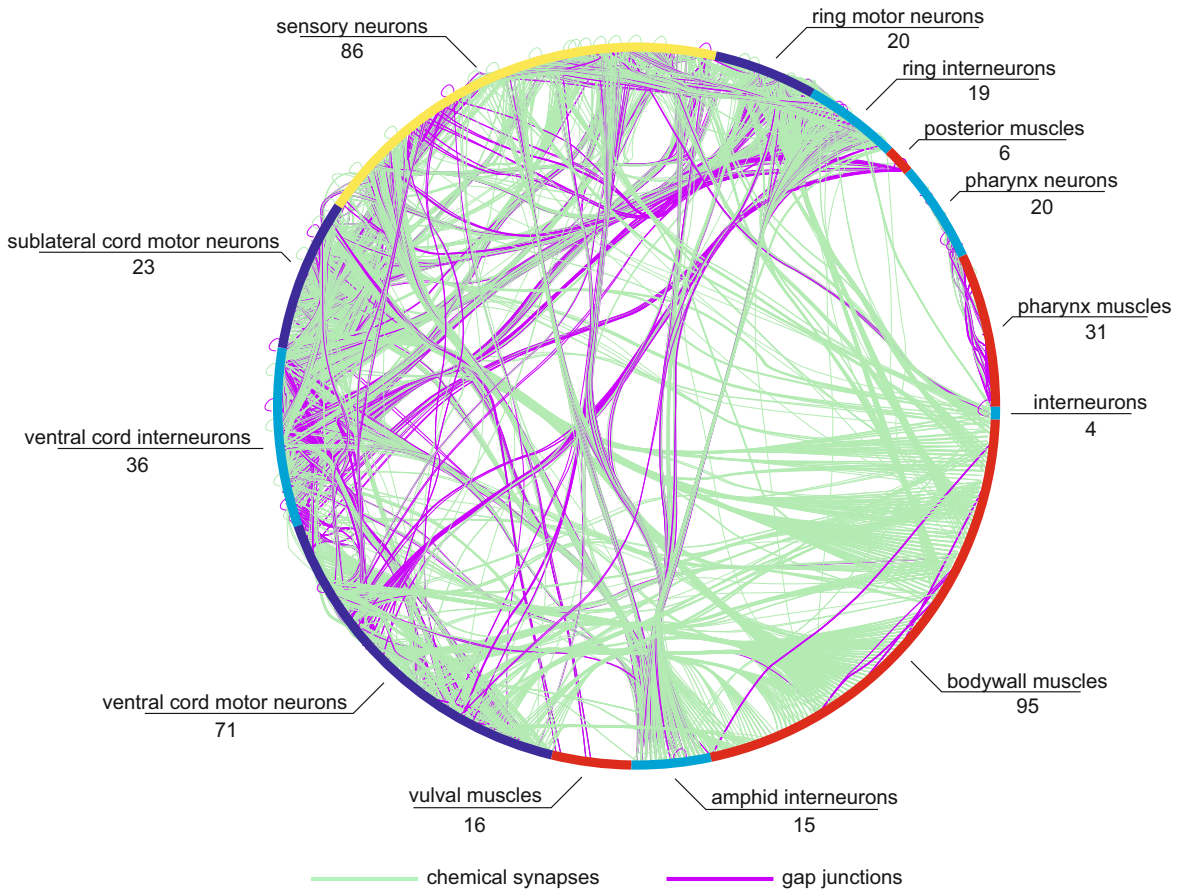

FIGURE 1.2. Wiring diagram of the nervous system of the nematode *Caenorhabditis elegans* hermaphrodite. Neurons and muscles are grouped by type. Below the labels the number of neurons represented by each wedge of the circle is provided. Chemical (synapses) and electric (gap junctions) connections are displayed as lines. Line width corresponds to the number of serial sections of the respective types of connection between pairs of cells. Data obtained from the WormWiring project (http://wormwiring.hpc.einstein.yu.edu/).

that date back as far as 1993 [McIntire et al., 1993].

The now famous article by White et al. [1986] is cited by 793 listed publications on PubMed Central - and that number is still rising. Surprisingly, John White himself perceived the reactions to his presentations of the analysis of the *C. elegans* connectome to be rather discouraging [Emmons, 2015]. Nevertheless, in the post-connectome years, *C. elegans* research has greatly contributed to the understanding of the genetic underpinnings of neuronal development [Hobert, 2010].

1.2.2 Vertebrate connectomes

The previous section covered exclusively neurobiological research in invertebrates. This section will give an overview about previous and current efforts to map neuronal networks in vertebrates.

As mentioned before, the size (i.e. number of neurons involved as well as physical dimensions) of vertebrate nervous systems are orders of magnitude larger than any of the invertebrate systems that have already been successfully mapped. Nevertheless, there are considerable efforts to create vertebrate connectomes albeit at lower resolution or limited dimension. So-called macroscale connectomes map connectivity between broad areas of the brain and have been generated for a range of different organisms such as monkeys [Young, 1993; Markov et al., 2011], rats [Burns and Young, 2000], cats [Scannell et al., 1999] and even post-mortem in humans [Galuske et al., 2000; Tardif and Clarke, 2001]. In the past these maps have been mostly based on tracings of axonal bundles using e.g. back-fills but also functional imaging [Sporns et al., 2005]. More recently, the use of viral vectors to label neurons has drastically increased the resolution and allowed for cell-type specific tracings (Fig. 1.3) [Oh et al., 2014; Zingg et al., 2014].

An alternative approach to large scale mapping is to break down the nervous system into elementary building blocks that are small enough to be studied at high resolution. Prominent examples of this are the so-called minicolumns of the visual cortex. Each minicolumn represents a sophisticated local network responsible for a particular receptive field. Many minicolumns are bound together by horizontal connections and form cortical columns. The relatively small number of neurons involved (80-100 neurons per minicolumn) has made them a very tractable system for functional and anatomical studies [Mountcastle, 1997; Buxhoeveden and Casanova, 2002; Ohki et al., 2005].

At a synaptic resolution, the largest vertebrate connectome to date is from the mouse retina. Here, neurons and their synaptic contacts were reconstructed within a section of the inner plexiform layer, the main computational region of the mammalian retina. This connectome consists of neurites from 950 neurons and has been used to identify new cell types and predict functional mechanisms based on the connectivity found [Briggman et al., 2011; Helmstaedter et al., 2013].

1.3 *Drosophila* in neurobiology

Ideally, a connectome is used as a resource to predict circuit function, generate models and design experiments [Sporns, 2014]. In mammals, this is complicated by the vast number and variability of individual neurons [Sporns et al., 2005]. *Drosophila* neurons, on the other hand, are highly stereotyped and can be uniquely identified across individual animals [Vogelstein et al., 2014; Manning et al., 2012]. At the same time, *Drosophila* offers a huge range of genetic tools and resources to facilitate the transition of connectomic data into neurobiological questions. This combination renders *Drosophila* an ideal organism to study neural networks. This section will provide some overview on some of the most commonly employed tools and resources.

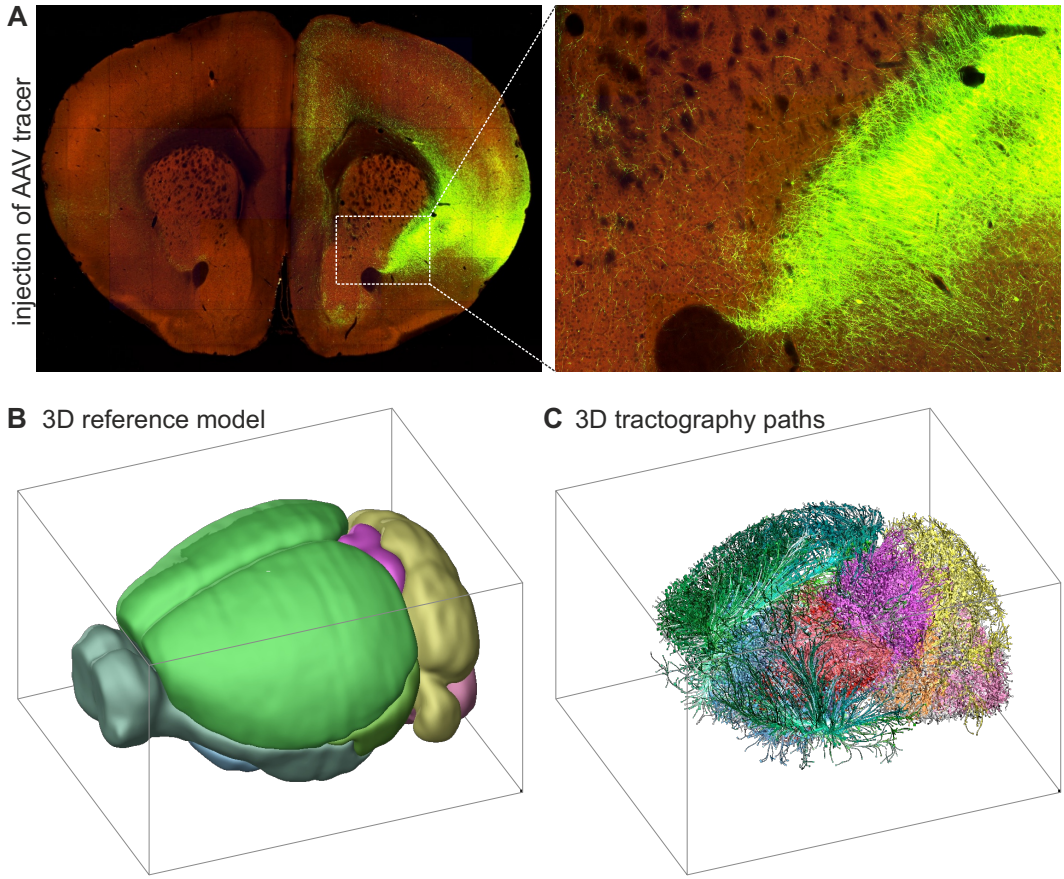

FIGURE 1.3. Mesoscale connectome of the mouse brain. **A**, Adeno-associated virus (AAV) were systematically injected in different areas of the brain to induce expression of a GFP tracer. Shown here is a coronal section through the *nucleus accumbens* from an AAV injection into the visceral area. **B**, Expression data was mapped onto a 3D reference model. **C**, 3D tractography shows connectivity between different areas of the brain [Oh et al., 2014]. Data shown was filtered for clarity. © 2015 Allen Institute for Brain Science. Allen Mouse Brain Connectivity Atlas [Internet]. Available from: http://connectivity.brain-map.org.

1.3.1 Targeting of specific neuronal populations

A challenge of studying neuronal circuits is to identify and access the neurons of interest. This poses less of a problem in small systems, such as the STG or the gill withdrawal reflex of *Aplysia*, that involve only a hand full of neurons as these can be identified based on e.g. position or morphology. But as the number of neurons increases this eventually becomes impossible. An alternative approach is the identification of neurons using their genetic fingerprint. For example, neurons that employ acetylcholine as a neurotransmitter produce choline acetyltransferase (ChAT) which is the rate-limiting enzyme in the synthesis of acetylcholine. The transcription of the ChAT gene is controlled by regulatory elements in the genome. In *Drosophila*, a number of expression systems make use of these regulatory elements to genetically target and manipulate

specific cells/cell types. The most famous of these is the UAS/GAL4 system that originates from the yeast *Saccharomyces cerevisiae* [Giniger et al., 1985]. The GAL4 protein binds the upstream-activating-sequence (UAS) and induces the transcription of neighboring genes. To target cholinergic neurons, the expression of *GAL4* would be put under the control of the same regulatory elements as *ChAT*. The challenge here is to identify and validate the correct regulatory elements of a given gene. The real power of UAS/GAL4 and similar systems is based on modularity: transgenic flies that have the GAL4 gene under the control of a given regulatory element inserted into their genome are called driver lines. GAL4 driver lines are combined with so-called UAS-responder lines. In these responder lines, the expression of a target gene, e.g. for a green-fluorescent protein (GFP), is put under the control of the upstream-activating-sequence (UAS). Circling back to the initial example, crossing of ChAT-GAL4 with UAS-GFP flies results in progeny in which all cholinergic neurons are fluorescent because *GFP* is expressed under the indirect (i.e. via GAL4→UAS) control of regulatory elements of *ChAT* [see Duffy, 2002, for an extensive review].

Since the UAS/GAL4 system has been adopted for *Drosophila* by Brand and Perrimon [1993], large public libraries that feature thousands of GAL4 lines have been generated and characterized in detail [e.g. Jenett et al., 2012; Milyaev et al., 2012]. In addition, there are a number of tools to refine expression patterns, such as GAL80 [Lee and Luo, 1999] or split-GAL4 [Luan et al., 2006]. These resources are invaluable to target specific neuronal populations, down to single neurons.

1.3.2 Manipulation of neuronal activity

Similar to the aforementioned public libraries of driver lines, a wide range of UAS-responder lines is available to help investigating neuronal function, e.g. by monitoring or manipulating neuronal activity.

Non-genetic methods, such as pharmacology, electrophysiology or lesions, have been used to manipulate neuronal function since the early days of neuroscience. In fact, until the emergence of functional imaging, much of the knowledge about the human brain was based on the study of people that had suffered accidental brain damage [Rorden and Karnath, 2004]. While pharmacology and lesions are very effective at manipulating neuronal function, they lack spatial control (i.e. which neurons will be affected). Electrophysiological manipulation on the other hand offers high spatial and temporal control but is technically very challenging.

Genetic methods to manipulate neuronal activity have become a powerful addition to the toolbox as they are extremely diverse and offer advantages over classical approaches. The genetic counterpart to the application of lesions, for example, is the ablation of cells by expressing apoptosis-inducing genes such as *rpr* and/or *hid* [Mohseni et al., 2009]. Combining this with previously mentioned methods to target gene expression gives precise control over exactly which cells will be ablated. Ion channels such as Kalium inward rectifying (Kir) or the bacterial sodium channel NaChBac can be used to increase or decrease neuronal activity without damaging the cell

[Hardie et al., 2004; Nitabach et al., 2006]. Even more sophisticated tools such as the thermosensitive cation channel dTrpA1 manipulate neuronal activity irreducibly and reversibly: dTrpA1 channels open at temperatures above 25°C, leading to a depolarization of the membrane potential. This effect is reversible by lowering the temperature again [Hamada et al., 2008; Pulver et al., 2009]. Most recently, optogenetic tools such as Channel- or Halorhodopsin have been used to manipulate neuronal activity using light as a stimulus [Zhang et al., 2007; Inada et al., 2011].

Summarizing, the innate stereotypy of *Drosophila* neurons in combination with a large genetic toolbox allows to take full advantage of connectomic data [see Ohyama et al., 2015; Fushiki et al., 2016; Zwart et al., 2016, for recent examples].

1.4 EM-based reconstruction of neuronal circuits in *Drosophila*

This section will illustrate the origins and work flow of the *larval EM project* in *Drosophila*.
In many cases, studies of neuronal circuits rely on standard light-microscopy techniques to establish connectivity either by simple overlap between neurites of distinct neuronal populations or by more sophisticated techniques such as GFP-reconstitution across synaptic partners (GRASP) [Feinberg et al., 2008; Hückesfeld et al., 2016; Cavanaugh et al., 2014]. These methods are based on the assumption that physical proximity is indicative of functional connectivity as they lack the resolution to look at the subcellular structures that actually determine connectivity: synapses and gap-junctions. Recent super-resolution microscopy has allowed to push these boundaries and observe many neuronal features such as synaptic structures but is difficult to implement on larger volumes or densely packed neurites. Either method has an inherent disadvantage: the neuronal populations of interest must be relatively sparse and need to be accessible either genetically (e.g. using binary expression systems like UAS/GAL4), (immuno-)histochemically or physically (e.g. using dye fills).

For these reasons, light microscopy is not well suited to investigate neuronal connectivity on a connectome scale - i.e. all the neurons and their connections within a given volume or population. For this purpose, recent electron microscopy (EM) techniques are the method of choice as they allow the generation of large image volumes at synaptic resolution. Similar to the method used to unravel the entire structure of the *C. elegans* nervous system, the EM volume used here to reconstruct the connectome of hugin-producing neurons is based on serial sectioning followed by serial section transmission electron microscopy (ssTEM).

The volume was generated by R. Fetter and Dr. A. Cardona (HHMI Janelia Research Campus, VA, USA) from a larval first instar brain [see Ohyama et al., 2015, for technical details]. The brain was sectioned into 4850 50nm-thick slices, scanned at a resolution of 3.5 nm and aligned into a cohesive image volume (Fig. 1.4A). This image data is freely available via the Open Connectome Project (http://www.openconnectomeproject.org/). The manual reconstruction of this entire first

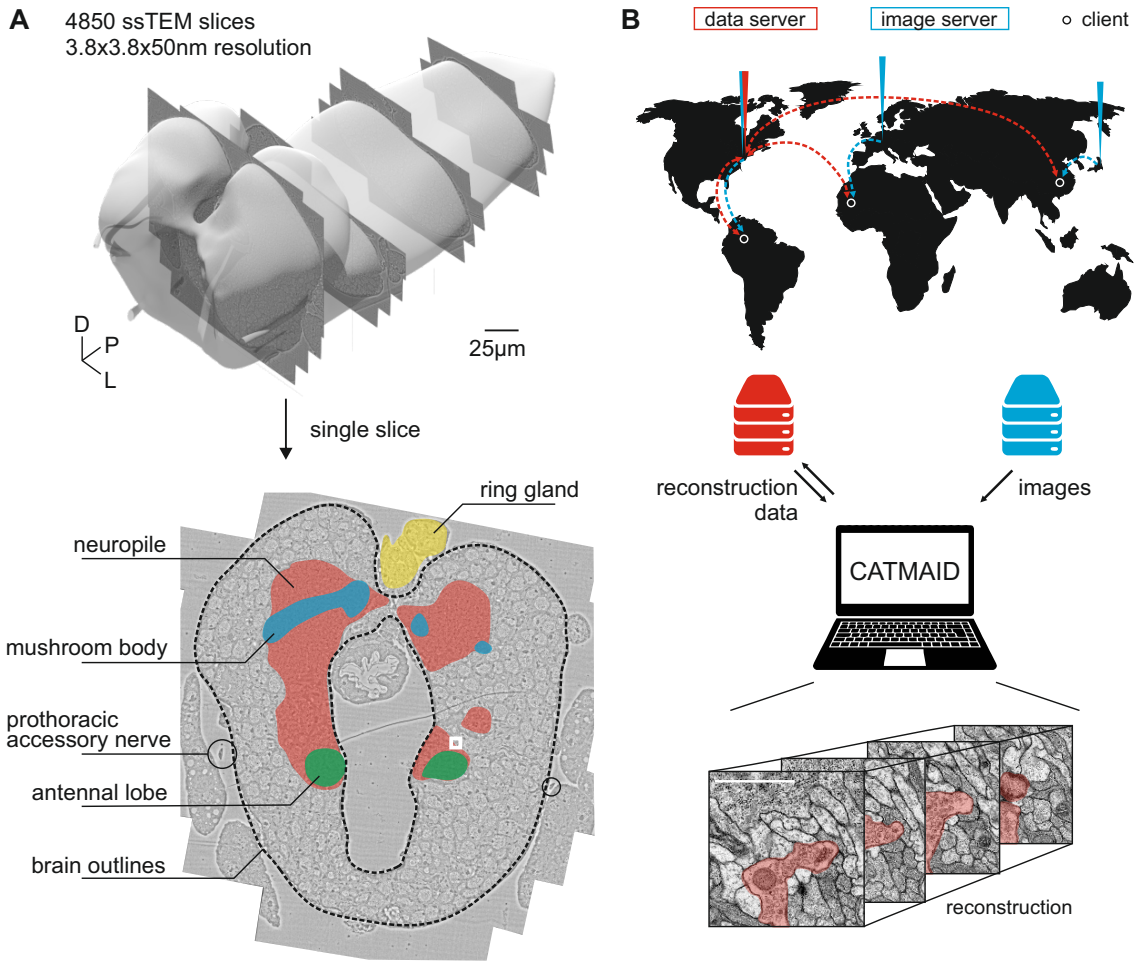

FIGURE 1.4. Collaborative EM-based reconstruction of neuronal circuits. **A**, 3D rendering (upper panel) and single slice (lower panel) of the serial section transmission electron microscopy (ssTEM) volume used for the reconstruction of the hugin connectome. Important neuropils and structures are highlighted. **B**, Sketch of information flow in the collaborative project. Clients running the CATMAID interface connect to the closest image server. Reconstruction data is synchronized between all clients by a single data server.

instar larval brain by a single individual was estimated to take 50 years. Therefore, Dr. Cardona started the larval EM project in 2012 to share the load and collaboratively reconstruct circuits of interest (Fig. 1.4B). As of November 2015, about 50% of the entire brain had been reconstructed this way (A. Cardona, personal communication).

1.5 The hugin neuropeptide

Studies of neural networks often focus on either anatomical connections (i.e. synapses and gap junctions) [Ohyama et al., 2015; Berck et al., 2016; Zwart et al., 2016] or non-anatomical peptidergic connectivity between neurons [Alfa et al., 2015; Dus et al., 2015; Dailey and Bartness, 2009].

Neuropeptide name	Acronym	Mammalian homolog
Adipokinetic hormone	AKH	Glucagon[1]
Allatostatin A/B/C	AstA/MIP/AstC	-
Corazonin	CRZ	-
Diuretic hormone 44	DH44	Corticotropin-releasing hormone (CRH) [2]
Drosophila insulin-like peptide	DILP	Insulin[3]
Hugin/Pyrokinin	Hug-PK2	NMU[4]
Neuropeptide F	NPF	Neuropeptide Y (NPY)[5]
Unpaired 2	Upd2	Leptin[6]

TABLE 1.1. List of selected *Drosophila* neuropeptides and hormones. References: [1] Kim and Rulifson [2004], [2]Cabrero et al. [2002], [3]Rulifson et al. [2002], [4]Melcher et al. [2006], [5]Nässel and Wegener [2011], [6]Rajan and Perrimon [2012], [1,2,4]Mirabeau and Joly [2013]

Only for few examples both types of connections have been investigated, e.g. co-transmission in *C.elegans* [Bentley et al., 2016], the mammalian hypothalamus [Cansell et al., 2012] or the frog sympathetic ganglion [Jan and Jan, 1983].

Neuropeptides are usually synthesized in the soma, packaged into vesicles and then trafficked to their sites of release [Zupanc, 1996]. These vesicles are larger than those for small molecule transmitters, appear electron-dense on EM images due to their protein content and are thus called dense core vesicles (DCVs). In contrast to synaptic small molecule transmitters such as acetylcholine or glutamate, neuropeptides are released independent of presynaptic sites and can then travel considerable distance before binding their receptors [van den Pol, 2012; Salio et al., 2006; Nusbaum et al., 2001]. This fact renders the mapping of peptidergic connections very challenging as source → target relations cannot be inferred just from anatomy.

The *Drosophila* genome has at least 42 genes that encode for precursors of neuropeptides and hormones, many of which are also found in other insects [Nässel and Winther, 2010]. Among those, some represent fundamental hormonal systems involved in regulation of metabolism that have been conserved in mammals and *Drosophila*. Prominent examples are glucagon [Kim and Rulifson, 2004], insulin [Ikeya et al., 2002; Rulifson et al., 2002] and leptin [Rajan and Perrimon, 2012] (Table 1.1). In addition, there are several less known peptidergic systems which are nevertheless highly conserved across bilaterians and represent clear cases of co-evolution of peptides and their receptors [Mirabeau and Joly, 2013].

The *Drosophila hugin*[3] gene encodes for a prepropeptide that is processed into two peptides. One of these peptides has a structure common to all known pyrokinins and was thus named pyrokinin 2 (hug-PK2) (also known as Drm-PK-2). Initially described as having myostimulatory effects, subsequent studies reported a range of different effects related to feeding behavior [Meng et al., 2002]. The first of these studies by Melcher and Pankratz [2005] found that

[3]The name is based on Scandinavian mythology: Hugin ("thought") is one of two ravens that are messengers to the god Odin [Meng et al., 2002]

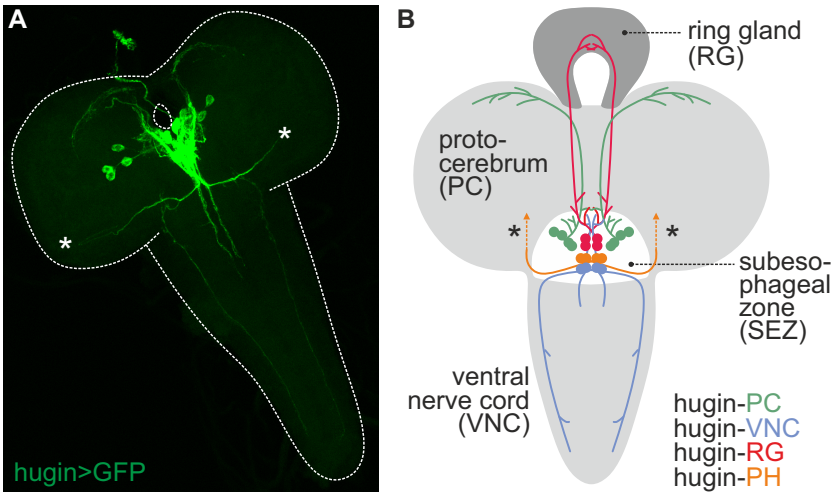

FIGURE 1.5. *Hugin* is expressed in 20 neurons in the central nervous system (CNS). **A**, *Hugin* promoter drives GFP expression in larval CNS (white outlines). **B**, Hugin-producing neurons subdivide into 4 classes based on their projection targets. Asterisks mark entry sites of the prothoracic accessory nerve (PaN).

hugin was upregulated in *klumpfuss* (*klu*) mutants and that ubiquitous overexpression of *hugin* phenocopied the *klu* feeding defect. They also showed that *hugin* is expressed in only 20 neurons in the subesophageal zone (SEZ) (also known as subesophageal ganglion), a region of the central nervous system involved in regulation of feeding and sensory processing [Colomb et al., 2007; Vosshall and Stocker, 2007; Hückesfeld et al., 2015] (Fig. 1.5A). This relatively small number of hugin-producing neurons (hereinafter also called hugin neurons) made them interesting targets for functional dissection of a neural circuit. In 2007, Bader et al. provided a comprehensive morphological description of all hugin neurons based on light microscopy scans of single-cell clones.

They found that the population of hugin neurons consists of four morphologically distinct classes (Fig. 1.5B). Each of the hugin classes is defined by common projection targets of the neurons within that class. Based on these projection targets the classes are called: hugin-PC (**p**roto**c**erebrum), hugin-VNC (**v**entral **n**erve **c**ord), hugin-RG (**r**ing **g**land) and hugin-PH (**ph**arynx). See sections 4.1 and 4.2.2 for a more detailed morphological description of hugin neurons.

In a follow up study, we found that artificial activation of hugin neurons led to a strong decrease in food intake in *Drosophila* larvae [Schoofs et al., 2014a]. This decrease was rescued by knocking-down *hugin* expression using RNA interference (RNAi), demonstrating that the neuropeptide is involved in regulation of feeding behavior. In-depth analysis showed that activation of hugin neurons simultaneously decelerates motor rhythms for pharyngeal pumping (an essential motor program for food ingestion) and accelerates motor rhythms for locomotion.

One cleavage product of the hugin peptide, hug-PK2, belongs to a peptidergic system that

mammalian	
human NMU-25	FRVDEEFQSPFASQSRGYFLFRPRN
human NMU-8	YFLFRPRN
mouse NMU-20	EYQSPSVGQSKGYFLFRPRN
C. lupus familiaris NMU-8	QFLFRPRN
avian	
Gallus gallus NMU-9	GYFFFRPRN
piscine	
C. auratus NMU-21	DDLQGPGRIQSRGFFLYRPRN
amphibian	
R. temporaria NMU-25	LKPDEELQGPGGVLSRGYFVFRPRN
insect	
P. americana PK2	LVPFRPRL
Drosophila hug-PK2	SVPFKPRL

TABLE 1.2. Comparison of amino acid sequences of neuromedinU (NMU) / pyrokinin 2 (hug-PK2) in selected vertebrate and insect species. Common residues (highlighted in red) lie in the last five C-terminal amino acids. References: Melcher et al. [2007] and Malendowicz et al. [2012].

shows strong conservation across bilaterians and serves as a clear example of co-evolution of peptides and receptors [Mirabeau and Joly, 2013]. Hug-PK2 and its vertebrate ortholog, neuromedinU (NMU), shows strong conservation across many species [Melcher et al., 2007; Malendowicz et al., 2012]. Both, hug-PK2 as well as the various NMUs are cleaved from larger prepropeptides and share common amino acid sequences among the last five C-terminal residues (Table 1.2). For NMU-8 it was shown that this highly conserved C-terminus is essential for its bioactivity [Brighton et al., 2004]. Conservation between hugin and NMU is not solely based on amino acid sequences but also covers their respective effects on behavior. As laid out above, increased hugin signaling decreases food intake and increases locomotion. Similarly, increased NMU signaling decreases food intake and increases physical activity in mammals [Howard et al., 2000; Hanada et al., 2004; Novak et al., 2007]. Similarities between hugin and NMU are discussed in detail in section 5.3.

Functional aspects of the hugin neuropeptide as well as the neurons employing this peptide have been extensively studied and subsets of hugin neurons were successfully linked to specific phenotypes. Just recently, Hückesfeld et al. [2016] showed that hugin-PC neurons are involved in the processing of aversive gustatory cues and subsequent reduction in food intake. In contrast, hugin-VNC neurons are not associated with feeding behavior at all but instead affect locomotion [Schoofs et al., 2014a]. These findings hint at a more diverse and intricate role of the hugin system in *Drosophila*.

1.6 Aims of the thesis

In order to devise meaningful hypotheses and experiments on the biological relevance of the different hugin neurons, it would be profoundly helpful to know more about their interaction partners. The only existing such data are on hugin-PC neurons which receive inputs from sensory neurons expressing a gustatory receptor for bitter substances [Hückesfeld et al., 2016] and from insulin-producing cells (IPCs) [Bader et al., 2013]. However, this data on the connectivity of hugin neurons is very limited and most certainly represents only a small fraction of the actual hugin network. The primary goal of this thesis is therefore to use recent advances in whole brain EM imaging and reconstruction to acquire the connectome of all hugin neurons. This connectivity map should represent a framework for further investigation of hugin neurons and help devising new hypotheses on the function of the hugin circuit.

CHAPTER 2

MATERIALS

2.1 Experimental Animals

2.1.1 Caretaking

Flies were kept on standard fly food in plastic vials. Unless otherwise stated they were stored at either 18°C or 25°C with air humidity between 50% and 60%. Flies at 18°C were kept at natural light conditions, flies at 25°C were kept at an artificial 12h:12h light cycle.

2.1.2 Fly strains

Fly strains used are listed in table 2.1.

Short name	Genotype	Source
hugS3-GAL4	w^{1118} ; ; hugS3-GAL4	Lab internal strain
CG8784-6kb-GAL4 also: PK2-R1-6kb-GAL4 or hugR84.6 L1.3	w^{1118} ; ; P{CG8784-6.0-GAL4}	Lab internal strain
CG8784::p65-GAL4 also: PK2-R1::p65-GAL4	w^{-} ;; CG8784::p65-GAL4	M. Texada, HHMI Janelia Research Campus
DH44-GAL4	w^{1118} ; ; P{w[+mC]=Dh44-GAL4.TH}2M	Bloomington #51987
InsP3-GAL4	; ; InsP3-GAL4	Lab internal strain
DMS5-GAL4	; ; DMS5-GAL4	J. Veenstra, University of Bordeaux

Continued on next page

Continued from previous page

Short name	Genotype	Source
ChAT-GAL4	w^{1118} ; ChAT-GAL4 7.4/CyO	Bloomington #6798
UAS-CaMPARI (high affinity)	w[*] ; P{y[+t7.7] w[+mC]=UAS-CaMPARI}attP40	Bloomington #58761
UAS-dTrpA1	w[*] ; UAS-dTrpA1	Bloomington #26263
UAS-NaChBac	w[*] ; ; UAS-NaChBac/TM6B,Tb	Bloomington #9468
hugin-YFP;UAS-mRFP	; hugS3-YFP ; UAS-DsRed	Lab internal strain
UAS-halorhodopsin	w^{1118} ; UAS-eNpHR-YFP; Sb/TM6B,Tb	Bloomington #41753
UAS-Kir2.1	w[*] ; ; UAS-Hsap\KCNJ2.EGFP/TM3,Sb	Bloomington #6595
UAS-HA-V5-FLAG	pJFRC201-10XUAS-FRT>STOP>FRT-myr::smGFP-HA in VK0005, pJFRC240-10XUASFRT>STOP>FRT-myr::smGFP-V5-THS-10XUAS-FRT>STOP>FRT-myr::smGFP-FLAG in su(Hw)attP1	A. Nern, HHMI Janelia Research Campus

Table 2.1: List of fly strains used.

2.2 Buffers and Media

Buffers and media used are listed in table 2.2.

Name	Composition
Apple juice agar	42,5g agar; 0,5l apple juice; 40g sucrose; 1,5l purified water, 3g nipagin solved in 20ml 100% EtOH
Standard Fly Food	13,3l H_2O; 330g beer yeast; 815g corn flour; 80g filamentous agar; 1l sugar beet syrup; 20g nipagin solved in 0,2 100% EtOH
Mowiol	12ml glycerin; 9,6g Mowiol40-88; 24ml H_2O; 48ml 0,2M TrisHCl; pH 8,5
phosphate-buffered saline (PBS) 10x	2g KCL; 2g KH_2PO_4; 11,5g Na_2HPO_4; 80g NaCl; topped of with ddH_2O to 1l; ph 7,4
PBT	0,1% or 0,5% Triton X-100 in 1X PBS
Intracellular ringer solution	140mM NaCl; 3mM KCl; 2mM $CaCl_2$; 4mM $MgCl_2$; 10mM sucrose; 5mM HEPES; pH 7,2
Red yeast paste	0,5g crimson red powder; 42g live yeast; 7ml H_2O
Fluorescent yeast paste	150mg (0,3%) fluoresceine; 42g live yeast; 7ml H_2O
Hybe buffer	50% (v/v) Formamid, 5x SSC, 200 μg/ml ssDNA, 100 μg/ml tRNA, 25 μg/ml Heparin, pH 5.0

Continued on next page

Continued from previous page

Name	Composition
Hybe-B buffer	50% (v/v) Formamid, 5x SSC
20X saline-sodium citrate (SSC)	3M NaCl, 300mM trisodium citrate, pH 7.0 (HCl)

Table 2.2: Buffers and media.

2.3 Reagents

Reagents and their sources are listed in table 2.3.

Name	Abbreviation	Source
Agar-Agar, Kobe I	Agar	Carl Roth, Karlsruhe
Apple juice		Lidl Dienstleistung, Neckarsulm
Beer yeast		Gewürzmühle Brecht, Eggenstein
Calcium chloride	$CaCl_2$	Carl Roth, Karlsruhe
Corn flour		Broicher Mühle, Bedorf
Crimson red powder		
Ethanol	EtOH	Carl Roth, Karlsruhe
Filamentous agar		Gewürzmühle Brecht, Eggenstein
Fluorescein		Sigma-Aldrich Chemie, Steinheim
Formaldehyde 37%		Carl Roth, Karlsruhe
Glycerin		Carl Roth, Karlsruhe
Goat serum		Life Technologies, Darmstadt
HEPES		
hugin pyrokinin 2	hug-PK2	Iris Biotech, Marktredwitz, Germany
Live yeast		Lidl, Neckarsulm
Magnesium chloride	$MgCl_2$	Acros Organics N.V., Geel, Belgium
Methyl-4-Hydroxybenzoat	Nipagin	Sigma-Aldrich Chemie, Steinheim
Mowiol40-88		Sigma-Aldrich Chemie, Steinheim
Petroleum jelly		
Poly-L-lysine 0.1%	Polylysine	Sigma-Aldrich Chemie, Steinheim
Potassium dihydrogen phosphate	KH_2PO_4	
Potassium chloride	KCl	Carl Roth, Karlsruhe
Sodium chloride	NaCl	Carl Roth, Karlsruhe
Sodium dihydrogren phosphate	Na_2HPO_4	Carl Roth, Karlsruhe
Sugar beet syrup		Grafschafter Krautfabrik, Meckenheim
Sucrose		VWR International, Darmstadt

Continued on next page

Continued from previous page

Name	Abbreviation	Source
Triton X-100		Carl Roth, Karlsruhe
Tris(hydroxymethyl)aminomethan	Tris	Carl Roth, Karlsruhe
SYBR Safe		Invitrogen, Carlsbad, CA

Table 2.3: Reagents and their sources.

2.4 Hardware

Hardware and their sources are listed in table 2.4.

Description	Model	Manufacturer
Binocular	Stemi 2000	Carl Zeiss, Jena
Cold light source	CL 1500 ECO	Zeiss, Jena
Confocal microscope	LSM780	Zeiss, Jena
Forceps	Dumont	Fine Science Tools, Heidelberg
Hot plate stirrer	RH Basic2	Ika, Staufen
Microscope camera	AxioCam ICc 1	Zeiss, Jena
Micro pipettes	Pipetman Neo 10/200/1000μl	Gilson, Inc., USA
Micro scissors		Fine Science Tools, Heidelberg
pH-meter	Hl 221	Hanna Instruments, Smithfield RI
Rotation wheel	Stuart SB3	Bibby Scientific Limited, Stone, UK
Pin holder	Moria MC1	Fine Science Tools, Heidelberg

Table 2.4: Hardware and their sources.

2.5 Kits and Consumables

Kits and consumables and their sources are listed in table 2.5.

Description	Article	Source
Tyramid signal amplification (TSA) Kit	TSA Plus Fluorescein System	Perkin & Elmer, Waltham, USA
Gel and PCR clean up	NucleoSpin Extract II	Macherey-Nagel, Düren
TOPO cloning	TOPO TA Cloning Kit	Thermofisher, Waltham, MA
Midiprep	PureLink HiPure Plasmid Filter Midiprep Kit	Invitrogen, Carlsbad, CA

Continued on next page

Continued from previous page		
Description	Model	Manufacturer
RNA clean up	NucleoSpin RNA II	Macherey-Nagel, Düren
In-vitro transcription	DIG RNA Labeling Mix	Roche Diagnostics, Mannheim
Cell sieve		VWR International, Darmstadt
Cover slides	24x24mm	Carl Roth, Karlsruhe
Glass slides	76x26mm	Carl Roth, Karlsruhe
Lab dishes		Schott, Mainz
Parafilm	Parafilm M	Pechiney Plastic Packaging, Menasha WI
Plastic vials		Greiner, Frickenhause & Nerbe plus, Winsen/Luhe
Pipette tips	w/ and w/o filter	Corning, NY
Tungsten wire	30-250μm	Goodfellow, Bad Nauheim

Table 2.5: Kits, consumables and their sources.

2.6 Antibodies

Antibodies and their sources are listed in table 2.6.

	Name	Host	Dilution	Source
Primary Antibodies	α-DMS		1:500	Jan Veenstra (Bordeaux)
	α-DH44		1:500	Jan Veenstra (Bordeaux)
	α-Dilp2		1:500	lab internal antibody
	α-GFP-FITC		1:500	Abcam plc, Cambridge, UK
	α-HA	rabbit	1:500	Cell Signaling Technologies, Inc.
	α-FLAG	rat	1:700	Novus Biologicals, Littleton, USA
	α-V5-AF647	mouse	1:200	AbD Serotec, Puchheim
Sec. Antibodies	α-mouse-AF488	donkey	1:500	Jackson ImmunoResearch, Suffolk, UK
	α-rabbit-AF594	donkey	1:500	Jackson ImmunoResearch, Suffolk, UK
	α-rat-Cy3	donkey	1:800	Jackson ImmunoResearch, Suffolk, UK
	α-Digoxigenin-POD	sheep	1:50	Roche Diagnostics, Mannheim

Table 2.6: Antibodies and their sources.

2.7 Software

Software and their sources are listed in table 2.7.

Name	Version	Source
AxioVision LE	AxioVs40 V4.8.1.9	Carl Zeiss, Jena
Excel	Microsoft Office 2010	Microsoft Cooperation, USA
Fiji/ImageJ	1.50	Wayne Rasband, National Institute of Health, USA
Mendeley	1.16	Elsevier, Inc.
SigmaPlot	12	Systat Software
Blender3D	2.7	Blender Foundation
Corel Draw	X8	Corel Cooperation
Anaconda	2.7/3.5	Continuum
Python	2.7/3.3/3.5	Python Software Foundation
GitHub		Github Inc.
iSpy	5.5	iSpyConnect.com
CytoScape	3.4.0	cytoscape.org

Table 2.7: Software and their sources.

CHAPTER 3

METHODS

3.1 Larval food intake assay

Age of experimental animals was synchronized by allowing adult flies to deposit eggs in plastic vials containing standard fly food and a small amount of live yeast paste. These egg collections were performed at 25°C over a duration of 4h resulting in a synchronized age of ±2h. Animals were subsequently kept at 25°C until they reached the required age for the experiment (96h for third instar larvae). If population density was too high (e.g. young larvae were found outside the fly food), collections were split into multiple vials. For the experiment, larvae were carefully removed from the vial, rinsed and pre-starved for 30 minutes on a wet filter paper at room temperature.

After starvation, larvae were placed on prewarmed (32°C) or precooled (18°C) apple juice agar plates containing a small amount of colored yeast paste (1:100 crimson red powder) and incubated for 20 minutes at the respective temperature. Afterwards the larvae were removed from the yeast and inactivated by rinsing them with 60°C water. For analysis, larvae were lined up on glass slides and pictures of single larvae were taken using an AxioCam microscope camera (Zeiss). To calculate the amount of food ingested, the area of the alimentary tract stained by the colored yeast paste was determined and divided by the total body surface area, giving in the percentage of the larval body stained. ImageJ was used to perform these measurements and calculations [Schneider et al., 2012].

3.2 Pupae size assay

To synchronize age of experimental animals, adult flies were allowed to deposit eggs on apple juice agar plates containing small amounts of live yeast paste. These egg collections were performed

at 25°C over a duration of 4h resulting in synchronized age of ±2h. After 1d, 20 newly hatched first instar larvae were transferred into small plastic vials and incubated at 25°C. These larvae started pupariation after 5-6 days. To analyze their size, pupae were carefully removed from the vials after 7 days and lined up on a glass slide with their ventral side down. Pictures of single pupae were taken using a AxioCam microscope camera (Zeiss). Basic acquisition settings (optical zoom, exposure time, image resolution) were kept constant across experiments. Pupae size was measured by counting the number of pixels constituting the pupa using the software Fiji [Schindelin et al., 2012]. Pixel count of individual pupae were normalized against the average over all pupae of the control.

3.3 Immunohistochemical stainings

Larvae were dissected in either 1X PBS or intracellular ringer [Rohrbough and Broadie, 2002]. First, the abdominal body wall, the alimentary tract and the fat body were removed, retaining the larval heads including the cephalopharyngeal skeleton, the central nervous system and the ring gland. The samples were fixed in 4% formaladehyde for 30-60 minutes. Next, they were washed 3 times for 20 minutes in 0,5% PBT and then blocked for 1h using 5% goat serum. Incubation with primary antibodies in 5% goat serum occurred overnight at 4°C. Subsequently, samples were washed again 3 times for 20 minutes in 0,5% PBT and then incubated with secondary antibodies overnight at 4°C. Before mounting, samples were washed again 3 times for 20 minutes in 0,5% PBT. If required, DAPI 1:1000 was applied for 5mins and subsequently washed 2 times for 5mins. Unless otherwise stated, all above steps were performed at room temperature and on a rotation wheel. Before mounting brains were separated from the larval heads, lined up on a glass slide and then embedded in MOWIOL mounting medium.

3.4 Fluorescence-in-situ-hybridization (FISH) of larval brains

3.4.1 Generation of riboprobes

First, a 500-800 base pair template DNA from a gene's exon was amplified from genomic DNA using standard polymerase chain reaction (PCR) reaction with GoTaq DNA-Polymerase to obtain products with adenine overhang at the 3' end (Tab. B.1). Primers used for amplification of the probe for the vesicular glutamate transporter (VGluT) were:

Forward:	`gtcggaaatcgtttgacgtt`
Reverse:	`tgcgcctacggctatctact`

PCR products were checked using gel electrophoresis (1.2% agarose, 1:1000 SYBR safe) and extracted using a gel extraction kit. After clean up, PCR fragments were cloned into a pCRII-TOPO vector using the TOPO TA Cloning Kit. Successful insertion disrupts the *lacZ*

gene allowing for X-Gal blue/white screening. Chemically competent bacteria were transformed following the kit's protocol. Afterwards bacteria were incubated for 1h at 37°C in LB media to allow development of ampicillin (Amp) resistance. Amp^+ LB agar plates were coated with X-Gal solution ($50\mu l$/plate) and prewarmed. Transformed bacteria were plated and incubated over night. The next day, white colonies (successful transformation with a vector containing the PCR fragment) were picked. 3ml Amp^+ LB medium were inoculated and incubated over night in a shaker (220rpm, slanted) at 37°C. To test the clones for insertion of the correct PCR fragment, a miniprep and a subsequent a digest with EcoRI were performed and run on a agarose gel. Clones showing bands of the correct sizes were amplified overnight in 30ml Amp^+ LB medium. The next day, plasmids were extracted using a midiprep kit (PureLink) and direction of the insertion was determined using restriction enzymes that produced asymmetric fragments. Simultaneously, clones were sequenced (GATC Biotech, Sanger sequencing, M13-FP primer). Both methods indicated that transcription with Sp6 polymerase would produce the antisense and T7 would produce the sense probe. To prevent transcript, the plasmids were linearized by digestion with XbaI for Sp6 and HindIII for T7 polymerase ($10\mu g$ DNA, $5\mu l$ enzyme, $100\mu l$ final volume, 2h at 37°C). Linearized template was cleaned up using a PCR clean up kit. Gel electrophoresis was performed to confirm complete digestion. For in vitro transcription, Digoxigenin (DIG) RNA labeling mix (Roche) was used following the manufacturer's protocol. Afterwards, DNA template was removed using a DNAse digest. Transcript was precipitated with ethanol and dissolved in $20\mu l$ RNAse free water. Of this $1\mu l$ was tested for degradation using gel electrophoresis. $200\mu l$ Hybe buffer was added to the remaining volume and the probe was stored at -20°C.

3.4.2 FISH protocol

Larvae were dissected in chilled ringer, fixed in 4% formaldehyde (in 1% PBT) for ±1h and afterwards extensively washed (5/5/15/30 min). Optionally, an additional methanol clearing was performed by step-wise transfer to 100% methanol (0%,30%,70%,100%; 5mins incubation in between) and subsequent storage over night at -20°C. Subsequently, samples were transferred step-wise back to PBT and extensively washed again.

For hybridization, Hybe and HybeB buffers were prewarmed to 65°C. Samples were transferred step-wise first from PBT to HybeB and then from HybeB to Hybe (0%,50%,100%; 5mins incubation at 65°C in between). Afterwards, samples were prehybridized in Hybe at 65°C for ±1h. For hybridization, most of the supernatant was discarded and 1-$5\mu l$ of each riboprobe (labelled with different antigens such as Digoxigenin (DIG), fluorescein or biotin) were added and incubated over night at 65°C (the exact annealing temperature depends on the riboprobe).

The next day, samples were first topped off with Hybe buffer. The supernatant was then discarded and samples were incubated for ±1h with fresh Hybe at 65°C. After this posthybridization, samples were transferred step-wise from Hybe to HybeB, from HybeB to PBT following the protocol laid out above and then extensively washed in PBT (5/5/15/30/60 min). Blocking was

performed in PBT plus 5% goat serum for ±1h. Next, peroxidase (POD)-coupled antibody against the first riboprobe and additional primary antibodies against other proteins were added (in PBT + 5% goat serum) and incubated over night at 4°C.

The following day, samples were extensively washed in PBT (5/5/15/30/60 min). Then supernatant was discarded and 150 μl 1X amplification diluent from the Tyramid signal amplification (TSA) kit was added. After 10 min 1st fluorochrome tyramide (TSA Plus Stock solution, 1:50) was added and incubated for another 10 min in the dark. This was followed by extensive washing in PBT (5/5/15/30 min).

If a second riboprobe had been used, the first peroxidase (POD) was now deactivated by washing samples in ringer solution and subsequent incubation with 10mM HCl (in ringer) for 10 min each. Then above steps of over night incubation with a second POD-coupled antibody were repeated. At this point, secondary antibody against protein was also added for over night incubation.

Finally, samples were washed extensively a last time (5/5/15/30/60 min) and mounted in Mowiol on glass slides.

3.5 Multi-Color Flp-Outs

multi-color flp-outs (MCFOs) were performed using the multi-color flp-out (MCFO)3-5 fly strains by Nern et al. [2015]. These flies express spaghetti monster GFPs (smGFPs), non-fluorescent GFP variants, with different epitopes (HA, V5 or FLAG) under the control of multiple upstream-activating sequences (10XUAS) and a core promotor. By default, a transcriptional terminator flanked by FRT sites prevents expression of smGFP. A weakened flipase is pan-neuronally expressed under the control of regulatory elements of the *N*-synaptobrevin gene. The flipase stochastically removes the terminator cassettes and allows expression of smGFP, allowing multi-color labeling of subsets of neurons.

HugS3-Gal4 flies were crossed with UAS-HA-V5-FLAG flies. Egg collections were performed by transferring flies into fresh plastic vials containing fly food and dry yeast. After 4h adult flies were transferred again and the vial with the collected eggs was incubated at 25°C. Larvae were dissected 1d and 4d after egg laying to investigate morphology of individual hugin-producing neurons in first and third instar larvae, respectively. Dissection and immunohistochemical staining procedure followed the standard protocol (see section 3.3). Rabbit anti-HA and rat anti-FLAG were used as primary antibodies. Anti-rabbit-AlexaFluor596, anti-rat-Cy3 and mouse anti-V5-AlexaFluor647 conjugated were used as secondary antibodies. See table 2.6 for details on dilution and supplier.

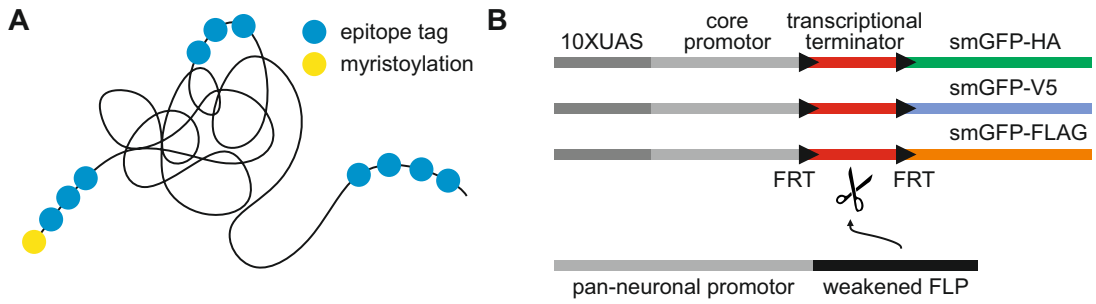

FIGURE 3.1. Principle of multi-color flp-outs (MCFOs). **A**, Schematic of non-fluorescent spaghetti monster GFP (smGFP) containing epitope tags and myristoylation. **B**, A weakened, pan-neuronally expressed flipase stochastically removes the terminator cassettes, allowing expression of different smGFP each with it's own epitope.

3.6 Calcium imaging using the calcium integrator CaMPARI

The effect of hugin-derived pyrokinin 2 (hug-PK2) on calcium activity in medial neurosecretory cells (mNSCs) was investigated using the calcium integrator CaMPARI (Fosque et al., 2015). Hug-PK2 was synthesized by Iris Biotech (Marktredwitz, Germany) using the amino acid sequence `SVPFKPRL-NH2` with an amidated C-terminus. CG8784-6kb-GAL4 flies were crossed to UAS-CaMPARI flies. Third instar larval brains were dissected in ringer solution and placed in ringer [Rohrbough and Broadie, 2002] containing either no, 100nM, 1µM or 10µM hug-PK2. After 1min of incubation, 405nm photoconversion light was applied for 15s. Afterwards brains were placed on a poly-l-lysine-coated cover slide and scanned using a confocal microscope. Settings were kept the same over all scans. Calcium activity was calculated as the ratio of the fluorescence of photoconverted (red) to unconverted (green) CaMPARI using ImageJ [Schneider et al., 2012].

3.7 Reconstruction of neuronal circuits

The following description of circuit reconstruction was modified from Schlegel et al. [2016]. Reconstructions were based on a ssTEM (serial section transmission electron microscopy) data set comprising an entire central nervous system including the ring gland of a first-instar *Drosophila* larva. Generation of this data set was described previously by Ohyama et al. [2015]. Neurons' skeletons were manually reconstructed using a modified version of CATMAID (http://www.catmaid.org) [Saalfeld et al., 2009]. Synaptic connections representing fast, chemical synapses were identified based on previously described typical criteria: thick black active zones, pre- (e.g. T-bar, vesicles) and postsynaptic membrane specializations [Prokop and Meinertzhagen, 2006]. Inputs and outputs of hugin neurons were traced by following the pre- and postsynaptically connected neurites to the respective neurons' somata or nerve entry sites in sensory axons. Subsequently, all sensory and endocrine neurons synaptically connected to hugin neurons were fully reconstructed. Interneurons were fully reconstructed if (a) homologous neurons were found in both

hemispheres/-segments (unless medially unpaired neurons) and (b) at least one of the paired neurons was connected by a minimum of 3 synapses to/from hugin neurons. Neurons that did not fit either criteria were not fully reconstructed and thus excluded from statistical analysis. This resulted in the reconstruction 177 synaptic partners that together covered 90%/96% of hugin neurons' above threshold pre-/postsynaptic sites. The same parameters were applied to the reconstruction of synaptic partners of median neurosecretory cells (mNSCs). Morphological plots and example synapse's volume reconstruction were generated using custom python scripts or scripts for Blender 3D (www.blender.org). The script for a CATMAID-Blender interface is available on Github (https://github.com/schlegelp/CATMAID-to-Blender). See appendix for supplemental neuron atlas of all reconstructed neurons and their connectivity with hugin neurons.

3.8 Circuit analysis

The following descriptions of methods for analyses of the reconstructed neuronal circuits were modified from Schlegel et al. [2016].

3.8.1 Localization of DCVs in respect to synaptic sites

Due to the neuronal reconstructions' being skeletons instead of volumes, distances were measured from the center of each given dense core vesicle to the center of the closest presynaptic site along the skeleton's arbors. Dense core vesicles (DCVs) within 3000 nm radius around the centers of neurons' somata were excluded. Data was smoothed for graphical representation (Fig. 4.9).

3.8.2 Normalized connectivity similarity score

To compare connectivity between neurons (Fig. 4.11 B; 4.14 C), a modified version of the similarity score described by Jarrell et al. [2012] was used:

$$f(A_{ik},A_{jk}) = min(A_{ik},A_{jk}) - C_1 max(A_{ik},A_{jk}) e^{-C_2 min(A_{ik},A_{jk})}$$

With the overall connectivity similarity score for vertices i and j in adjacency matrix A being the sum of $f(A_{ik},A_{jk})$ over all connected partners k. C_1 and C_2 are variables that determine how similar two vertices have to be and how negatively a dissimilarity is punished. Values used were: $C_1 = 0.5$ and $C_2 = 1$. To simplify graphical representation, we normalized the overall similarity score to the minimal (sum of $-C_1 max(A_{ik},A_{jk})$ over all k) and maximal (sum of $max(A_{ik},A_{jk})$ over all k) achievable values, so that the similarity score remained between 0 and 1. Self-connections (A_{ii}/A_{jj}) and A_{ij} connections were ignored.

3.8.3 Synapse similarity score

To calculate similarity of synapse placement between two neurons, the synapse similarity score was calculated (Fig. 4.12):

$$f(i_s, j_k) = e^{\frac{-{d_{sk}}^2}{2\sigma^2}} e^{-\frac{|n(i_s)-n(j_k)|}{n(i_s)+n(j_k)}}$$

With the overall synapse similarity score for neurons i and j being the average of $f(i_s, j_k)$ over all synapses s of i. Synapse k being the closest synapse of neuron j to synapses s [same sign (pre-/postsynapse) only]. d_{sk} being the linear distance between synapses s and k. Variable σ determines which distance between s and k is considered as close. $n(j_k)$ and $n(i_s)$ are defined as the number of synapses of neuron j/i that are within a radius ω of synapse k and s, respectively (same sign only). This ensures that in case of a strong disparity between $n(i_s)$ and $n(j_k)$, $f(i_s, j_k)$ will be close to zero even if distance d_{sk} is very small. Values used: $\sigma = \omega = 2000$ nm.

3.8.4 Clustering

Unless otherwise stated, clusters for dendrograms were created based on the mean distance between elements of each cluster using the average linkage clustering method. Clusters were formed at scores of 0.2 for synapse similarity score (Fig. 4.12) and 0.4 for connectivity similarity score (Fig. 4.11 B; 4.14 C).

3.9 Statistics

For statistical analysis SigmaPlot 12 (Systat Software) was used. CorelDraw X8 (Corel) was used to generate figures.

CHAPTER 4

RESULTS

4.1 Morphology of hugin neurons in first instar larvae

Previous studies have produced detailed descriptions of the morphology of hugin neurons at single cell level, e.g. by clonal analysis in third instar larva [Bader et al., 2007a] (see also introduction, Fig. 1.5). However, the EM volume of the larval CNS that was going to be used for the reconstruction of hugin neurons stemmed from a first instar larva [Ohyama et al., 2015]. The smaller size of the CNS in the first instar reduces the amount of image data and the time it takes to reconstruct a neuron. As a consequence, the morphology of hugin neurons had to first be confirmed in the first instar. Hugin promoter-driven expression of a GFP and immunohistochemical stainings against the hugin neuropeptide [Melcher and Pankratz, 2005] showed that the expression pattern of hugin in the first instar is similar to that in the third instar (Fig. 4.1 A,B). In both developmental stages a set of 20 neurons in the SEZ is labeled by both the hugin promoter-GAL4 as well as the hugin antibody.

Exact knowledge of their morphology is crucial to unambiguously identify neurons in the EM volume. Therefore, first instar hugin neurons were additionally investigated at single cell level using multi-color flp-outs (MCFOs) [Nern et al., 2015]. MCFOs in addition to standard fluorescent labeling showed that individual hugin neurons have similar morphology in first and third instar (Fig. 4.1 C-H). The only notable difference were less pronounced fine arborizations in first as compared to third instar hugin neurons.

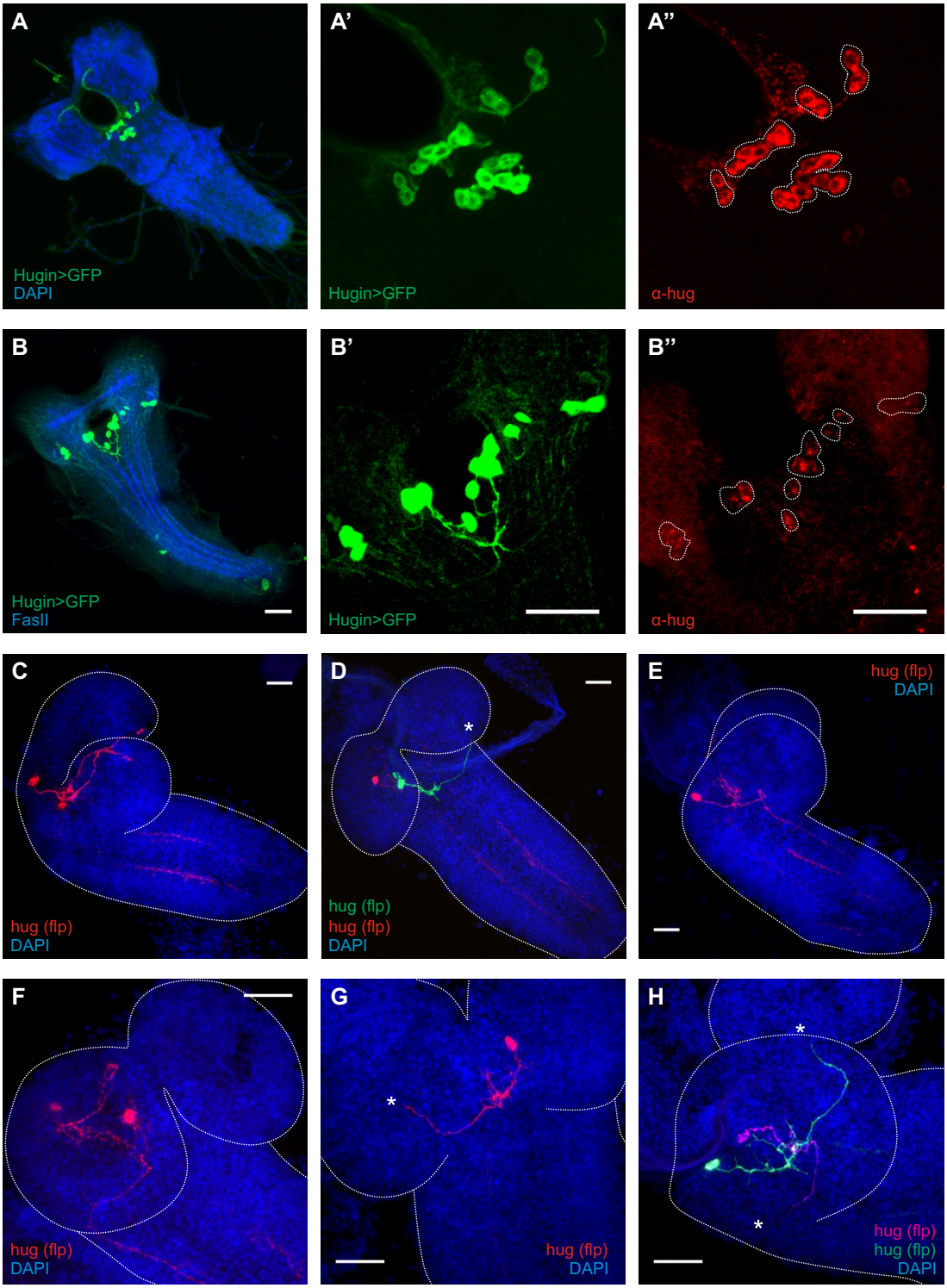

FIGURE 4.1. Morphology of hugin neurons in first instar larvae. **A**, CNS of a third instar larva. **A'**, Zoom-in. GFP expression driven by a [continued on next page]

Figure 4.1: [continued from previous page] hugin promoter-GAL4 line (HugS3-GAL4). **A"**, Co-staining against the hugin neuropeptide. **B-B"**, CNS of a first instar larva, same setup as A-A". All 20 hugin neurons are labeled by hugin promoter line as well as by hugin antibody. **C-H**, Sparse multicolor flp-outs (flp) show that first instar hugin neurons have similar morphology but fewer fine arborizations as in third instar. **C**, Single hugin-PC and hugin-RG neurons. **D**, Single hugin-PC and hugin-PH neurons. **E**, Single hugin-VNC neuron. **F**, Single hugin-PC and hugin-VNC neuron. **G**, Single hugin-PH neuron. **H**, Two hugin-PH neurons. Scale bars represent 20 μm. Asterisks mark PaN entry site

4.2 The Hugin Connectome

4.2.1 Identification and reconstruction of hugin neurons within the EM volume

Reconstruction of hugin neurons and their synaptic partners was conducted as part of the larval EM project. For details on the project, the serial section EM volume and the work flow see introduction 1.4 and methods 3.7. Finding and unambiguously identifying all hugin-producing neurons within an EM volume encompassing an estimated 10.000-12.000 neurons in total [Ohyama et al., 2015] was unlikely to succeed by randomly sampling neurons within the SEZ. In order to increase feasibility, a reconstruction strategy was developed that allowed to limit the number of neurons that needed to be sampled. Each class of hugin neurons has some unique features that can be used to focus reconstruction efforts on a small subset of potential candidates:

Hugin-PH neurons leave the central nervous system via the prothoracic accessory nerve (PaN). This thin nerve was readily identifiable in the EM volume as it is situated dorso-laterally of the antennal nerve but ventral to the optic nerve [Schoofs et al., 2010]. A cross section through that nerve showed only very few axons projecting from or to the CNS, limiting the number of hugin-PH candidates to 12. As expected, reconstruction of all these neurons revealed exactly two neurons per hemisegment that matched with hugin-PH morphology (Fig. 4.2A).

Hugin-RG neurons leave the CNS via the *nervi corporis cardiaci* (Ncc) that innervate the ring gland. These nerves were found to carry 30 axons each including those of prominent neuroendocrine neurons such as the IPCs. Similar to hugin-PH, full reconstruction of all the neurons with axons in the Ncc revealed exactly two neurons per hemisphere that matched hugin-RG morphology (Fig. 4.2B).

Hugin-PC neurons' ascending projections into the protocerebrum were previously shown to travel close to the descending projections of IPCs [Bader et al., 2013]. The IPCs and other mNSCs had already been reconstructed as byproduct of identifying hugin-RG neurons. Consequently, they were used as a landmark to reconstruct hugin-PC candidates. Only the expected four neurons per hemisegment showed an exact match with known hugin-PC neurons morphology (Fig. 4.2C).

Hugin-VNC neurons' main neurites travel in the same axon bundle as those of hugin-PH neurons as they traverse the commissure laterally before branching off towards the ventral nerve cord and the PaN, respectively. This bundle in the commissure contains approximately 20 axons,

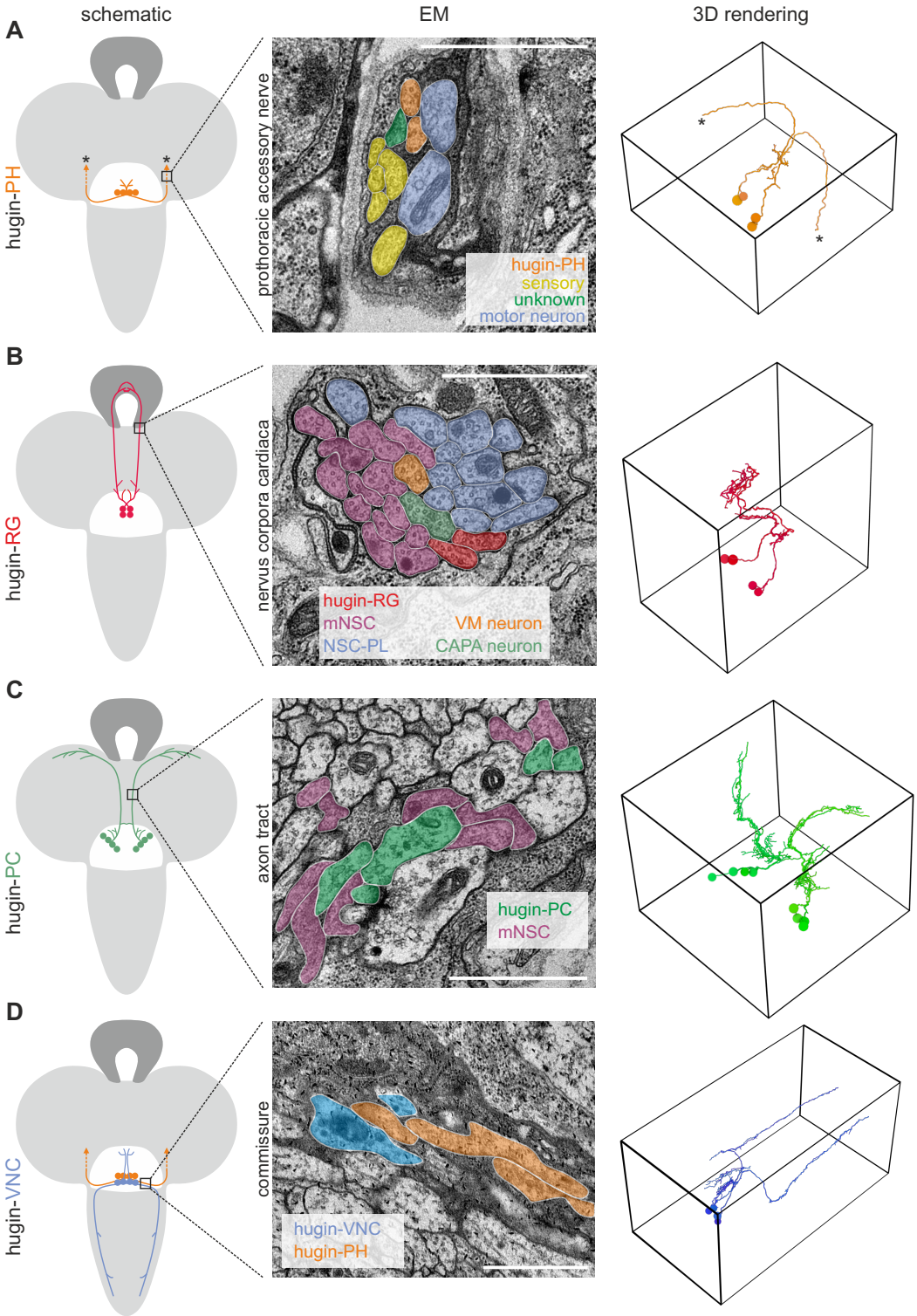

FIGURE 4.2. Strategies used for identification of hugin neurons in the EM volume. **A**, Hugin-PH neurons were identified by reconstructing all neurons in the prothoracic accessory nerve (PaN). Asterisks mark PaN entry site. [continued on next page]

Figure 4.2: [continued from previous page] **B**, Hugin-RG neurons were identified by reconstructing all neurons in the *nervi corporis cardiaci* (Ncc). Other neurons in the Ncc include median neurosecretory cells (mNSCs), neurosecretory cells of the *pars lateralis* (NSCs-PI), ventromedial (VM) and capability (CAPA) neurons. **C**, Hugin-PC neurons were identified by reconstructing neurons close to mNSCs along the axon tract. **D**, Hugin-VNC neurons were identified by reconstructing neurons close to Hugin-PH in the commissure. See text for detailed explanation. Scale bars represent 1 μm. A, anterior; D, dorsal; L, lateral.

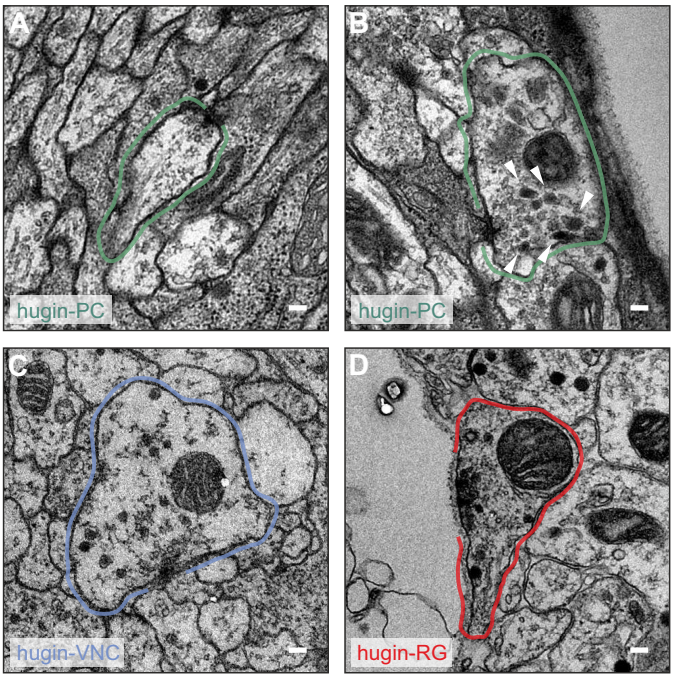

Figure 4.3: Examples of presynaptic sites in different hugin neurons. Neuronal profiles of respective hugin neurons are outlined. Opening in outline indicates synaptic site. **A**, Presynaptic site of a hugin-PC neuron. **B**, Presynaptic site of a hugin-PC neuron with closeby dense core vesicles (DCVs) (arrowheads). **C**, Presynaptic site of hugin-VNC neuron. **D**, Presynaptic site of a hugin-RG neuron within the ring gland. Note that in this case the neuron borders the haemal space. Scale bars represent 100nm.

only two of which belong to neurons that match hugin-VNC morphology (Fig. 4.2D).

4.2.2 Morphological analysis of hugin neurons

4.2.2.1 Occurrence of synaptic sites and dense core vesicles

As mentioned in the introduction, neurons are able to communicate by different modes of transmission. These are electrical transmission via gap junctions, chemical synaptic transmission using small molecule transmitters and synapse-independent diffuse transmission via peptide transmitters [Agnati et al., 1995].

Gap junctions are visible as focal points of cell-to-cell contacts in EM images [Sloper, 1972; Bennett et al., 1991]. However, in the EM volume at hand, the extracellular matrix was not preserved during fixation, making it difficult to unambiguously identify gap junctions. Synapses on the other hand were readily identifiable. The protein complexes required for synaptic processes such as fusion of transmitter-filled vesicles with the cell membrane are electron-dense and thus show up as dark structures on EM images. As pre- and postsynaptic sites are generally easy to discern, synapses can be assigned a direction: Presynapses are sites of output whereas

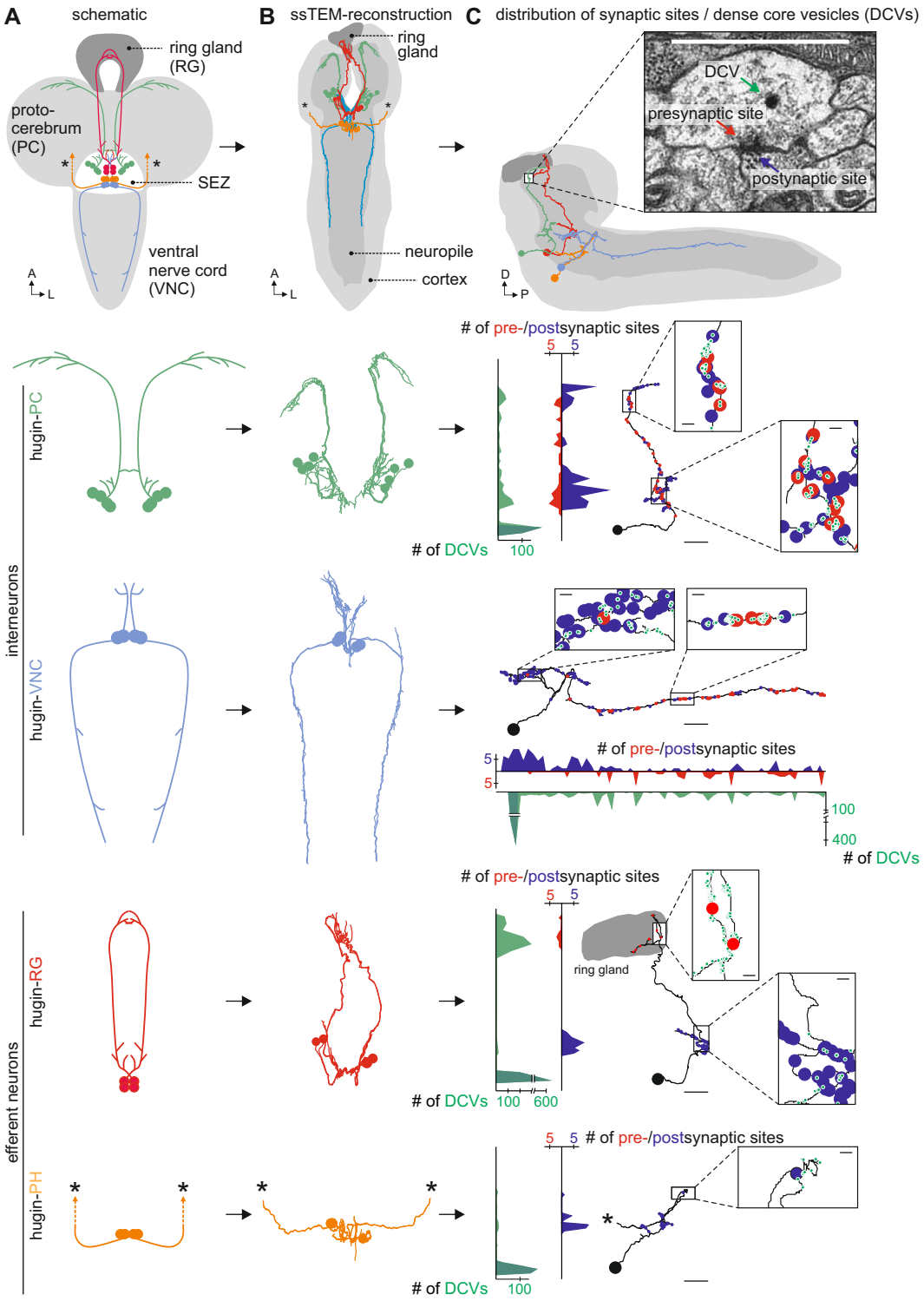

FIGURE 4.4. Spatial distribution of synaptic sites and dense core vesicles (DCVs). [Continued on next page]

postsynapses are sites of input. In *Drosophila*, synapses are characterized by the existence of

Figure 4.4: [continued from previous page] **A**, Schematic representation of each hugin class. **B**, Hugin neurons as reconstructed from the ssTEM volume. **C**, Distribution of pre- (red) and postsynaptic (blue) sites and DCVs (green) for exemplary hugin neurons. Dark green represents fraction of DCVs in the soma. Note that hugin interneurons exhibit presynaptic sites whereas efferent hugin neurons exhibit either none (hugin-PH) or only few (hugin-RG). Scale bars represent 10 μm for the overviews and 100nm for inlays.

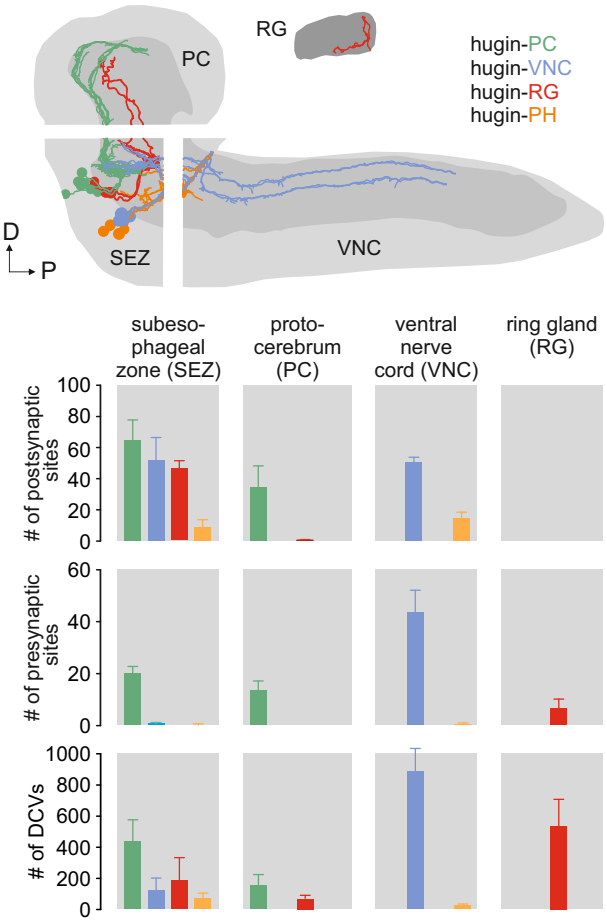

Figure 4.5: Quantification of synaptic sites and DCVs. Occurrence of synapses and DCVs in four broad compartments of the brain: ring gland (RG), protocerebrum (PC), subesophageal zone (SEZ) and ventral nerve cord (VNC). Whiskers represent standard deviation.

presynaptic vesicles, pre- and postsynaptic membrane thickening and presynaptic so-called T-bars [Prokop and Meinertzhagen, 2006]. Both, pre- and postsynaptic sites of each individual hugin neurons were annotated based on the co-occurrence of at least two out of those three criteria. Dense core vesicles (DCVs), the packaging units of neuropeptides, were likewise readily traceable in EM images as their protein content makes them electron-dense.

In the process of reconstructing the hugin neurons, synaptic sites as well as dense core vesicles (DCVs) were annotated. Previous studies on hugin neurons had been focused on the hugin neuropeptide, the common denominator for these neurons. As a result, although not uncommon, co-transmission of a classical small molecule transmitter in addition to the neuropeptide had never been suggested for hugin neurons [Burnstock, 2004; Nusbaum et al., 2001].

Hence unexpected, the two hugin interneuron classes, hugin-PC and hugin-VNC, were found

to have a large number of presynaptic sites with close-by small clear core vesicles (SCVs) (Fig. 4.3). SCVs are the packaging unit of small molecule transmitters such as GABA, glutamate or acetylcholine. Hugin-RG neurons showed only few presynaptic sites that were exclusively located within the ring gland and in contrast to those of hugin interneurons they did not have close-by SCVs. All hugin neurons had postsynaptic sites within the SEZ. In addition, the hugin interneurons, hugin-PC and hugin-VNC, had a large number of postsynaptic sites along their main neurites (Fig 4.4).

In general, hugin neurons of the same class had similar numbers and distribution of pre- and postsynaptic sites as well as DCVs (Fig. 4.5 and Appendix A, Tab. A.1).

4.2.2.2 Compartmentalization and polarity of Hugin neurons

To investigate their polarity, each hugin neuron was compartmentalized (Fig 4.6 A). This was done by first calculating the distance along the arbor from each synapse to each other synapse. Ward's agglomerative hierarchical clustering was performed on the resulting distance matrix [Ward, 1963]. Assuming that most polar neurons can be split into two distinct compartments, the resulting hierarchical clusters were cut at a distance that separated them into two large clusters of synapses.

The resulting compartments corresponded in most cases with an intuitive compartmentalization (Fig 4.6 B). Hugin-PC split approximately in the middle of the ascending neurite, resulting in one SEZ and one protocerebrum (PC) compartment. Hugin-VNC split into one SEZ and one ventral nerve cord (VNC) compartment. Hugin-RG split into one SEZ and one ring gland (RG) compartment due to aforementioned ambiguous synaptic sites that were found in the ring gland. Only for hugin-PH the split was counter-intuitive as all synaptic sites are very closely localized.

Next, the segregation index was calculated for each hugin neuron [Schneider-Mizell et al., 2016]. This was done by calculating the entropy as the amount of input/output mixing within each of the two compartments, normalized by that of the whole neuron. Low segregation indices mean that pre- and postsynaptic sites intermingle and that defining designated input and output compartments is inappropriate. Hugin-PH neurons were excluded as their lack of presynaptic sites within the CNS made the calculation of entropy obsolete. Assuming that they exhibit presynaptic sites at their target site in the pharynx, they obviously represent prime examples of polar neurons.

For the remainder of hugin neurons, calculation of the segregation scores showed strong differences between hugin classes (Fig 4.6 C). Hugin-RG neurons showed the highest polarity (between 0.8 and 1.0) due to the clear separation of postsynaptic sites in the SEZ and presynaptic sites in the ring gland. Segregation scores of hugin-VNC neurons were lower (between 0.21 and 0.34) due to mixing of inputs and outputs along the descending projections. Albeit lower, these indices are nevertheless indicative of one clear input domain in the SEZ and one mixed input/output compartment in the VNC. Hugin-PC neurons had very low segregation indices between 0.0001

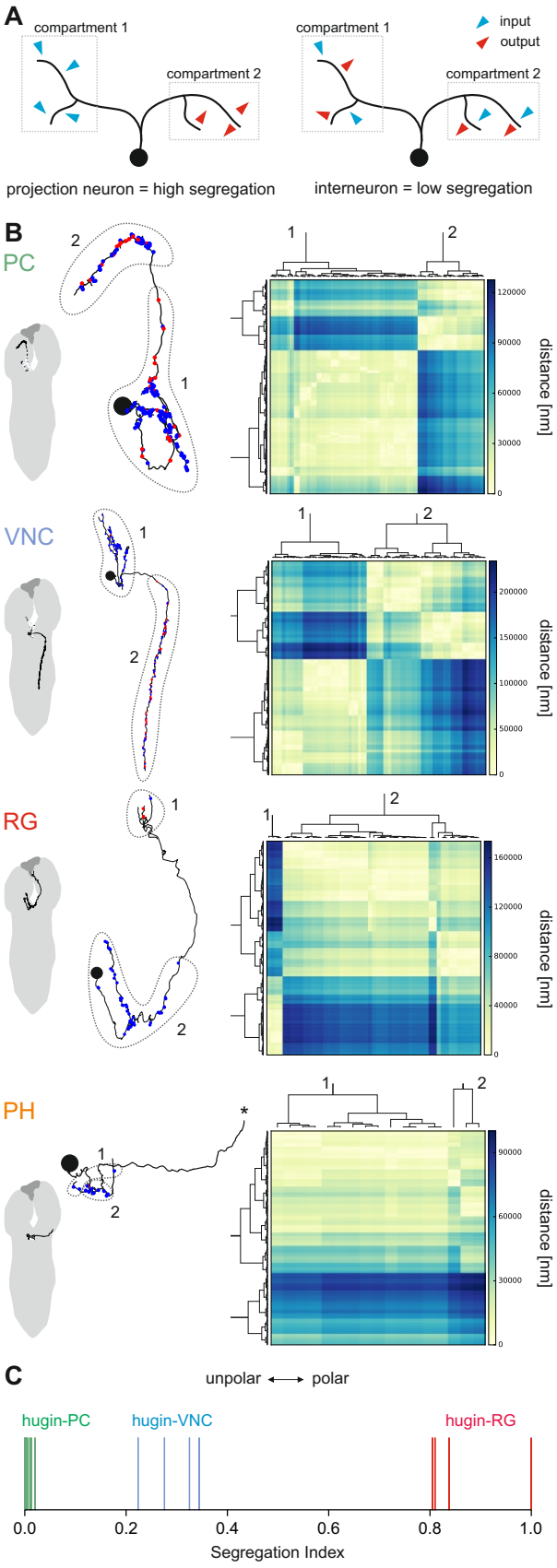

Figure 4.6: Polarity of hugin neurons. **A**, Explanation of the compartment model. First, neurons were split into two main compartments based on spatial clustering of their synapses. Next, the segregation index was calculated. Neurons with high polarity have clear input and output compartments and thus a high segregation index. Conversely, inputs and outputs mix in unpolar neurons resulting in a low segregation index. **B**, Compartmentalization of exemplary hugin neurons. Left: Morphology with pre- (red circles) and postsynaptic (blue circles) sites. Right: Matrix shows distance along the arbor between all pairs of synapses. Based on this distance matrix, synapses were hierarchically clustered (Ward's). The two largest clustered were defined as compartments. **C**, Segregation indices of hugin neurons. Note that hugin-PH neurons are not included due to their lack of presynaptic sites. See text for details.

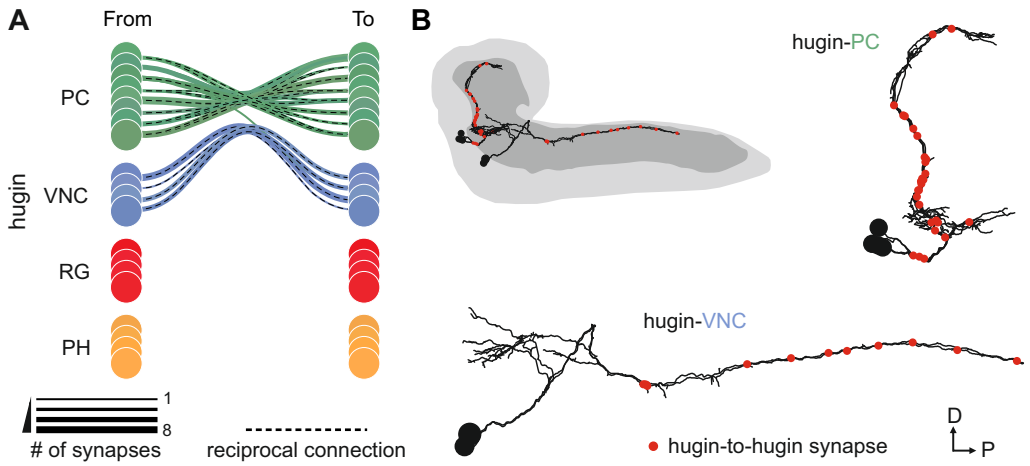

FIGURE 4.7. Hugin-to-hugin synapses. **A**, Line graph shows synaptic connections from hugin neurons to other hugin neurons. Note that connections are predominantly made reciprocally between hugin interneurons of the same class. **B**, Connections between hugin interneurons of the same class, hugin-PC and hugin-VNC, are found as axo-axonic synapses along their primary neurites. Only hugin neurons of one hemisphere are shown.

and 0.02. Despite the very intuitive splits into one SEZ and one PC compartment, they are highly unpolar neurons with similar numbers of pre-/postsynaptic sites in both compartments.

4.2.2.3 Hugin to hugin synapses

Reconstruction of the hugin neurons and annotation of their synaptic sites showed that hugin interneurons, hugin-PC and hugin-VNC, are synaptically connected. Reciprocal synaptic connections were found only between neurons of the same hugin-class (Fig 4.7 A). These connections made up a considerable fraction of their inputs. For hugin-PC neurons, input from other hugin-PC neurons accounted for $9.3\% \pm 3.2\%$ of their total synaptic input. For hugin-VNC neurons, the fraction of inputs from other hugin-VNC neurons was lower with $5.5\% \pm 2\%$ of their total synaptic input. These connections were made predominantly as axo-axonic synapses along the neurons' primary neurites (Fig 4.7 B).

4.2.2.4 DCV analysis

In contrast to small molecule transmitters, release of neuropeptides from dense core vesicles (DCVs) is not restricted to active zones of synaptic sites [Zupanc, 1996]. To investigate the spatial relation between DCVs and synaptic sites, locations of DCVs had been annotated similar to those of synaptic sites (Fig 4.5 C). Hugin-RG neurons had DCVs predominantly in the ring gland and hugin-PH showed overall small numbers of DCVs within the EM volume (Fig 4.5). In contrast, hugin interneurons, hugin-PC and hugin VNC, DCVs were found to not be evenly distributed within a neuron. While scattered DCVs were found all along their larger neurites, they appeared

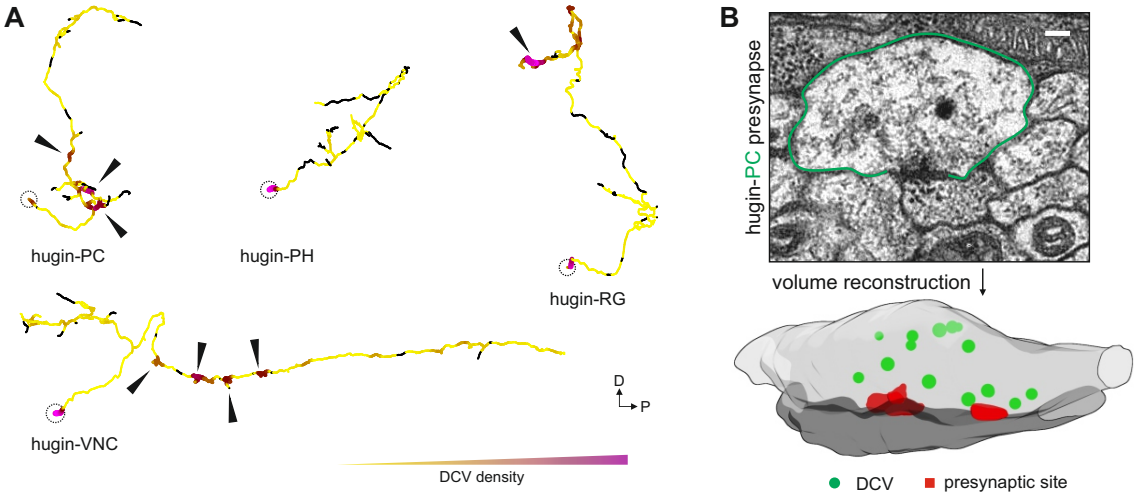

FIGURE 4.8. Intracellular distribution of dense core vesicles (DCVs). **A**, Exemplary hugin neurons color-coded by density of DCVs. With the exception of hugin-PH, all hugin neurons exhibit local spots with very high DCV density (arrowheads). Note that DCVs in the somata (dotted circles) may represent lysosomes. **B**, Exemplary volume reconstruction of a local swelling with presynaptic sites of a hugin-PC neuron shows close-by DCVs. Scale bar represents 100nm.

to aggregate in higher numbers at local axon swellings (Fig 4.8 A). These swellings often feature multiple presynaptic sites with close-by DCVs.

To quantify the spatial relation between synapses and DCVs, the distance from each DCV to the closest pre- and postsynaptic site was calculated (Fig. 4.9). For hugin-PC and hugin-VNC more DCVs were closer to pre- than to postsynaptic sites. Similarly, the minimal distances observed were smaller for pre- than for postsynaptic sites. For DCVs of the efferent hugin neurons, hugin-RG and hugin-PH, no distances to presynaptic sites were calculated due to the lack thereof. For postsynaptic sites however, their DCVs were located at much larger distances than those of the other two hugin classes.

4.2.3 Reconstruction of synaptic partners

Having reconstructed all 20 hugin neurons, the next step was to generate a hugin connectome: a map of all first order synaptic up- and downstream partners. To do so, the following reconstruction strategy was employed (Fig. 4.10 A). First, for each hugin neuron all synaptically connected neuronal profiles were partially reconstructed up to the point where all branches must meet: for central neurons this was the soma, for sensory neurons the entry site of the respective nerve. While not fully reconstructed, the resulting neurons already had their final number of synapses from and to hugin neurons. Under the assumption that the number of synapses between two neurons is indicative of connection strength and importance of that connection, further reconstruction efforts were focused on strongly connected partners. Therefore, only synaptic

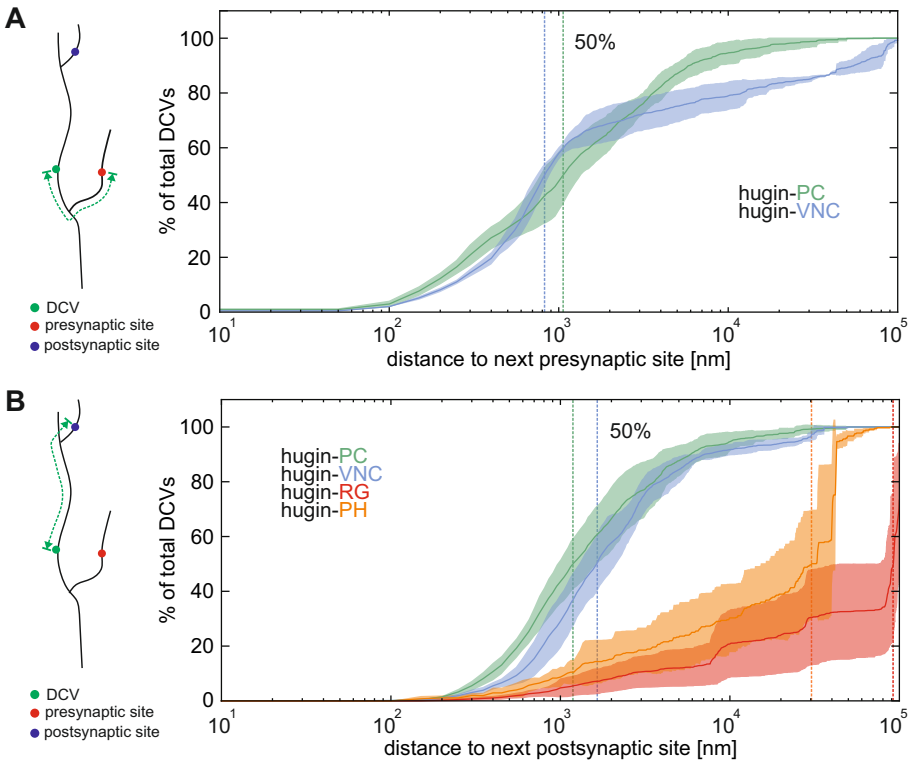

FIGURE 4.9. Spatial relation between synaptic sites and dense core vesicles (DCVs). Shown is the percentage of DCVs within a given distance to the closest synaptic site. **A**, Distances to the closest presynaptic site. Note that hugin-PH and hugin-RG were excluded due to their general lack of presynaptic sites. **B**, Distances to the closest postsynaptic site. Envelopes represent standard deviation. Distances were measured along the arbor.

partners with at least a single connection consisting of 3 or more synapses from or to a hugin neuron were subsequently fully reconstructed. This threshold did not apply for sensory neurons which were fully reconstructed regardless. Note that above-threshold partners may still have below-threshold connections to other hugin neurons.

As a final step of quality control, these fully reconstructed neurons were checked for symmetry by finding matching pairs of neurons in both hemispheres. Medial unpaired neurons were excepted from this due to their lack of a paired neuron. Only neurons that fulfilled all of the above criteria were used for subsequent analysis. The completeness of the final connectome as measured by the fraction synapses covered by all fully reconstructed and symmetry matched partners was 70.1% across all hugin neurons (Fig. 4.10 B). This number varied between the different hugin classes. The hugin-PC connectome being the most complete as it covered 79% and hugin-VNC being the most incomplete at 53% of the respective synapses. For a comprehensive neuron atlas of all neurons in the hugin connectome and their connectivity, see supplemental data of Schlegel et al. [2016].

The fraction of fully reconstructed and symmetry-matched partners increased with the number of synapse per connection (Fig. 4.10 C). Conversely, neurons that had only few-synapse

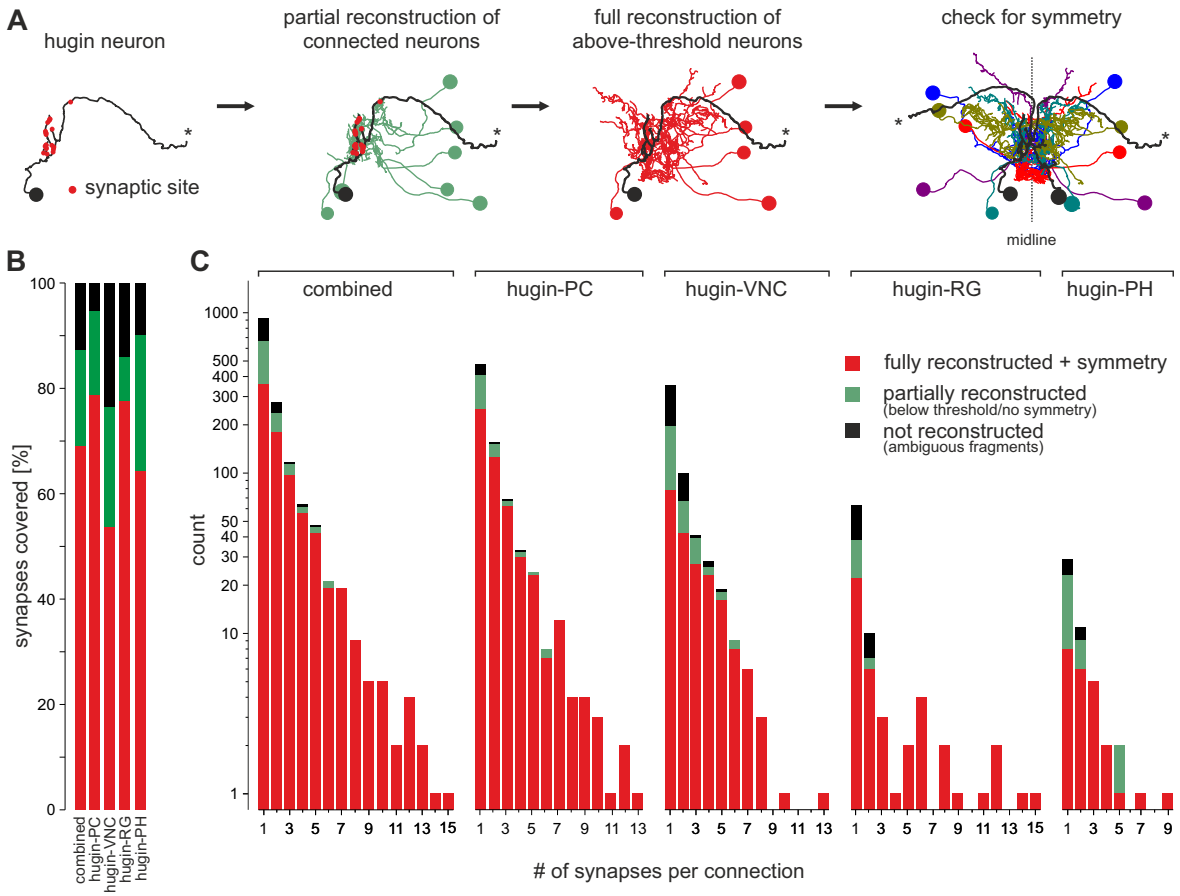

FIGURE 4.10. Completeness of the hugin connectome. **A**, Reconstruction strategy for synaptic partners of hugin neurons using a hugin-PH neuron as example. **B**, Synapse completeness of the hugin connectome. Bar plot shows the percentage of synapses from or to hugin neurons that connect to fully reconstructed, symmetrical neurons (red), partially reconstructed neurons (green) and ambiguous fragments (black). **C**, Completeness of the hugin connectome by connections. A connection can consists of single or multiple synapses with more synapses indicating a stronger connection. Histograms show the distribution of connection completeness along increasing connection strength for all hugin neurons combined (left-most) and separated by hugin classes. Threshold for full reconstruction of synaptic partners was at least a single 3-synapse connection to any of the hugin neurons.

connections to or from a hugin neuron were more likely to not be fully reconstructed. There are several reasons for this. First, small fragments (< 10 μm) occurred when a neuronal profile pre- or postsynaptic to a hugin neuron could not be unambiguously followed to its larger main branch. This generally happened due to glitches, noise or misalignment in the EM images. Larger, not fully reconstructed fragments were in most cases due to lost sections in the EM volume. This was especially severe in case of larger projection neurons that were more likely to cross several of the gaps in the dataset. These gaps range between a single (50nm) and eleven (550nm) lost consecutive sections. The larger the gap, the more difficult it was to follow a neurite across that

gap.

4.2.4 Analysis of the hugin network

Reconstruction of the hugin connectome as laid out above generated a dataset of 260 neurons and their synaptic connections. Unexpectedly, each hugin class appeared to connect to a very unique set of partners with little overlap between neurons of different hugin classes (Fig. 4.11 A). To quantify this, the *connectivity similarity score* based on Jarrell et al. [2012] was used: neurons that are connected to the same synaptic partners in a similar manner (number of synapses, pre- or postsynaptic) have a high connectivity similarity score and vice versa (Fig. 4.11 B, schematic; see methods 3.8.2 for details). This similarity score was calculated pairwise between all hugin neurons, resulting in a distance matrix which could then be clustered using agglomerative clustering. These data showed that hugin neurons of the same class had very similar sets of synaptic partners whereas neurons from different hugin classes showed common features in their connectivity (Fig. 4.11 B).

4.2.5 Sensory inputs to hugin neurons

From their first description on, hugin neurons have been implied to receive sensory inputs based on their arborization within the SEZ [Melcher and Pankratz, 2005; Hückesfeld et al., 2016]. This region of the CNS represents a first order chemosensory center that receives input from a range of anterior sensory organs [Ghysen, 2003]. To address if and what kind of sensory input hugin neurons receive, the hugin connectome was searched for neurons that do not have a soma within the CNS but instead enter via a peripheral nerve. Two major types of sensory neurons were found to synapse onto hugin neurons. The first group consisted of neurons entering the CNS via the antennal nerve (Fig. 4.12 A). To break down this large, morphologically heterogeneous group into meaningful components, the sensory neurons were clustered based on their synapse placement: neurons which have their synapses spatially close to each other were grouped (see section 3.8.3 for details). This resulted in 6 clusters (C1-6) that each covered distinct areas of the SEZ (Fig. 4.12 B). Clusters C1-C5 all input onto hugin-PC with C1 additionally connecting onto hugin-VNC. Cluster C6 was exclusively inputting onto hugin-RG, albeit with few synapses.

The second, more homogeneous group of sensory neurons enters the CNS via abdominal nerves, projects laterally towards the thoracic segments, then curves toward the midline and projects into the SEZ. Here, this type of sensory neurons made synaptic contacts predominantly with hugin-VNC neurons (Fig. 4.13 A). Notably, they also showed synaptic contacts between each other. Abdominal nerves innervate internal and external sensory organs of the peripheral nervous system. This includes proprioceptive (chordotonal), tactile, nociceptive (multi dendritic neurons) and a range of sensory neurons whose function is yet unknown [Hwang et al., 2007; Ghysen et al., 1986; Bodmer and Jan, 1987]. Abdominal sensory neurons with central projection patterns like the ones at hand were not found in current literature. To investigate origin and thus

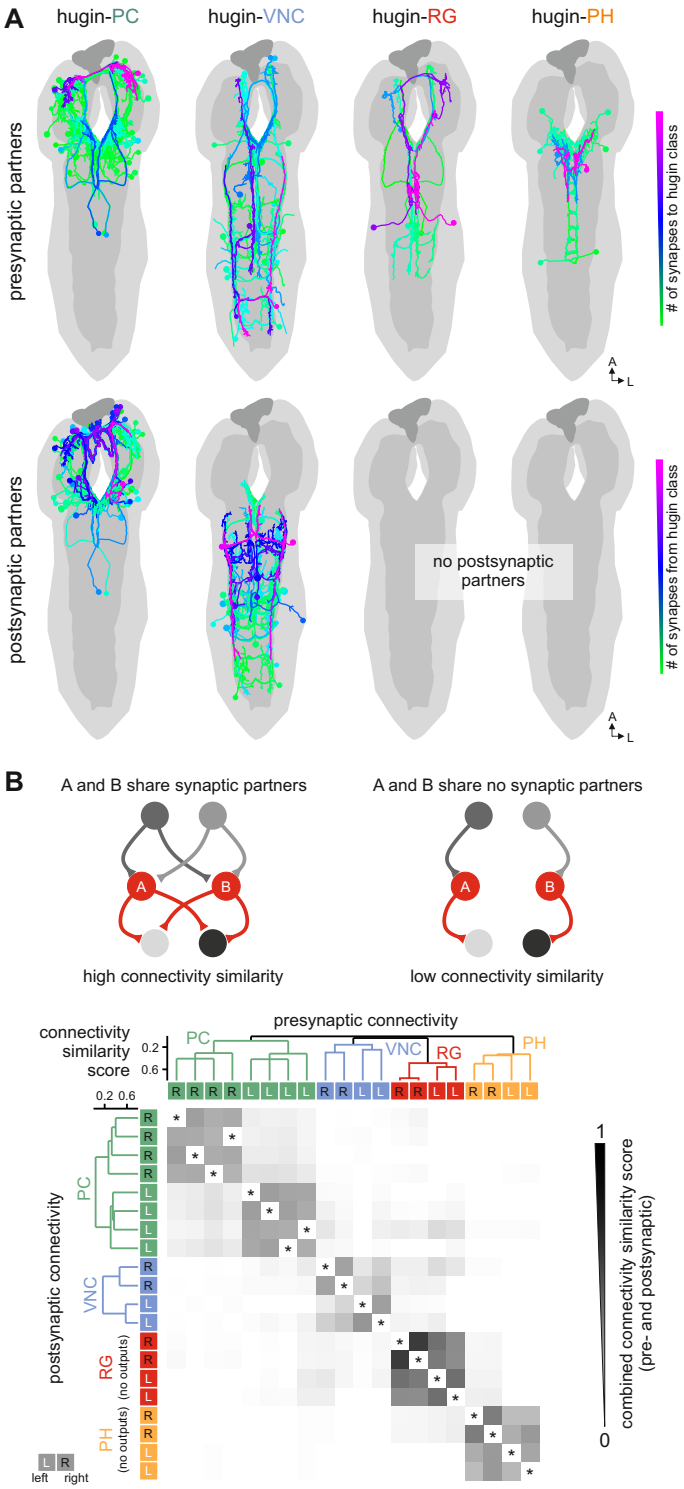

Figure 4.11: Synaptic partners of hugin neurons and connectivity analysis. **A**, All pre- and postsynaptic partners by hugin class. Neurons are color-coded based on total number of synapses to given hugin class [minimum=1; maximum (pre-/postsynaptic): hugin-PC=53/16, hugin-VNC=21/18, hugin-RG=39/none, hugin-PH=23/none]. Hugin-RG and hugin-PH neurons do not have postsynaptic partners within the CNS. **B**, Connectivity similarity between hugin neurons. Schematic illustrates basic principle of connectivity similarity score: neurons that connect to the same set of neurons by similar number of synapses have a high connectivity similarity. Conversely, neurons that do not share synaptic partners have a low connectivity similarity. Matrix shows combined pre- and postsynaptic similarity score. Neurons are ordered by dendrogram of similarity score of pre- (x-axis) and postsynaptic (y-axis) partners. Self-self comparisons were omitted (asterisks). Hugin classes connect to unique sets of pre- and postsynaptic partners. Neurons of each hugin class have the same synaptic partners and there is little to no overlap with other classes.

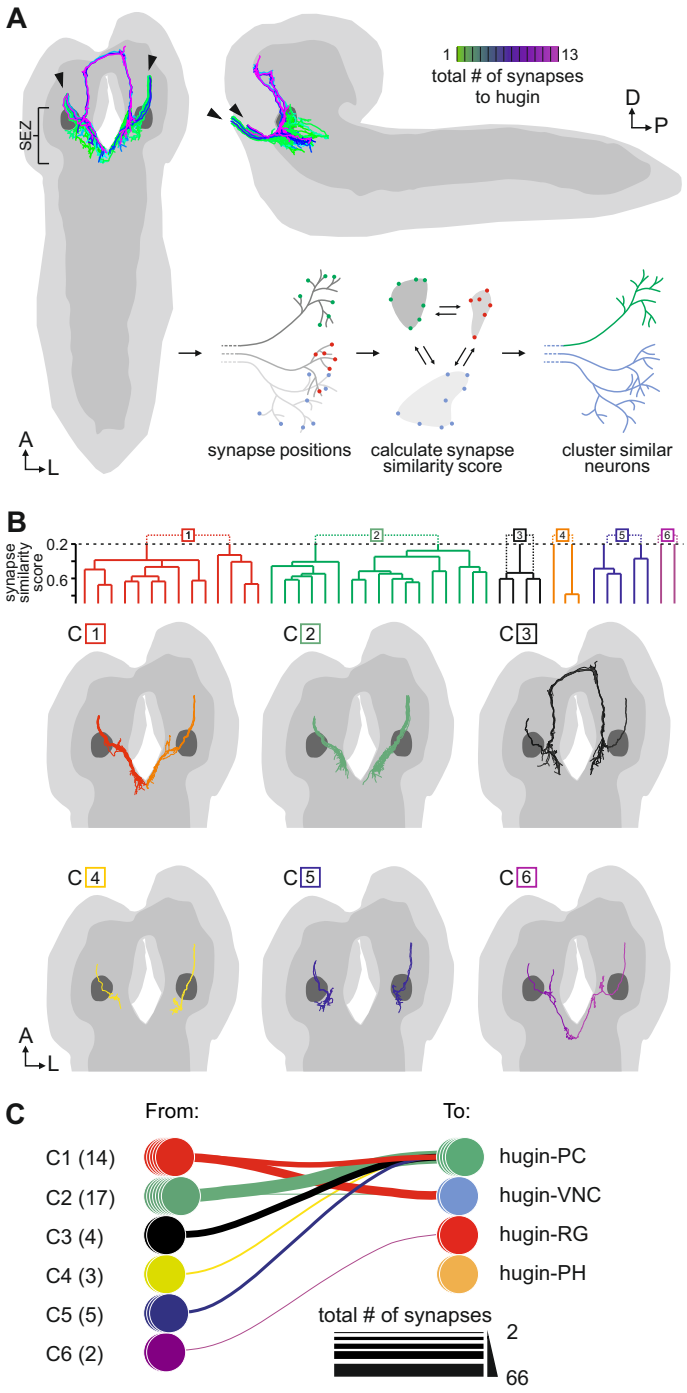

Figure 4.12: Sensory inputs from the antennal nerve (AN). **A**, Sensory neurons from the AN (arrowheads) that make synapses onto hugin neurons. Color codes for the total number of synapses with hugin neurons. To compare sensory neurons' morphologically, a synapse similarity score was calculated based on the spatial distribution of their synaptic sites. **B**, Dendrogram shows clustering of sensory neurons based on synapse similarity score. Trees were cut to position corresponding clusters of each hemisphere next to each other. Resulting clusters C1-6 cover distinct areas of the SEZ. **C**, Connectivity between AN sensory clusters and each hugin class. Numbers in brackets is the number of neurons represented by each pile. Line thickness corresponds to total number of synapses between a sensory cluster and given hugin class.

potential function of these sensory neurons, GAL4 lines were screened for neurons with similar projection patterns. One line, PK2-R1-GAL4 (hugR84.6 L1.3) generated by Peters [2013], was found to include sensory neurons with the above described projection patterns. These neurons originate in the larval body wall where they wrap around trachea (Fig. 4.13 B). Bodmer and Jan [1987] describe similar neurons, which they termed tracheal dendritic (td) neurons.

In summary, efferent hugin neurons, hugin-PH and hugin-RG, receive little to no sensory input.

The hugin interneurons, hugin-PC and hugin-VNC, on the other hand receive a significant fraction of their individual incoming synapses (up to 39%) from sensory neurons. These sensory inputs are much more diverse and heterogeneous than previous publication have suggested [Melcher and Pankratz, 2005; Hückesfeld et al., 2016].

4.2.6 Neuroendocrine targets of hugin neurons

Knowledge about interneurons is sparse compared to those neurons that enter (afferent) or leave (efferent) the CNS. Efferent neurons encompass motor neurons, efferent modulatory neurons and endocrine neurons such as hugin-RG [Siegmund and Korge, 2001; Schoofs et al., 2014b; Hückesfeld et al., 2015]. Knowledge about these neuron types is usually larger mostly because they are easier to access experimentally. This fact allows on one hand a relatively easy identification within the EM volume and on the other hand there is a wealth of scientific data to put them into context. Hugin neurons had previously been shown to affect motor neurons for the pharyngeal pump Schoofs et al. [2014a] and to be targets of insulin signaling from the insulin-producing cells (IPCs) [Bader et al., 2013]. Therefore downstream targets of hugin neurons were screened for efferent neurons, i.e. for neurons that have neurites leaving the CNS. No connections[1] between hugin and motor or efferent modulatory neurons were found.

However, a cluster of neuroendocrine neurons that target the ring gland (RG) received a large number of synapses from hugin-PC neurons. These neurons form a cluster of 24 cells (12 per hemipshere) in the *pars intercerebralis* (PI) of the medial protocerebrum and are thus called median neurosecretory cells (mNSCs) (Fig. 4.14 A) [Siegmund and Korge, 2001; Rajan and Perrimon, 2012]. Three different types of mNSCs produce distinct neuropeptides in a non-overlapping manner: 3 mNSCs produce diuretic hormone 44 (DH44), 2 mNSCs produce Dromyosuppressin (DMS) and 7 mNSCs produce *Drosophila* insulin-like peptides (DILPs) [also called insulin-producing cells (IPCs)] [Park et al., 2008]. While these neurosecretory cells have been long known, their individual morphology is largely unknown [see Siegmund and Korge, 2001, for a comprehensive description]. The EM reconstruction showed that all mNSCs have essentially the same morphology: ipsilateral projections descending towards the SEZ and contralateral projections into the RG (Fig. 4.14 B). Consequently, it was impossible to identify the different types of mNSCs based on morphology.

Therefore, identification had to be attempted by different means: it was hypothesized that similar to the different hugin classes, neurons of the same mNSC type would be more likely to have the same synaptic partners as neurons of different types (see section 4.2.4). To test this, presynaptic partners (inputs) of all mNSCs were reconstructed using the same criteria as for the hugin network previously (see section 4.2.3). Next, connectivity similarity scores for all mNSCs were calculated and neurons with high similarity were clustered. This resulted in 3 distinct clusters for each hemisphere that contained the exact number of neurons expected for each of the

[1] above reconstruction threshold of 3 synapses and with left/right symmetry

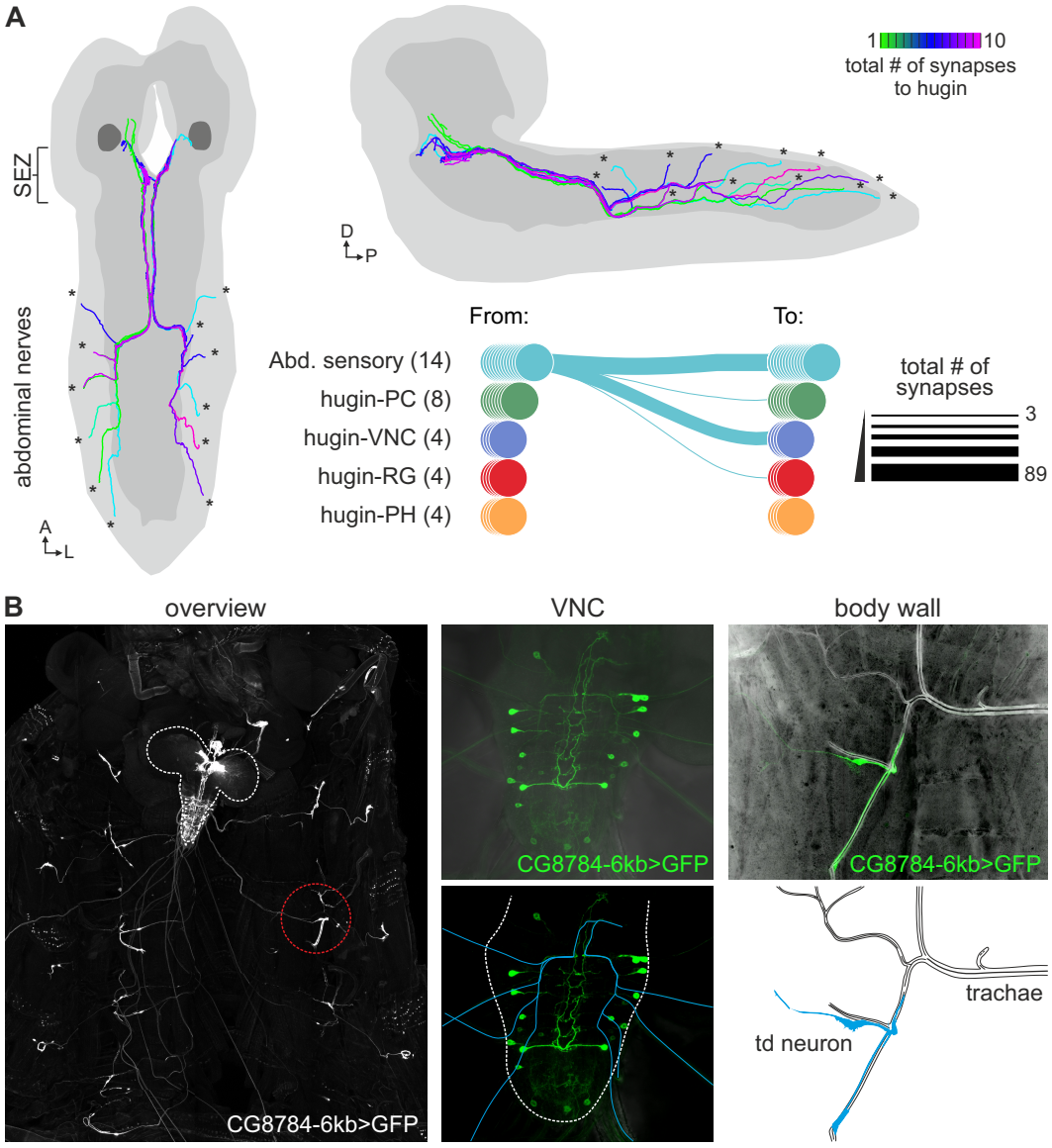

FIGURE 4.13. Sensory inputs from abdominal nerves. **A**, Sensory inputs from abdominal nerves (asterisks) colored by their total number of synapses onto hugin neurons. Line graph shows connectivity of abdominal sensory neurons to each other and to classes of hugin neurons. Numbers in brackets is the number of neurons represented by each pile.**B**, Sensory neurons with matching morphology were identified in a GAL4 driver line, *PK2-R1-GAL4*. Overview shows the larval body wall with the CNS (white outlines) still attached. A distinct set of segmentally repeated neurons (red circle) shows the same projection pattern within the CNS: see zoom on ventral nerve cord (VNC). These sensory neurons are called tracheal dendritic (td) neurons as their dendrites wrap around the trachea [see body wall zoom; Bodmer and Jan, 1987].

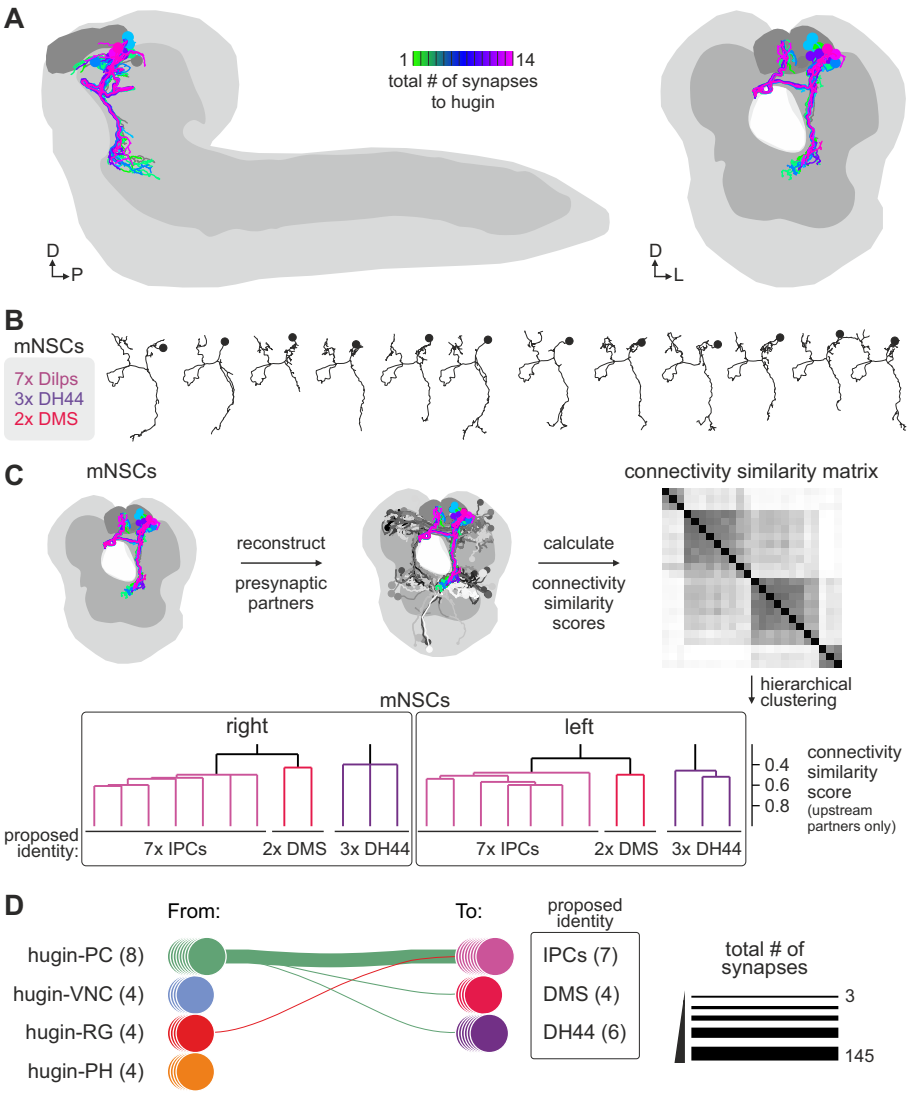

FIGURE 4.14. Neurosecretory targets of hugin. **A**, Median neurosecretory cells (mNSCs) of the *pars intercerebralis* (PI) were found downstream of hugin neurons. For clarity, only mNSCs of the left hemisphere are shown. **B**, The cluster of mNSCs consists of 7 insulin-producing cells (IPCs), 3 diuretic hormone 44 (DH44)-producing and 2 Dromyosuppressin (DMS)-producing cells per hemisphere. The reconstructed mNSCs were morphologically too similar to allow a differentiation into these three groups. **C**, To identify the mNSCs based on connectivity, their presynaptic partners were reconstructed and used to calculate connectivity similarity scores between all pairs of mNSCs. Hierarchical clustering resulted in clusters of 7, 3 and 2 neurons with similar connectivity. To assign identities, these cluster sizes were matched against the number of neurons expected for each mNSC type. **D**, Connectivity between hugin neurons and mNSCs of both hemispheres. Based on the proposed identities of the mNSCs, hugin-PC neurons connect strongly to IPCs but only weakly to DH44- or DMS-producing neurons. Number of neurons represented by each stack is provided in brackets. Line thickness corresponds to total number of synapses.

three mNSCs types (3, 2 and 7 neurons). From this observation, each of the reconstructed mNSCs was assigned a putative identity (Fig. 4.14 C). Based on this identity, IPCs are strongly connected to hugin-PC neurons whereas connections to the other mNSCs are comparatively weak (Fig. 4.14 B). Synapses from hugin-PC neurons onto mNSCs constitute a large fraction of their respective synaptic connections: up to 35% of hugin-PC neurons' outgoing and up to 17% of mNSCs incoming synapses.

4.2.7 Network topology

In the process of fully reconstructing all synaptic partners of hugin neurons, all other synapses of these partners were also annotated. As a result, these data included information on how hugin partners are themselves interconnected. This *hugin network* consisted of 260 neurons and 3372 edges (synaptic connections, composed of ≥1 synapses) (Fig. 4.15 A). Surprisingly, even though neurons of each hugin class have unique sets of synaptic partners (see section 4.2.4), these synaptic partners are themselves strongly interconnected and thus form a larger, tight network. One notable exception of this are hugin-PH neurons and their synaptic partners which appear to be more separated from the rest of the network (Fig. 4.15 B,C).

In order to analyze this hugin network, several abstraction techniques were tested. Two general types of clustering methods can be employed to partition a network: density-based and similarity-based clustering algorithms. Density-based clustering tries to find sets of neurons that are highly interconnected internally and are isolated against other such groups. None of the tested density-based clustering methods (edge pruning, edge betweenness, relative neighbor graph, MCODE) resulted in a meaningful partition of the hugin network (data not shown) [Bader and Hogue, 2003; Zhou et al., 2009]. Instead, a similarity based clustering was employed. Like for hugin neurons and mNSCs, a connectivity similarity score was calculated for each pair of neurons in the network [Jarrell et al., 2012]: neurons that connect to the same synaptic partners are assigned a high similarity score and vice versa. Next, hierarchical clustering was performed on the resulting similarity matrix. This approach clusters neurons that share connectivity motifs and may thus represent functional units.

This revealed very well defined clusters/units, each with distinct connectivity features (Fig. 4.15 D,E). For example, neurons of cluster 1 (as annotated in Fig. 4.15 D) were almost exclusively associated with hugin-VNC neurons. Similarly, cluster 2 was mostly associated with hugin-PC and mNSCs. In contrast to that, cluster 3 contained many of the neurons that were responsible for keeping the hugin network from splitting into individual subnetworks for each hugin class. These neurons connect directly to hugin-VNC and hugin-PC neurons but additionally they input onto neurons of cluster 2 which - as mentioned before - targets hugin-PC and mNSCs. This third cluster is composed of a large number of AN sensory and abdominal tracheal dendritic (td) neurons.

Due to synapses having a clear polarity (pre- → postsynapse), any synaptic connection between

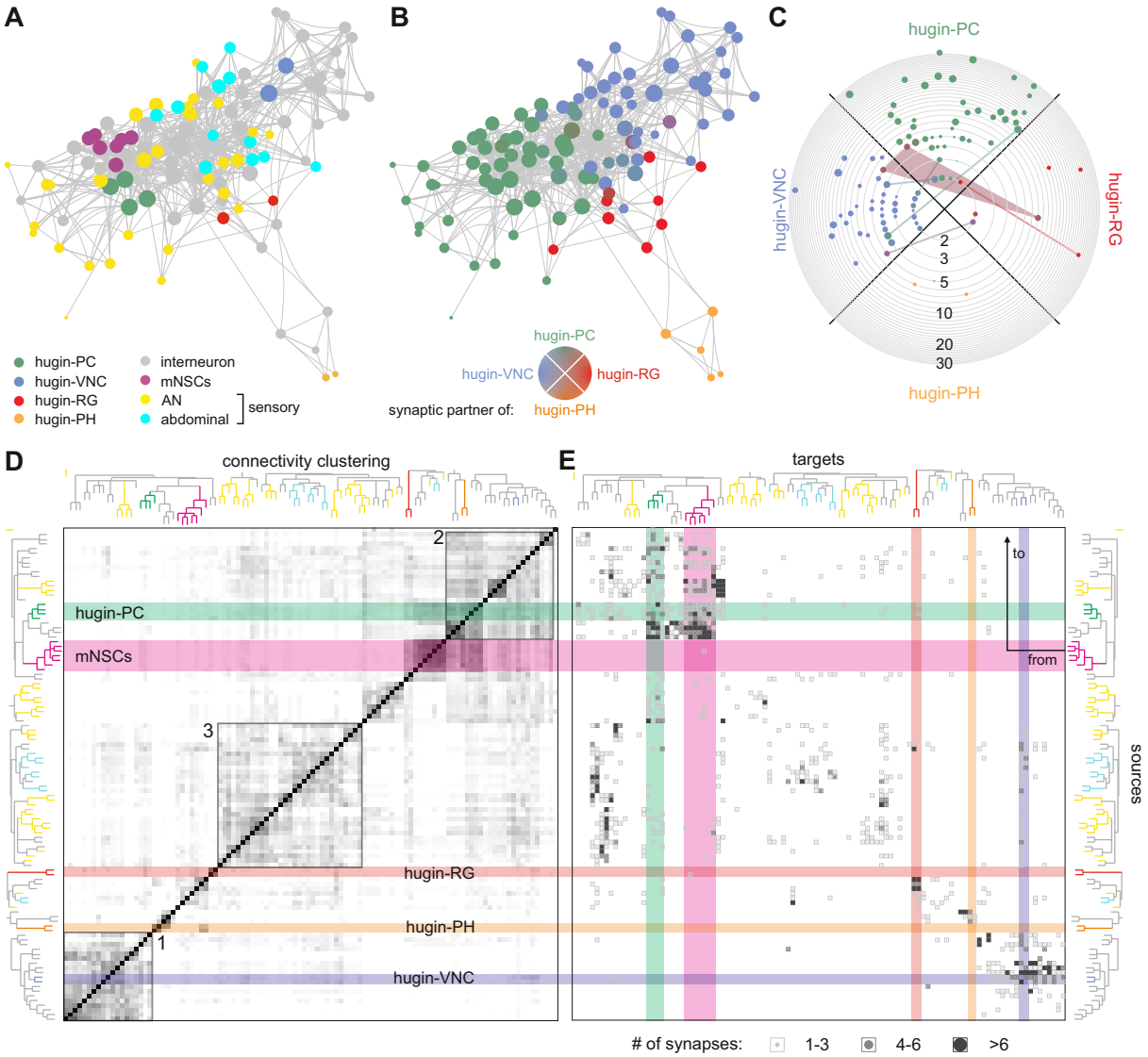

FIGURE 4.15. Clustering of the hugin network. For clarity, only left hugin neurons and their synaptic partners are shown. **A**, Hugin network with force-directed layout. With the exception of hugin-PH, the network is tightly interconnected and does not split into separate sub-networks for each hugin class. **B**, Same network as A. Colors indicate which hugin class a neuron directly connects to. Most neurons are connected exclusively to a single hugin class. Lines in A and B represent synaptic connections. Thickness indicates number of synapses between two neurons. **C**, Quantification of B. Each circle represents a neuron. Quadrant indicates which hugin class they connect to. Radius indicates total number of synapses to the respective hugin class. Neurons that appear in more than one quadrant are connected by lines. Circle sizes in A-C represent neuron's degree (number of direct synaptic partners within the network). **D**, Clustering of the hugin network based on connectivity similarity (see also Fig. 4.11 B). Dendrogram is colored according to the legend in A. See text for details on the outlined clusters 1-3. **E**, Adjacency matrix of the hugin network as clustered in D. Rows are sources, columns targets.

two neurons is directed. A network made up of synaptic connections is consequently likewise directed. To visualize and quantitatively investigate hierarchies within the hugin network, a topological sorting was performed [Sugiyama et al., 1981]. This required the network at hand to not have one-way loops of edges, also called directed cycles (e.g. A → B → C → A). To transform a network (also called *graph*) into a directed acyclic graph (DAG), connections between neurons can be either selectively inverted or removed entirely. A set of connections whose removal/inverting turns a network into a directed acyclic graph (DAG) is called a feedback arc set.

To minimize the effect on the layout of the network, a feedback arc set was calculated using Eades et al. [1993] greedy cycles removal algorithm. The resulting DAG was layered such that neurons without outputs, so-called sinks, are at the bottom of the graph and all other neurons are on top, organized into layers based on their maximal distance to a sink. Note that interneuron sinks are only sinks within the context of the hugin network and may well have downstream neurons of their own that are not part of the hugin network. Within each layer, neurons are positioned horizontally based on their barycenters, i.e. at the center between all their postsynaptic partners (Fig. 4.16 A). The topology plot of the left hugin network illustrates some of the key findings (Fig. 4.16 B).

First, hugin-PH and hugin-RG neurons represent sinks as they do not have synaptic outputs within the CNS. In contrast, hugin interneurons (hugin-PC and hugin-VNC) do have synaptic outputs and are thus positioned higher up in the hierarchy. Second, hugin-PC and hugin-VNC neurons are often reciprocally (pre- *and* postsynaptically) connected to their synaptic partners. During cycles removal the weaker of these reciprocal connections is removed. This has a bigger impact on hugin-PC neurons as many of their outputs are at the same time much stronger inputs. As a result, hugin-PC neurons have a larger number of neurons above than below them in the topology plot. However, mNSCs remain the most strongly connected downstream targets of hugin-PC neurons. Third, while the majority of the neurons in the hugin network directly (monosynaptically) connect to only a single hugin class (see also Fig. 4.15 B,C), some neurons connect the otherwise separated parts of the network indirectly over several synapses (polysynaptical). Due to the barycenter placement, these neurons are positioned horizontally in between the different hugin neurons in the topology graph.

4.3 Peptide-receptor connectivity

In contrast to synaptically released, small molecule transmitters, neuropeptides can diffuse over a larger distance after they have been released. Consequently, their action is not dependent on physical contact between source and target cells. As a result, mismatches between localization of the peptide and the receptor have been observed in several cases [Zupanc, 1996; Nässel, 2009]. In order to shed some light on the relation between the hugin neuropeptide and potential target neurons, the expression pattern of one of the hugin receptors was investigated. *CG8784*, also

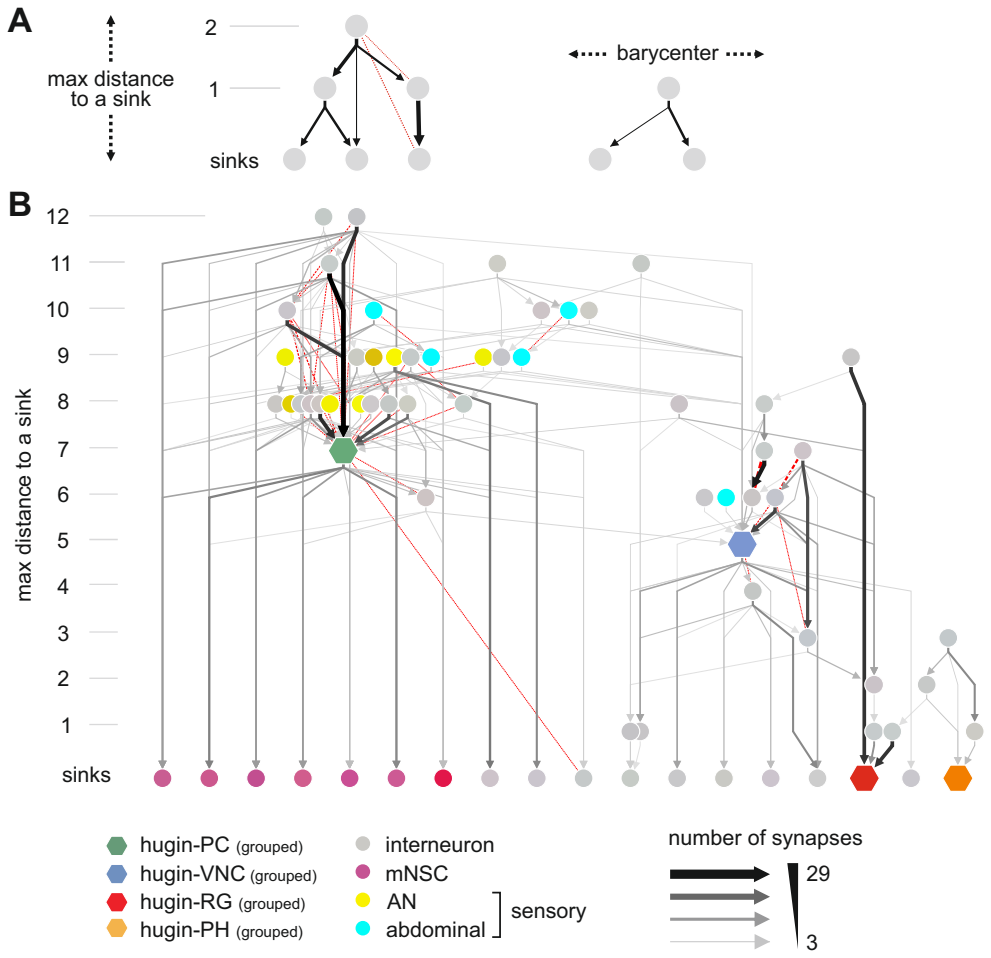

FIGURE 4.16. Topology of the hugin network. **A**, Explanation of topology graph. Hugin network was turned into a directed acyclic graph (DAG) by removal of a feedback arc set (red lines). Neurons are arranged in layers based on their maximum distance to a sink (a neuron without outputs). Within a layer, neurons are positioned along the x-axis based on the barycenter to their downstream neuron. **B**, Topology plot of the left hugin network. For clarity hugin neurons of each class have been grouped and only edges consisting of >2 synapses are shown. See text for detailed explanation.

called PK2-R1 (pyrokinin-2 receptor 1), was previously shown to be activated by both products of the hugin prepropeptide [Park et al., 2002; Rosenkilde et al., 2003].

Two different existing *CG8784* promoter *GAL4* lines were investigated: *CG8784-6kb-GAL4* drives expression of *GAL4* under the control of a 6 kilobase (kb) fragment of the intergenic region upstream of *CG8784*. The second *GAL4* line, *CG8784-GAL4::p65*, is very similar to a knock-in line: the first coding exon of *CG8784* in a bacterial artificial chromosome (BAC) clone of ≈80 kb of flanking genomic context was replaced with *GAL4* and the whole BAC clone was integrated into the third chromosome [Schlegel et al., 2016].

Both lines drove expression of a GFP reporter in the prominent cluster of mNSCs in addition to varying number of neurons distributed over the CNS (Fig. 4.17 A,B). The mNSCs were most

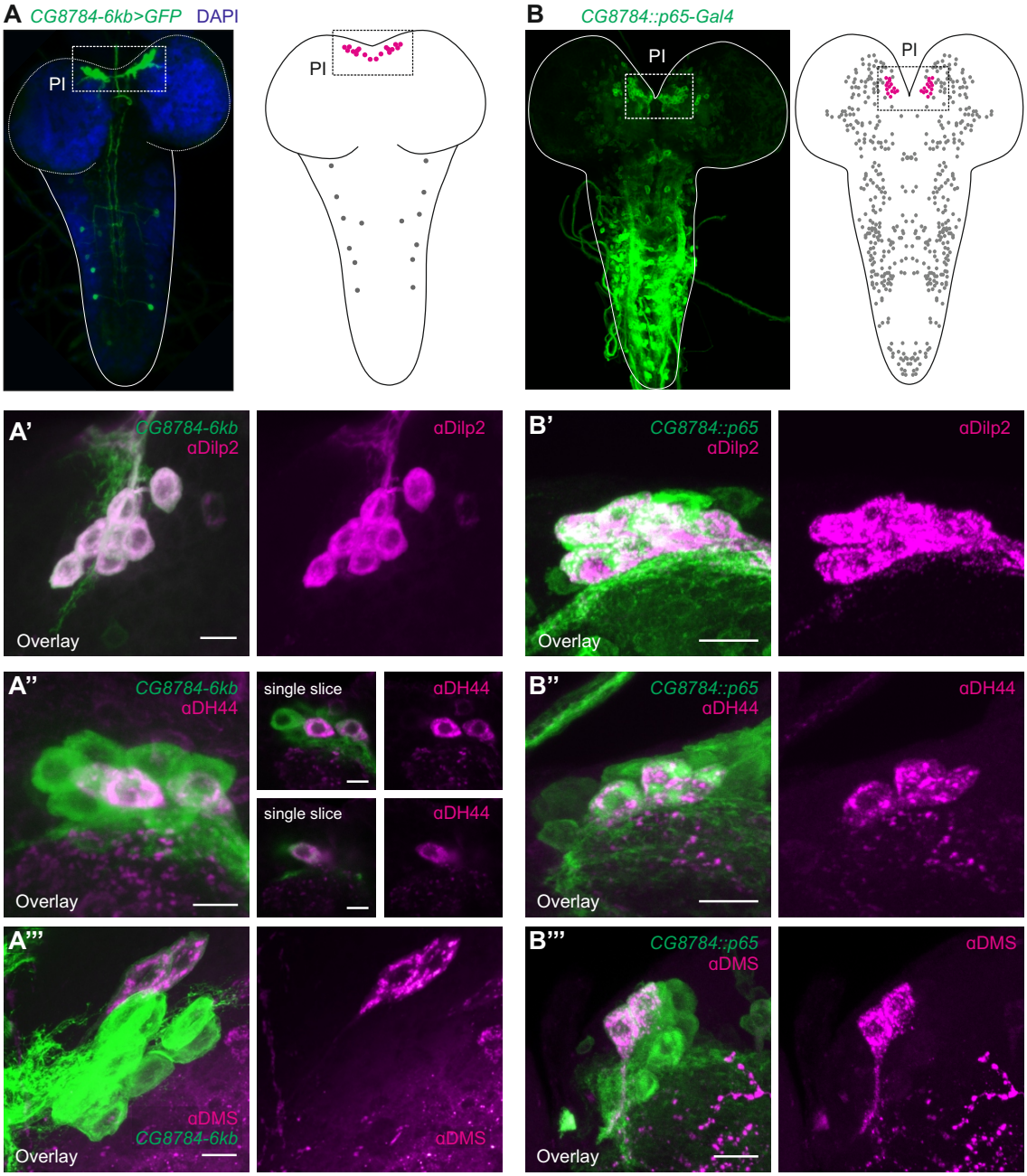

FIGURE 4.17. Expression analysis of a hugin receptor *CG8784* (PK2-R1) using two independent *GAL4* driver lines. **A-A'''**, PK2-R1 promoter *GAL4* line, *CG8784-6kb-GAL4*. **A**, Overview shows expression in mNSCs of the *pars intercerebralis* (PI). **A'-A'''**, Immunohistochemical counterstainings of *CG8784-6kb-GAL4* against peptides produced by mNSCs: expression of *CG8784-6kb-GAL4* co-localizes with *Drosophila* insulin-like peptide (DILP) 2, diuretic hormone 44 (DH44) and Dromyosuppressin (DMS). **B-B'''**, Second PK2-R1 *GAL4* knock-in driver line, *CG8784:p65b-GAL4*. The same counterstainings as in A-A''' were performed. *CG8784:p65b-GAL4* stainings were performed in collaboration with Michael Texada, Janelia Research Campus, USA. Scale bars represent 5μm. Modified from Schlegel et al. [2016].

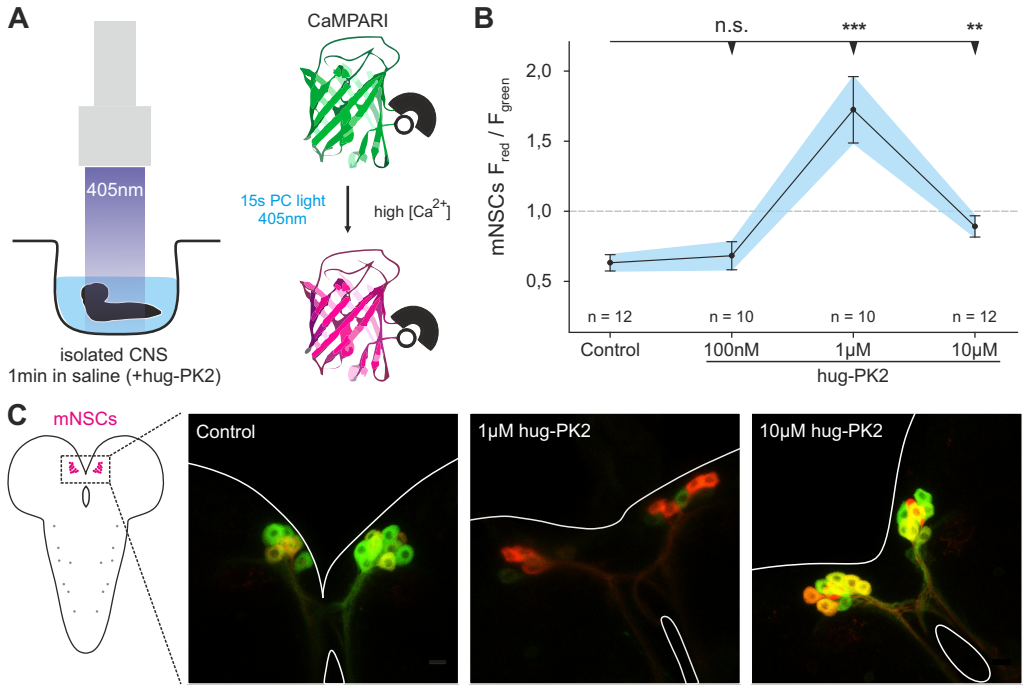

FIGURE 4.18. Effect of hug-PK2 neuropeptide on neurosecretory cells. **A**, Experimental setup and functional principle of CaMPARI. *CG8784-6kb-GAL4* was used to drive expression of *UAS-CaMPARI* in the mNSCs. Isolated CNS were placed in saline (control) or saline + pyrokinin 2 (hug-PK2). Application of 405nm photo-conversion (PC) light irreversibly switches CaMPARI from green to red state in the presence of high calcium. Calcium activity is quantified as ratio of red to green fluorescence F_{red}/F_{green}. **B**, Effect of hugin derivate hug-PK2 on calcium activity in mNSCs. N gives numbers of CNS. Mann-Whitney Rank Sum Test; **, p<0.01; ***, p<0.001. **C**, Exemplary scans showing calcium activity of mNSCs at different concentrations of hug-PK2.

interesting because of their previously demonstrated synaptic interaction with hugin neurons. To look at the mNSCs in more detail, immunohistochemical counterstainings against the peptides produced by the different subsets of mNSCs were performed (see also section 4.2.6). For both *CG8784* lines, immunohistochemical stainings against *Drosophila* insulin-like peptide (DILP) 2, diuretic hormone 44 (DH44) and Dromyosuppressin (DMS) showed co-localization with the GAL4-driven GFP reporter expression. The fact that this observation was made in two independent driver lines strongly suggested that hugin receptor *CG8784* is indeed expressed in the full complement of mNSCs.

4.3.1 Effect of hugin neuropeptide on the neuroendocrine system

As validation of the expression of hugin receptor *CG8784*, the effect of one of the hugin derivates, pyrokinin 2 (hug-PK2), on the mNSCs was investigated. To do so, a genetically encoded calcium sensor, Calcium Modulated Photoactivatable Ratiometric Integrator (CaMPARI), was expressed in the mNSCs using the *CG8784-6kb-GAL4* driver line. In contrast to widely used GCaMPs,

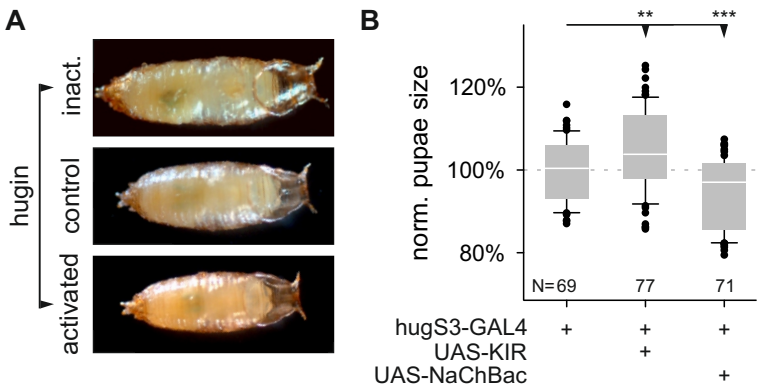

Figure 4.19: Effect of constitutive activation (UAS-NaChBac) or inactivation (UAS-KIR) of hugin neurons on pupae size. **A**, Exemplary images of pupae. **B**, Quantification of pupae size normalized to the control. Mann-Whitney Rank Sum Test (**,p<0.05;***,p<0.001)

CaMPARI is a calcium integrator: its fluorophore changes emission from green to red when high levels of free intracellular calcium coincides with 405nm photoconversion (PC) light [Fosque et al., 2015]. Calcium transients are directly correlated with neuronal activity [Sugimori and Llinas, 1990; Baker et al., 1971]. Based on this, CaMPARI allows to take snapshots of a neuron's activity during the time window of PC light conversion. Isolated CNS were incubated with hug-PK2 for 1min, then PC light was applied for 15s. Afterwards the brains were scanned using a confocal microscope. Calcium activity was measured as the ratio between green and red fluorescence. Results showed that calcium activity in mNSCs increased when hug-PK2 was applied (Fig. 4.18). The strongest increase was observed at a concentration of $1\mu M$.

4.3.1.1 Effect of hugin signaling on pupae size

Data strongly suggested that the endocrine system is a major downstream target of hugin neurons, both by synaptic as well as peptide-receptor connections. The insulin-producing cells (IPCs) are the best studied neurons of the endocrine system. They are a major regulators of growth, energy homeostasis, stress resistance and lifespan [Rulifson et al., 2002; Wu and Brown, 2006; Broughton et al., 2005], and as such act as funnel for a wide range of other pathways [Géminard et al., 2009; Luo et al., 2011; Enell et al., 2010; Rajan and Perrimon, 2012]. A well-established read-out for altered insulin activity is body size [Li and Gong, 2015; Grönke et al., 2010; Andersen et al., 2013]. To investigate their effect on insulin signaling, hugin neurons were constitutively activated or inactivated and the sizes of the pupae were measured upon pupariation. For activation the bacterial sodium channel NaChBac [Nitabach et al., 2006] and for inactivation the kalium (potassium) inward rectifying channel KIR [Hardie et al., 2001] were used. Decreased activity of hugin neurons led to an increase in pupa size indicating increased insulin signaling. Conversely, increased activity of hugin neurons led to a decrease in pupae size (Fig. 4.19).

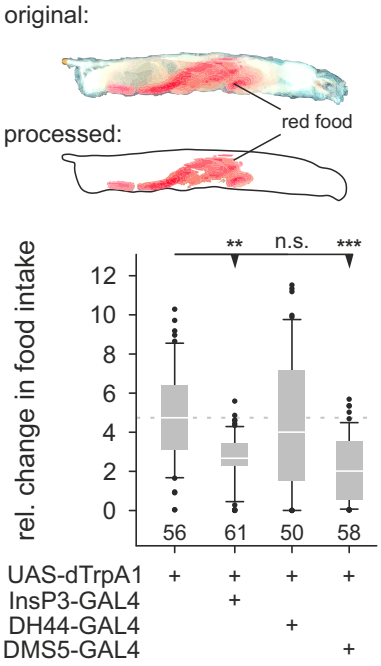

Figure 4.20: Effect of temperature-induced activation of mNSCs on food intake. Larvae were allowed to feed on colored yeast pastes and food intake of individual larvae was calculated as area stained divided by total body surface area. Box plot shows relative change in food intake between control condition (18°C) and dTrpA1-induced activation (32°C). Activation of IPCs (InSP3-GAL4) and DMS-producing cells led to a significant decrease in food intake. Numbers below box plots represent N. Mann-Whitney Rank Sum Test (**,p<0.05;***,p<0.001)

4.3.1.2 Effect of endocrine activity on food intake

Activation of hugin neurons severely decreases food intake [Schoofs et al., 2014a]. Just recently, this effect was narrowed down to hugin-PC neurons [Hückesfeld et al., 2016]. With the mNSCs as major downstream target of hugin-PC neurons, it stood to reason that the negative effect of hugin neurons on feeding behavior might be mediated via the endocrine system. To investigate this possibility, subsets of mNSCs were activated using the thermosensitive cation channel dTrpA1 [Hamada et al., 2008] and food intake was measured.

GAL4 driver lines used to target expression to IPCs [InsP3-GAL4: Buch et al., 2008] and diuretic hormone 44 (DH44)-producing neurons [DH44-GAL4 Dus et al., 2015] were specific for mNSCs of the *pars intercerebralis* (PI). DMS5-GAL4 however expresses in more DMS-producing neurons than just the mNSCs (Appendix A, Fig. A.1) [Park et al., 2008]. Activation of IPCs or DMS-producing neurons severely decreased food intake. In contrast, activation of DH44-producing neurons had no effect on food intake (Fig. 4.20).

Summarizing, pharmacological experiments demonstrated that hug-PK2 has - on average - an activating effect on the population of mNSC but it should be noted that subpopulations may respond differently. In agreement with these results, short-term induced activation of DMS-producing neurons or IPCs led to a decrease in food intake resembling previously reported effects of a direct activation of hugin neurons [Schoofs et al., 2014a].

The effect of hugin neuron's activity on pupae size, however, contradicted an activation of IPCs by hugin: here, activation of hugin neurons led to a decrease in pupae size which is thought to indicate decreased insulin signaling and vice versa [Li and Gong, 2015]. There are several

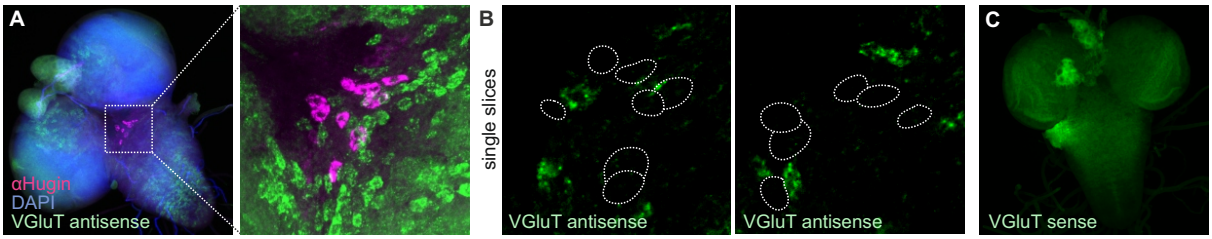

FIGURE 4.21. Colocalization of glutamate and hugin. **A**,**B**, FISH with antisense riboprobe against vesicular glutamate transporter (VGluT) and α-hugin antibody shows no VGluT transkript in hugin neurons. Z-projection (A) and single slices (B). **C**, VGluT sense riboprobe control shows no signal.

potential explanations for this discrepancy. First, the results may reflect the suppressive effect of hugin on food intake thereby masking any effect additional effect on insulin signaling. Second, the constitutive activation/inactivation of hugin neurons might cause long-term compensatory mechanisms (e.g. hugin tolerance due to decreased receptor expression). Third, hugin neurons have previously been demonstrated to take-up insulin upon starvation resulting in increased intracellular insulin signaling [Bader et al., 2013]. This might be indicative of a feedback loop that could also change the effect of long-term hugin activation/inactivation. Finally, constitutive over-activation of hugin neurons may ultimately leads to a depletion of neuropeptide and/or small molecule neurotransmitters. Such observations have been made e.g. in the mammalian superior cervical sympathetic ganglion and the frog neuromuscular junction [Wiley et al., 1987; Lynch, 1980]. It is unclear whether long term inactivation may also have side effects.

4.4 Small molecule transmitters employed by hugin neurons

The EM reconstruction data had shown that some hugin classes have presynaptic sites containing SCVs. This strongly suggested that the hugin interneurons, hugin-PC and hugin-VNC, and possibly also hugin-PH as their pharyngeal target site might also contain SCVs, employ small molecule transmitters in addition to the hugin neuropeptide. Therefore, three of the major small molecule neurotransmitters were checked for their occurrence in hugin neurons: γ-Aminobutyric acid (GABA), acetylcholine (ACh) and glutamate.

4.4.1 Co-localization of glutamate and hugin

As there are no commercially available antibodies for immunohistochemical stainings of glutamatergic neurons, a riboprobe against mRNA of the vesicular glutamate transporter (VGluT) was generated (see methods 3.4). This transporter is responsible for the uptake of glutamate into synaptic vesicles. FISHs using this riboprobe did not co-localize in hugin neurons indicating that glutamate is not used as synaptic transmitter (Fig. 4.21).

4.4.2 Co-localization of acetylcholine and hugin

In the past, immunohistochemical and promoter expression analyses of choline acetyltransferase (ChAT), the biosynthetic enzyme for acetylcholine (ACh), have been used to demonstrate the occurrence of ACh in neurons [Barnstedt et al., 2016; Miyamoto et al., 2012; Yapici et al., 2016]. Both these methods were employed to investigate co-localization of ACh and hugin. Immunohistochemical stainings against ChAT gave relatively weak signals in hugin cell bodies (Fig. 4.22 A). This however was to be expected: First, ChAT preferentially localizes in the neuropil not in the soma [Sámano et al., 2006]. Second, in the EM data hugin neurons showed comparatively few SCVs, indicating low amounts of small molecule transmitter. Because these signals varied strongly between brains, fluorescence of individual hugin neurons was quantified and normalized to the background. Based on soma position and morphology, hugin-PC and hugin-RG neurons were easily identifiable. Hugin-VNC and hugin-PH on the other hand, were in most cases too tightly clustered to be unambiguously classified and thus treated as a single, mixed hugin-VNC/PH group. Highest levels of ChAT were found in hugin-PC neurons and the mixed hugin-VNC/PH group.

In addition to ChAT immunoreactivity, ChAT expression was analyzed using a ChAT-promoter GAL4 line. Similar to the immunohistochemical analysis, the ChAT-GAL4 drove expression in all hugin-PC neurons plus a subset of hugin-VNC/PH neurons (Fig. 4.22 B).

4.4.3 Co-localization of GABA and hugin

Immunohistochemical stainings against GABA were performed to investigate co-localization with hugin. GABA immunoreactivity was generally low in hugin-PC and hugin-RG neurons but high in subsets of hugin-VNC/PH neurons (Fig. 4.22 C).

Summarizing, none of the hugin neurons employ glutamate as indicated by the absence of VGluT transcript. Immunohistochemical stainings as well as promoter expression analysis consistently showed hugin-PC neurons to be cholinergic. Hugin-VNC and hugin-PH neurons had to be treated as a single cluster due to their tight packing. The presented data suggests both GABAergic as well as cholinergic neurons within this mixed cluster. It stands to reason that neurons of each hugin class employ the same transmitter(s). Therefore, the most likely explanation is that either all hugin-VNC neurons are cholinergic and all hugin-PH neurons are GABAergic, or vice versa.

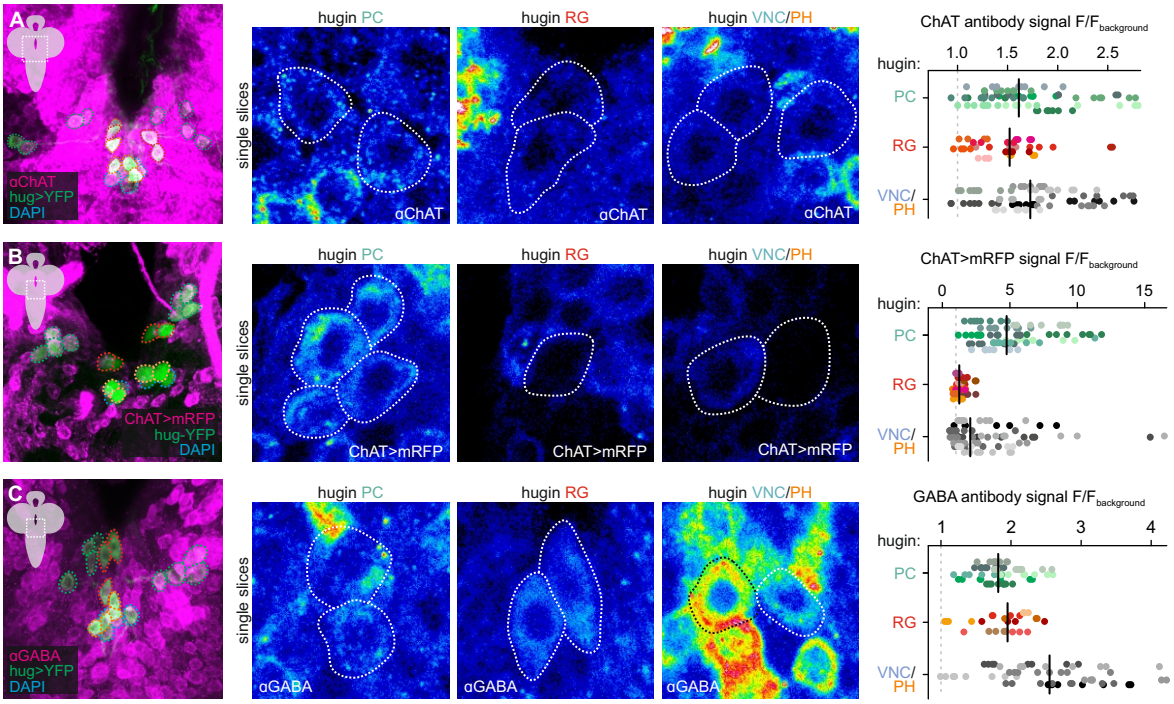

FIGURE 4.22. Colocalization of acetylcholine (ACh)/γ-Aminobutyric acid (GABA) and hugin. **A**,**B**, Occurrence of ACh in hugin neurons was investigated using immunohistochemical stainings (A) against ChAT, the biosynthetic enzyme for ACh, and a ChAT-promoter GAL4 driving a fluorescent reporter (B). Highest levels of ChAT were detected in hugin-PC neurons and subsets of hugin-VNC/PH. **C**, Occurrence of GABA in hugin neurons. Highest levels of GABA immunoreactivity were found in subsets of hugin-VNC/PH neurons. To identify hugin neurons, fluorescent reporters were expressed in these neurons using either a tagged halorhodopsin (hugS3-GAL4;UAS-eNpHR-YFP) or a hugin promoter fused to *YFP* (hug-YFP). Dot plots show normalized fluorescence of single cells. Total number of brains analyzed: $N_{\alpha ChAT}$=10; $N_{ChAT>GFP}$=11; $N_{\alpha GABA}$=7.

CHAPTER 5

DISCUSSION

5.1 Hugin neurons connect the sensory and the endocrine system

Due to their arborizations within the SEZ, the chemosensory center of the *Drosophila* brain [Ghysen, 2003], hugin neurons have long been suspected to receive sensory inputs [Melcher and Pankratz, 2005]. Likewise, projections into the *pars intercerebralis* (PI) have raised the question about interaction with the neuroendocrine system.

5.1.1 Sensory integration

Just recently, Hückesfeld et al. [2016] showed that hugin-PC neurons are responsive to gustatory stimuli and are necessary for the avoidance of bitter substrates. Furthermore, these neurons are also mediating the suppressive effect of hugin on feeding behavior. The data presented in this thesis provides the connectivity underlying these observations. EM reconstructions showed that hugin-PC neurons receive monosynaptic chemosensory input from a range of morphologically diverse sensory neurons of the antennal nerve (AN) (Fig. 4.12). Previous morphological and physiological data indicates that some of these sensory neurons express Gr66a, a gustatory bitter receptor [Hückesfeld et al., 2016].

However, it is reasonable to assume that hugin-PC neurons do not simply act as one-to-one relay station for chemosensory information, like e.g. projection neurons (PN) of the olfactory system. Most PNs innervate single glomeruli of the antennal lobe [Wang et al., 2003; Ng et al., 2002]. They receive stereotyped input from olfactory receptor neurons (ORNs) and relay that information mostly unchanged onto higher brain centers (mushroom body calyx and lateral horn). In the larva, these uniglomerular PNs were shown to receive 58% of their synaptic input from

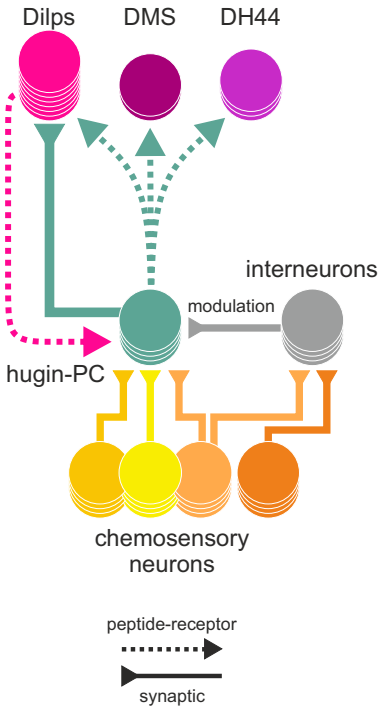

Figure 5.1: Summarizing schematic. Hugin-PC neurons connect sensory and endocrine systems. Morphologically diverse chemosensory neurons from the antennal nerve make direct synaptic connections onto hugin-PC neurons. MNSCs that produce *Drosophila* insulin-like peptides (DILPs), diuretic hormone 44 (DH44) and Dromyosuppressin (DMS), express a hugin receptor. Only DILP-producing mNSCs are also synaptically connected to hugin-PC neurons. Conversely, hugin neurons have been shown to take up DILP2 under starvation leading to increased intracellular insulin signaling [Bader et al., 2013]. Interneurons partially share chemosensory inputs with hugin-PC and likely have a modulatory/integrative function. These interneurons also directly synapse onto the mNSCs but for clarity these connections have been omitted.

ORNs [Berck et al., 2016]. In comparison, hugin-PC neurons receive only up to 28% of their inputs from sensory neurons. Most of their inputs come from other interneurons that might be involved in the integration and modulation of sensory information. Furthermore, sensory neurons synapsing onto hugin-PC were found to be very heterogeneous in respect to connectivity as well as morphology. Based on the fact that gustatory neurons from various sensory organs have previously been shown to compartmentalize the SEZ, this suggests that hugin-PC neurons integrate across multiple sensory organs and/or chemosensory stimuli [Colomb et al., 2007]. In support of this, hugin-PC neurons are not merely activated by bitter substances but additionally respond to other gustatory cues (i.e. high salt, fructose or amino acids) with a decrease in activity [Hückesfeld et al., 2016]. Understanding how different chemosensory cues are integrated to affect hugin neurons' activity would be of great interest for future investigations.

5.1.2 Endocrine regulation

Both, synaptic (Fig. 4.14) as well as peptide-receptor (Fig. 4.17) connectivity points at the endocrine system as a main target of hugin-PC neurons (Fig. 5.1). Strikingly, in case of insulin-producing cells (IPCs), this connection appears to be reciprocal: Bader et al. [2013] demonstrated that hugin-PC neurons take up DILP2 in a nutrient-dependent manner which in turn leads to increased insulin signaling in these neurons. This may be indicative of a regulatory feedback loop between hugin neurons and the IPCs. In accordance with hugin-PC neurons' sensory inputs, the PI as the major endocrine center has previously been shown to be responsive to aversive cues in adult *Drosophila* [Harris et al., 2015]. It is thus well conceivable that hugin-PC neurons play a

role in such chemosensory control over endocrine activity.

Calcium imaging showed that the hugin neuropeptide (hug-PK2) increases neuronal activity in mNSCs (Fig. 4.18). In subsequent food intake experiments, activation of IPCs and DMS- but not DH44-producing neurons resulted in severely decreased food intake (Fig. 4.20). DMS (which belongs to the FMRFamide peptide family) has not been well studied in the context of regulation of feeding behavior [Nichols, 2003]. In *Drosophila*, DMS has so far only been implicated in behavioral responses to environmental stress [Klose et al., 2010; Kiss et al., 2013]. In mice however, intracerebroventricular administration of FMRFamide is known to also inhibit feeding [Kavaliers and Hirst, 1986].

For insulin/insulin-like peptides, on the other hand, there is a wide range of studies linking them to very specific aspects of feeding [for reviews see Fernandez and Torres-Alemán, 2012; Schwartz et al., 2000]. In contrast to *Drosophila*, insulin expression in the adult mammalian CNS is controversial. Consensus is that no or only little insulin is present in central neurons but that peripheral insulin has access to the CNS [for discussions see Banks, 2004; Schwartz et al., 2010]. However, Insulin-like growth factors (IGFs) are widely expressed throughout the CNS [Lee et al., 1996; Stylianopoulou et al., 1988]. Accordingly, receptors for insulin and IGF are widely distributed in the CNS, with high concentrations in the hypothalamus [Bondy, 1991; Valentino et al., 1990; Havrankova et al., 1978]. In accordance with data presented here, several studies have demonstrated inhibitory effects of insulin on feeding behavior across species. IGF treatment ameliorates hyperphagia and obesity in rats with metabolic disorders [Vickers et al., 2001]. In baboons, intracerebroventricular infusion of insulin leads to reduced food intake [Woods et al., 1979]. There is also evidence that misregulation of insulin signaling in general has negative effects on feeding behavior. In *Drosophila*, inactivation or ablation of IPCs can cause decreases in food intake under certain dietary conditions [Broughton et al., 2010; Cognigni et al., 2011]. At the same time, IPCs co-express drosulfakinins, satiety-inducing peptides whose knockdown increases food intake [Söderberg et al., 2012]. Similarly, decreased insulin-signaling in neuropeptide F (NPF) receptor neurons promotes feeding on noxious (bitter) food sources [Wu et al., 2005]. Such connection between chemosensory systems and insulin signaling has been reported multiple times. In *C. elegans*, insulin-like peptides are involved in food related sensory integration [Jiu et al., 2010]. Similarly, insulin signaling in combination with short neuropeptide F (sNPF) sensitizes olfactory receptor neurons (ORNs), thereby enhancing odor-driven food-search behavior in *Drosophila* [Root et al., 2011].

Summarizing, the endocrine system is a good candidate through which hugin-PC neurons could exert their effect on feeding behavior. Whether endocrine regulation is the sole pathway or rather a new, additional aspect of hugin function remains to be seen. Future investigations should focus on dissecting the effect of hugin neurons on each component of the endocrine system separately. Furthermore, it would be of great interest to understand how exactly they are involved in feeding/feeding-related behavior. E.g. the role of DH44 in the *Drosophila* feeding behavior

remains unclear. This knowledge will ultimately help placing hugin neurons in a larger context.

5.1.3 Conserved sensory to endocrine connections

Hugin neurons connect the chemosensory with the endocrine system (Fig. 5.1). It has been suggested that neuroendocrine centers evolved from a simple brain consisting of cells with dual sensory/neurosecretory properties. Only later they diversified into optimized single-function cells. Neurosecretory cells that share the same genetic fingerprint in zebrafish and the annelid *Platynereis dumerilii* have conserved such dual sensory/neurosecretory function [Tessmar-Raible et al., 2007]. Accordingly, these cell types were suggested to have been part of a primitive urbilaterian[1] brain in which they directly relayed sensory cues into changes in body physiology. Such comparisons across large evolutionary distances are difficult. Nevertheless, there is more evidence that connections between sensory and endocrine centers have been conserved throughout evolution despite the increase in complexity and neuronal specialization. In the sea squirt *Ciona*, neurons producing gonadotropin-releasing hormone (GnRH) likely also possess chemosensory function [Abitua et al., 2015]. This is strikingly similar to the situation in mammals: GnRH neurons of the rodent hypothalamus receive direct input from olfactory sensory neurons [Yoon et al., 2005]. These findings strongly suggest that sensory to endocrine connections are fundamental building blocks of nervous systems and the connection between endocrine and chemosensory centers provided by hugin neurons may well represent such a conserved circuit.

5.2 Co-Transmission of neuropeptide and synaptic transmitter

EM data revealed the occurrence of small clear core vesicles (SCVs) at presynaptic sites of hugin interneurons, hugin-PC and hugin-VNC. This led to the assumption that these and possibly also hugin-PH neurons (whose peripheral target sites were not part of the EM volume) employ synaptic small molecule transmitters in addition to hugin neuropeptide. Indeed, immunohistochemical and expression analyses strongly suggested that hugin neurons produce acetylcholine (ACh) and/or γ-Aminobutyric acid (GABA). In detail, hugin-RG neurons did not produce any of these small molecule transmitters which is in accordance with them not showing SCVs in the EM data. Hugin-PC neurons clearly employed ACh but not GABA. In support of this, synaptic targets of hugin-PC neurons, the IPCs, correspondingly express a muscarinic ACh receptor [Cao et al., 2014]. Hugin-VNC and hugin-PH were positive for both ACh and GABA. Unfortunately, their tight clustering made it impossible to unambiguously assign a neurotransmitter to either hugin class. However, given the homogeneity of synaptic partners within each hugin class, it is logical that this should be reflected in the use of synaptic transmitters. Therefore, likely all hugin-VNC neurons will be cholinergic while all hugin-PH neurons are GABAergic, or vice versa.

[1] German ur - 'original'

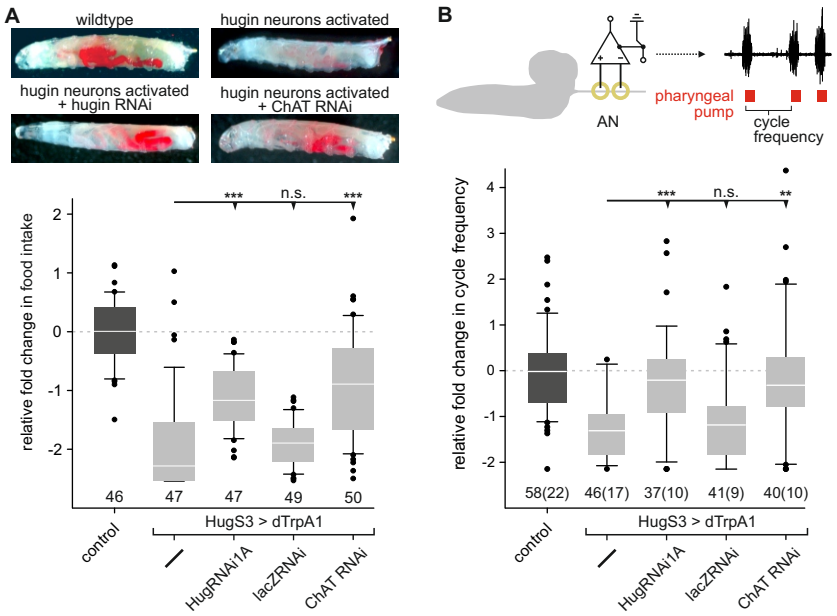

FIGURE 5.2. Cholinergic transmission in hugin neurons. Activation of hugin neurons decreases food intake (**A**) and activity of the pharyngeal pump (**B**). RNAi-induced knockdown of either acetylcholine (via choline acetyltransferase [ChAT], the biosynthetic enzyme) or the hugin neuropeptide itself rescues these hugin phenotypes. Modified from Schlegel et al. [2016].

The concept of multiple transmitters within a single neuron is well established and appears to be the rule rather than the exception [for reviews see Nusbaum et al., 2001; Merighi, 2002; Burnstock, 2004; Brezina, 2010]. However, there are only few examples in which specific targets of both synaptic and peptidergic transmission have been described. In sympathetic ganglia of frogs neurons use both ACh and a neuropeptide to target so-called C cells, but only the neuropeptide additionally targets B cells. For either target, the neuropeptide has a late, slow depolarizing effect on the membrane potential whereas ACh causes a fast excitatory postsynaptic potential [Jan and Jan, 1983]. This illustrates, that neuropeptides and synaptic transmitters may operate on different timescales.

For hugin neurons, this raises the question of how neuropeptide and synaptic transmitter interact to affect e.g. food intake. The importance of hugin neuropeptide for the decrease in food intake had previously been demonstrated using RNAi-induced knockdown of hug-PK2. This hugin knockdown partially rescued the suppressive effect of activation of hugin neurons on food intake and feeding motor patterns [Schoofs et al., 2014a]. Among hugin neurons, hugin-PC neurons are mainly responsible for this decrease in food intake and motor patterns [Hückesfeld et al., 2016]. As ACh is co-localized in these neurons, they are well suited to investigate the importance of synaptic transmission versus hugin neuropeptide. Indeed, RNAi-induced knockdown of the biosynthetic enzyme for ACh, choline acetyltransferase (ChAT), also ameliorates the suppressive effect of hugin neurons (Fig. 5.2) [Schlegel et al., 2016]. These findings prove the employment

of ACh by hugin neurons but at the same time they also raise more questions. Are hugin neuropeptide and ACh both employed under natural conditions? What is the purpose of targeting downstream neurons by either ACh or hug-PK2 alone or a combination of both? A system in which this question has been addressed is the radula closer muscle of *Aplysia*. Here, motor neurons employ ACh and additionally several neuropeptides. ACh is released at lower firing rates than the neuropeptides. Nevertheless, baseline activity of the motor neurons is high enough to release both under natural conditions to ensure optimal motor output. The neuropeptides modulate the contraction of the muscle to reduce the probability of tetanic contractions [for reviews see Weiss et al., 1993; Vilim et al., 1996].

An interesting possibility of how hugin and ACh may interact is illustrated by the so called synaptic gain hypothesis. Based on work in frog sympathetic ganglia, Horn [1992] proposed that co-transmission has an integrative role that can drastically alter the response of postsynaptic targets. One of the core postulates of the synaptic gain hypothesis can be rephrased such that different modes of transmission (e.g. fast synaptic and slow peptidergic) are optimally elicited at distinct parameters of neuronal activity. Consequentially, this leads to a complex interaction of co-transmitters which in turn multiplies the effects a neuron can exert on its downstream targets. For hugin neurons, this could imply that ACh and hug-PK2 are selectively employed to serve very specific purposes. In case of IPCs for example, ACh might trigger short bursts of insulin release, whereas hug-PK2 modulates excitability in the long term. In light of the comprehensive morphological, physiological and connectivity data provided by this work and previous publications, the hugin system is well suited to investigate the interaction of peptide vs. synaptic transmitter in greater detail.

5.3 Common features in flies and mammals

Previous studies reported similar effects of hugin and its mammalian homolog NMU: both neuropeptides decrease food intake while promoting locomotion/physical activity [Schoofs et al., 2014a; Howard et al., 2000; Hanada et al., 2004]. Data presented in this study reveal additional striking parallels between the homologous neuropeptides. On a circuit level, hugin-PC neurons act as integrator between chemosensory and endocrine system where they specifically target IPCs, DMS- and DH44-producing neurons. Similarly, NMU acts on the mammalian homologs of both DILP and DH44. First, insulin-producing β cells express a NMU receptor that allows NMU to potently suppress glucose-induced insulin secretion [Alfa et al., 2015]. Unlike in *Drosophila*, β cells are not part of the CNS but of the pancreas. Nevertheless, the mammalian CNS is linked to the pancreas by sympathetic and parasympathetic efferents that innervate β cells [Thorens, 2011, 2014]. Second, the main anorexigenic effect of NMU is localized to the hypothalamus [Wren et al., 2002; Malendowicz et al., 2012]. Here, its most important effect is the increased release of corticotropin-releasing hormone (CRH) [Hanada et al., 2001, 2003] which is an homolog of

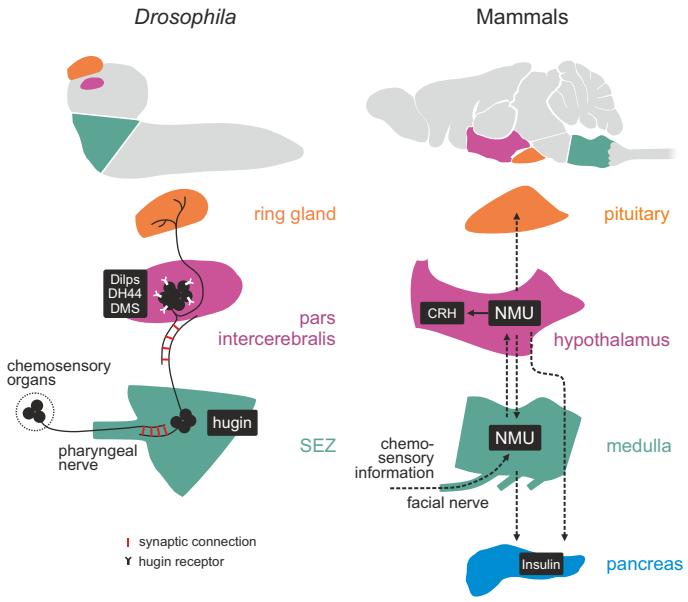

FIGURE 5.3. Comparison of hugin and neuromedinU (NMU). Hugin neurons connect the chemosensory with the endocrine system in *Drosophila*. In mammals, NMU is found in regions of the brain that are analogous or even homologous to those innervated by hugin neurons. Both neuropeptides share similarities in their chemical connectivity as they target homologous peptides: DH44/CRH and DILPs/insulin. Indicated connections between areas of NMU occurrence have been demonstrated but whether they play any role for NMU signaling or effect has yet to be addressed. Subesophageal zone, SEZ; diuretic hormone 44, DH44; *Drosophila* insulin-like peptides, Dilps; Dromyosuppressin, DMS; corticotropin-releasing hormone (CRH).

Drosophila DH44 [Mirabeau and Joly, 2013]. These parallels in hugin/NMU to DH44/CRH and DILP/insulin suggest a conservation in chemical connectivity between both neuropeptides (Fig. 5.3).

As mentioned earlier, comparisons across such large evolutionary distance are generally difficult. The mammalian CNS is indisputably more complex in respect to both number and types of neurons involved. Nevertheless, hugin and NMU exhibit parallels beyond the chemical connectivity. NMU peptide, NMU-positive fibers and NMU-expressing cells have been found in many parts of the nervous system. While neither the total number of NMU neurons nor their morphology is known, high levels of NMU have been found in the *arcuate nucleus* (ARC) of the hypothalamus, the pituitary, the nucleus of the solitary tract (NTS) in the *medulla oblongata* and the spinal cord [Domin et al., 1987; Ballesta et al., 1988; Howard et al., 2000; Ivanov et al., 2004]. Despite being much simpler, hugin neurons and their projections cover corresponding regions of the *Drosophila* CNS: based on morphological, functional and genetic similarities, the ring gland, the *pars intercerebralis* (PI) and the ventral nerve cord (VNC) have been suggested to correspond to the pituitary gland, the hypothalamus and the spinal cord, respectively [Ghysen, 2003; Hartenstein, 2006].

Combined data on hugin in *Drosophila* has revealed many parallels to NMU in mammals. It is conceivable, that the obvious differences are merely a result of the larger size and volume of the mammalian CNS which required a larger number of specialized neurons dedicated to each of the target neuropils even though the basic function remains the same. In light of this, findings on hugin should encourage research in other organisms to specifically look for other similar features, e.g. responsiveness of NMU neurons in the NTS to chemosensory stimuli or a direct connection between NMU neurons and pancreatic islet β cells.

Acronyms

klu *klumpfuss*. 12

ACh acetylcholine. 56–58, 62–64

AN antennal nerve. 44, 48, 59

BAC bacterial artificial chromosome. 51

CaMPARI Calcium Modulated Photoactivatable Ratiometric Integrator. 53, 54

CAPA capability. 33

ChAT choline acetyltransferase. 7, 8, 57, 58, 63

CNS central nervous system. 12, 29–31, 36, 42, 45, 50, 51, 53, 54, 61, 64–66

CPG central pattern generator. 2, 3

CRH corticotropin-releasing hormone. 11, 64, 65

DAG directed acyclic graph. 50, 51

DCV dense core vesicle. 11, 26, 33–36, 38–40, 72

DH44 diuretic hormone 44. 45, 47, 52, 53, 55, 60, 61, 64, 65

DIG Digoxigenin. 23

DILP *Drosophila* insulin-like peptide. 45, 52, 53, 60, 64, 65

DMS Dromyosuppressin. 45, 47, 52, 53, 55, 60, 61, 64

EM electron microscopy. 4, 9, 45

FISH fluorescence-in-situ-hybridization. 56

GABA γ-Aminobutyric acid. 56–58, 62

GFP green-fluorescent protein. 7, 8, 30, 51, 53

GnRH gonadotropin-releasing hormone. 62

GRASP GFP-reconstitution across synaptic partners. 9

hug-PK2 pyrokinin 2. 11–13, 25, 53–55, 61, 63, 64

IGF insulin-like growth factor. 61

IPC insulin-producing cell. 14, 31, 45, 47, 48, 54, 55, 60–62, 64

Kir Kalium inward rectifying. 8

MCFO multi-color flp-out. 24, 25, 29

mNSC median neurosecretory cell. 26, 31, 33, 45, 47, 48, 50–55, 60, 61, 72

Ncc *nervi corporis cardiaci*. 31, 33

NMU neuromedinU. iii, v, 11, 13, 64–66

NPF neuropeptide F. 61

NPY neuropeptide Y. 11

NSCs-PI neurosecretory cells of the *pars lateralis*. 33

PaN prothoracic accessory nerve. 12, 31, 32

PBS phosphate-buffered saline. 16, 22

PC protocerebrum. 35, 36, 38

PCR polymerase chain reaction. 22

PI *pars intercerebralis*. 45, 47, 52, 55, 59, 60, 65

POD peroxidase. 24

RG ring gland. 35, 36, 45

RNAi RNA interference. 12, 63

SCV small clear core vesicle. 36, 56, 57, 62

SEZ subesophageal zone. 12, 29, 31, 35, 36, 38, 42, 44, 45, 59, 60

smGFP spaghetti monster GFP. 24, 25

sNPF short neuropeptide F. 61

SSC saline-sodium citrate. 17

ssTEM serial section transmission electron microscopy. 9, 10

STG stomatogastric ganglion. 2, 3, 7

STNS stomatogastric nervous system. 4

td tracheal dendritic. 44, 46, 48

TSA Tyramid signal amplification. 18, 24

UAS upstream-activating-sequence. 8

VGluT vesicular glutamate transporter. 22, 56, 57

VM ventromedial. 33

VNC ventral nerve cord. 35, 36, 46, 65

Appendix A: Supplementary data and figures

Neuron	Smooth Cable [nm]	N postsynaptic sites	N presynaptic sites	N DCVs
hugin-PC left 1	225212	129	38	585
hugin-PC left 2	194394	93	29	552
hugin-PC left 3	165623	74	31	315
hugin-PC left 4	227867	121	36	905
hugin-PC right 1	209580	127	40	767
hugin-PC right 2	196333	98	35	356
hugin-PC right 3	187933	90	28	577
hugin-PC right 4	211920	99	38	639
hugin-PH left 1	150832	16	1	99
hugin-PH left 2	180658	32	0	138
hugin-PH right 1	155747	22	1	90
hugin-PH right 2	165740	28	0	99
hugin-RG left 1	234030	49	5	710
hugin-RG left 2	241573	50	3	569
hugin-RG right 1	219573	40	8	897
hugin-RG right 2	258717	53	11	810
hugin-VNC left 1	373114	129	56	1302
hugin-VNC left 2	294802	82	40	808
hugin-VNC right 1	342651	115	48	1023
hugin-VNC right 2	331927	106	39	1109

Continued on next page

Continued from previous page

Neuron	Smooth Cable [nm]	N postsynaptic sites	N presynaptic sites	N DCVs

Table A.1: Statistical analysis of the morphology of hugin neurons. Size of neuron as measured by smoothed cable length, number of pre- and postsynaptic sites as well as dense core vesicles (DCVs). DCVs within a $3\mu m$ radius around the soma were not counted.

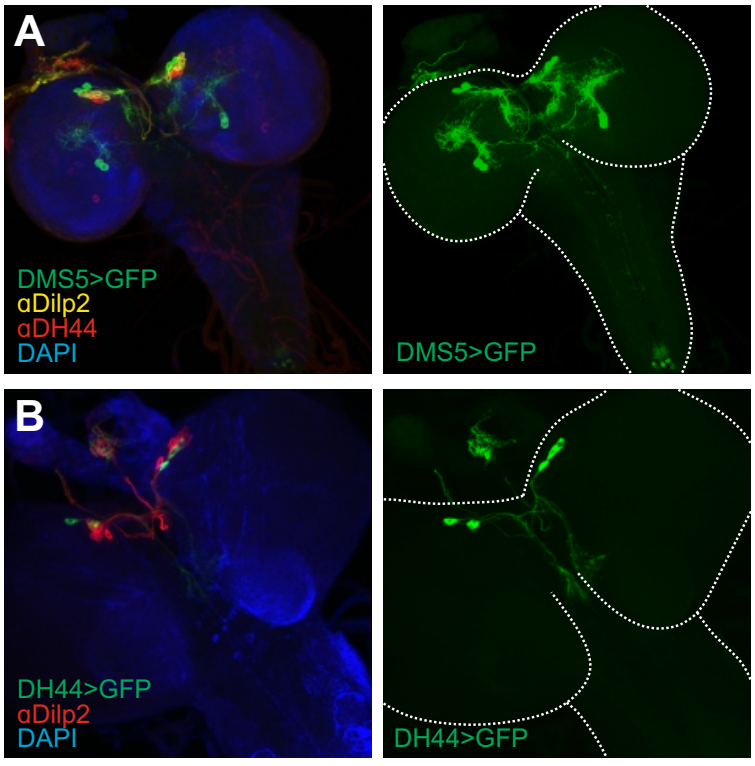

Figure A.1: Expression patterns of driver lines DMS5-GAL4 and DH44-GAL4. **A**, DMS5-GAL4 drives expression in mNSCs and some additional neurons in the protocerebrum and the last abdominal segments of the ventral nerve cord. **B**, DH44-GAL4 drives expression exclusively in mNSCs.

APPENDIX B

Appendix B: Reactions

Components	Amount
Primer Mix	
forward primer	20 μM
reverse primer	20 μM
PCR reaction (25 μl)	
DNA Template	2 μl
5X GoTaq Green	5 μl
10mM dNTPs	0.5 μl
GoTag Pol.	0.125 μl
primer mix	1 μl
bidest	16.375 μl
PCR protocol	
Initial denaturation	95°C $2'$
35 cycles	95°C $30''$
	55°C $30''$
	72°C $1'$
Final extension	72°C $5'$
Hold	4°C ∞
Test digest	
DNA	10 μg
10X buffer	3 μl
restriction enzyme	0.5 μl

Continued on next page

Continued from previous page

Components	Amount
bidest	16.5 μl
incub. for 1h at 37°C	
InVitro transcription	
DNA template	1 μg
10X buffer	2 μl
DIG labeling mix	2 μl
RNAse inhibitor	0.5 μl
T7/Sp6	2 μl
final volume	20 μl
incub. for 1h at 37°C	

Table B.1: Cloning reactions.

BIBLIOGRAPHY

Abitua, P. B., Gainous, T. B., Kaczmarczyk, A. N., Winchell, C. J., Hudson, C., Kamata, K., Nakagawa, M., Tsuda, M., Kusakabe, T. G., and Levine, M. (2015).
The pre-vertebrate origins of neurogenic placodes.
Nature, 524(7566):462–5.

Agnati, L. F., Zoli, M., Strömberg, I., Fuxe, K., Strömberg, I., and Fuxe, K. (1995).
Intercellular communication in the brain: Wiring versus volume transmission.
Neuroscience, 69(3):711–726.

Albertson, D. G. and Thomson, J. N. (1976).
The pharynx of *C. elegans*.
Philosophical transactions of the Royal Society of London. Series B, Biological sciences, 275(938):299–325.

Alfa, R. W., Park, S., Skelly, K.-r. R., Poffenberger, G., Jain, N., Gu, X., Kockel, L., Wang, J., Liu, Y., Powers, A. C., and Kim, S. K. (2015).
Suppression of Insulin Production and Secretion by a Decretin Hormone.
Cell metabolism, 21(2):323–333.

Andersen, D. S., Colombani, J., and Léopold, P. (2013).
Coordination of organ growth: Principles and outstanding questions from the world of insects.
Trends in Cell Biology, 23(7):336–344.

Bader, G. D. and Hogue, C. W. V. (2003).
An automated method for finding molecular complexes in large protein interaction networks.
BMC bioinformatics, 4:2.

Bader, R., Colomb, J., Pankratz, B., Schröck, A., Stocker, R. F., and Pankratz, M. J. (2007a).
Genetic dissection of neural circuit anatomy underlying feeding behavior in *Drosophila*: distinct classes of hugin-expressing neurons.
The Journal of Comparative Neurology, 502(5):848–56.

Bader, R., Sarraf-Zadeh, L., Peters, M., Moderau, N., Stocker, H., Köhler, K., Pankratz, M. J., and Hafen, E. (2013).

The IGFBP7 homolog Imp-L2 promotes insulin signaling in distinct neurons of the *Drosophila* brain.
Journal of cell science, 126(Pt 12):2571–6.

Bader, R., Wegener, C., and Pankratz, M. J. (2007b).
Comparative neuroanatomy and genomics of hugin and pheromone biosynthesis activating neuropeptide (PBAN).
Fly, 1(4):228–31.

Baker, P. F., Hodgkin, A. L., and Ridgway, E. B. (1971).
Depolarization and calcium entry in squid giant axons.
The Journal of Physiology, 218(3):709–755.

Ballesta, J., Carlei, F., Bishop, A. E., Steel, J. H., Gibson, S. J., Fahey, M., Hennessey, R., Domin, J., Bloom, S. R., and Polak, J. M. (1988).
Occurrence and developmental pattern of neuromedin U-immunoreactive nerves in the gastrointestinal tract and brain of the rat.
Neuroscience, 25(3):797–816.

Banks, W. A. (2004).
The source of cerebral insulin.
European journal of pharmacology, 490(1-3):5–12.

Barnstedt, O., Owald, D., Felsenberg, J., Brain, R., Moszynski, J. P., Talbot, C. B., Perrat, P. N., and Waddell, S. (2016).
Memory-Relevant Mushroom Body Output Synapses Are Cholinergic.
Neuron, 89(6):1237–1247.

Bennett, M. V., Barrio, L. C., Bargiello, T. a., Spray, D. C., Hertzberg, E., and Sáez, J. C. (1991).
Gap junctions: new tools, new answers, new questions.
Neuron, 6:305–320.

Bentley, B., Branicky, R., Barnes, C. L., Bullmore, E. T., Vértes, P. E., and Schafer, W. R. (2016).
The multilayer connectome of *C. elegans*.
arXiv.

Berck, M. E., Khandelwal, A., Claus, L., Hernandez-Nunez, L., Si, G., Tabone, C. J., Li, F., Truman, J. W., Fetter, R. D., Louis, M., Samuel, A. D., and Cardona, A. (2016).
The wiring diagram of a glomerular olfactory system.
eLife, 5:1–21.

Bodmer, R. and Jan, Y. N. (1987).
Morphological differentiation of the embryonic peripheral neurons in *Drosophila*.

Rouxs Archives Of Developmental Biology, 196:69–77.

Bondy, C. A. (1991).
Transient IGF-I gene expression during the maturation of functionally related central projection neurons.
The Journal of neuroscience : the official journal of the Society for Neuroscience, 11(11):3442–55.

Brand, a. H. and Perrimon, N. (1993).
Targeted gene expression as a means of altering cell fates and generating dominant phenotypes.
Development (Cambridge, England), 118(2):401–15.

Brezina, V. (2010).
Beyond the wiring diagram: signalling through complex neuromodulator networks.
Philosophical transactions of the Royal Society of London. Series B, Biological sciences, 365(1551):2363–74.

Briggman, K. L., Helmstaedter, M., and Denk, W. (2011).
Wiring specificity in the direction-selectivity circuit of the retina.
Nature, 471(7337):183–188.

Brighton, P. J., Szekeres, P. G., and Willars, G. B. (2004).
Neuromedin U and its receptors: structure, function, and physiological roles.
Pharmacological reviews, 56(2):231–48.

Broughton, S. J., Piper, M. D. W., Ikeya, T., Bass, T. M., Jacobson, J., Driege, Y., Martinez, P., Hafen, E., Withers, D. J., Leevers, S. J., and Partridge, L. (2005).
Longer lifespan, altered metabolism, and stress resistance in *Drosophila* from ablation of cells making insulin-like ligands.
Proceedings of the National Academy of Sciences of the United States of America, 102(8):3105–10.

Broughton, S. J., Slack, C., Alic, N., Metaxakis, A., Bass, T. M., Driege, Y., and Partridge, L. (2010).
DILP-producing median neurosecretory cells in the *Drosophila* brain mediate the response of lifespan to nutrition.
Aging cell, 9(3):336–46.

Buch, S., Melcher, C., Bauer, M., Katzenberger, J., and Pankratz, M. J. (2008).
Opposing effects of dietary protein and sugar regulate a transcriptional target of *Drosophila* insulin-like peptide signaling.
Cell metabolism, 7(4):321–32.

Burns, G. A. and Young, M. P. (2000).

Analysis of the connectional organization of neural systems associated with the hippocampus in rats.
Philosophical transactions of the Royal Society of London. Series B, Biological sciences, 355(1393):55–70.

Burnstock, G. (2004).
Cotransmission.
Current opinion in pharmacology, 4(1):47–52.

Buxhoeveden, D. P. and Casanova, M. F. (2002).
The minicolumn hypothesis in neuroscience.
Brain : a journal of neurology, 125(Pt 5):935–51.

Cabrero, P., Radford, J. C., Broderick, K. E., Costes, L., Veenstra, J. a., Spana, E. P., Davies, S. a., and Dow, J. a. T. (2002).
The Dh gene of *Drosophila melanogaster* encodes a diuretic peptide that acts through cyclic AMP.
The Journal of experimental biology, 205(Pt 24):3799–3807.

Cansell, C., Denis, R. G. P., Joly-Amado, A., Castel, J., and Luquet, S. (2012).
Arcuate AgRP neurons and the regulation of energy balance.
Frontiers in Endocrinology, 3(DEC):1–7.

Cao, J., Ni, J., Ma, W., Shiu, V., Milla, L. a., Park, S., Spletter, M. L., Tang, S., Zhang, J., Wei, X., Kim, S. K., Scott, M. P., Shi, V., Milla, L. a., Park, S., Spletter, M. L., Tang, S., Zhang, J., Wei, X., Kim, S. K., and Scott, M. P. (2014).
Insight into Insulin Secretion from Transcriptome and Genetic Analysis of Insulin-Producing Cells of *Drosophila*.
Genetics, 197(1):175–192.

Cavanaugh, D. J., Geratowski, J. D., Wooltorton, J. R. a., Spaethling, J. M., Hector, C. E., Zheng, X., Johnson, E. C., Eberwine, J. H., and Sehgal, A. (2014).
Identification of a circadian output circuit for rest: Activity rhythms in drosophila.
Cell, 157(3):689–701.

Chalfie, M. and Sulston, J. (1981).
Developmental genetics of the mechanosensory neurons of *C. elegans*.
Developmental Biology, 82(2):358–370.

Clarac, F. and Pearlstein, E. (2007).
Invertebrate preparations and their contribution to neurobiology in the second half of the 20th century.
Brain Research Reviews, 54(1):113–161.

Cognigni, P., Bailey, A. P., and Miguel-Aliaga, I. (2011).
Enteric neurons and systemic signals couple nutritional and reproductive status with intestinal homeostasis.
Cell metabolism, 13(1):92–104.

Colomb, J., Grillenzoni, N., Ramaekers, A., and Stocker, R. F. (2007).
Architecture of the primary taste center of *Drosophila melanogaster* larvae.
The Journal of comparative neurology, 502(5):834–47.

Dailey, M. J. and Bartness, T. J. (2009).
Appetitive and consummatory ingestive behaviors stimulated by PVH and perifornical area NPY injections.
American journal of physiology. Regulatory, integrative and comparative physiology, 296(4):R877–R892.

Domin, J., Ghatei, M. a., Chohan, P., and Bloom, S. R. (1987).
Neuromedin U – a study of its distribution in the rat.
Peptides, 8(5):779–784.

Duffy, J. B. (2002).
GAL4 system in *Drosophila*: a fly geneticist's Swiss army knife.
Genesis (New York, N.Y. : 2000), 34(1-2):1–15.

Dus, M., Lai, J. S.-Y. Y., Gunapala, K. M., Min, S., Tayler, T. D., Hergarden, A. C., Geraud, E., Joseph, C. M., and Suh, G. S. B. (2015).
Nutrient Sensor in the Brain Directs the Action of the Brain-Gut Axis in *Drosophila*.
Neuron, 87(1):139–51.

Eades, P., Lin, X., and Smyth, W. F. (1993).
A fast and effective heuristic for the feedback arc set problem.
Information Processing Letters, 47(6):319–323.

Emmons, S. W. (2015).
The beginning of connectomics: a commentary on White et al. (1986) 'The structure of the nervous system of the nematode *C. elegans*'.
Philosophical transactions of the Royal Society of London. Series B, Biological sciences, 370(1666):20140309–.

Enell, L. E., Kapan, N., Söderberg, J. a. E., Kahsai, L., Nässel, D. R., and Nässe, D. R. (2010).
Insulin signaling, lifespan and stress resistance are modulated by metabotropic GABA receptors on insulin producing cells in the brain of *Drosophila*.
PLoS ONE, 5(12):e15780.

Feinberg, E. H., Vanhoven, M. K., Bendesky, A., Wang, G., Fetter, R. D., Shen, K., and Bargmann, C. I. (2008).
GFP Reconstitution Across Synaptic Partners (GRASP) defines cell contacts and synapses in living nervous systems.
Neuron, 57(3):353–63.

Fernandez, A. M. and Torres-Alemán, I. (2012).
The many faces of insulin-like peptide signalling in the brain.
Nature Reviews Neuroscience, 13(4):225–239.

Fosque, B. F., Sun, Y., Dana, H., Yang, C.-t., Ohyama, T., Tadross, M. R., Patel, R., Zlatic, M., Kim, D. S., Ahrens, M. B., Jayaraman, V., Looger, L. L., and Schreiter, E. R. (2015).
Labeling of active neural circuits in vivo with designed calcium integrators.
Science (New York, N.Y.), 347(6223):755–60.

Fushiki, A., Zwart, M. F., Kohsaka, H., Fetter, R. D., Cardona, A., and Nose, A. (2016).
A circuit mechanism for the propagation of waves of muscle contraction in *Drosophila*.
eLife, 5:e13253.

Galuske, R. A., Schlote, W., Bratzke, H., and Singer, W. (2000).
Interhemispheric asymmetries of the modular structure in human temporal cortex.
Science (New York, N.Y.), 289(5486):1946–9.

Géminard, C., Rulifson, E. J., and Léopold, P. (2009).
Remote control of insulin secretion by fat cells in *Drosophila*.
Cell metabolism, 10(3):199–207.

Ghysen, A. (2003).
The origin and evolution of the nervous system.
The International journal of developmental biology, 47(7-8):555–62.

Ghysen, A., Dambly-Chaudière, C., Aceves, E., Jan, L. Y., and Jan, Y. N. (1986).
Sensory neurons and peripheral pathways in *Drosophila* embryos.
Roux's Archives of Developmental Biology, 195(5):281–289.

Giniger, E., Varnum, S. M., and Ptashne, M. (1985).
Specific DNA binding of GAL4, a positive regulatory protein of yeast.
Cell, 40(4):767–74.

Grönke, S., Clarke, D.-F., Broughton, S., Andrews, T. D., and Partridge, L. (2010).
Molecular evolution and functional characterization of *Drosophila* insulin-like peptides.
PLoS genetics, 6(2):e1000857.

Hamada, F. N., Rosenzweig, M., Kang, K., Pulver, S. R., Ghezzi, A., Jegla, T. J., and Garrity, P. A. (2008).
An internal thermal sensor controlling temperature preference in *Drosophila*.
Nature, 454(7201):217–20.

Hanada, R., Nakazato, M., Murakami, N., Sakihara, S., Yoshimatsu, H., Toshinai, K., Hanada, T., Suda, T., Kangawa, K., Matsukura, S., and Sakata, T. (2001).
A role for neuromedin U in stress response.
Biochemical and Biophysical Research Communications, 289(1):225–228.

Hanada, R., Teranishi, H., Pearson, J. T., Kurokawa, M., Hosoda, H., Fukushima, N., Fukue, Y., Serino, R., Fujihara, H., Ueta, Y., Ikawa, M., Okabe, M., Murakami, N., Shirai, M., Yoshimatsu, H., Kangawa, K., and Kojima, M. (2004).
Neuromedin U has a novel anorexigenic effect independent of the leptin signaling pathway.
Nature medicine, 10(10):1067–1073.

Hanada, T., Date, Y., Shimbara, T., Sakihara, S., Murakami, N., Hayashi, Y., Kanai, Y., Suda, T., Kangawa, K., and Nakazato, M. (2003).
Central actions of neuromedin U via corticotropin-releasing hormone.
Biochemical and Biophysical Research Communications, 311:954–958.

Hardie, R. C., Gu, Y., Martin, F., Sweeney, S. T., and Raghu, P. (2004).
In vivo light-induced and basal phospholipase C activity in *Drosophila* photoreceptors measured with genetically targeted phosphatidylinositol 4,5-bisphosphate-sensitive ion channels (Kir2.1).
The Journal of biological chemistry, 279(46):47773–82.

Hardie, R. C., Raghu, P., Moore, S., Juusola, M., Baines, R. A., and Sweeney, S. T. (2001).
Calcium influx via trp channels is required to maintain PIP2 levels in *Drosophila* photoreceptors.
Neuron, 30(1):149–159.

Harris, D. T., Kallman, B. R., Mullaney, B. C., and Scott, K. (2015).
Representations of Taste Modality in the *Drosophila* Brain.
Neuron, 86(6):1–12.

Hartenstein, V. (2006).
The neuroendocrine system of invertebrates: A developmental and evolutionary perspective.
Journal of Endocrinology, 190(3):555–570.

Hartline, D. K. (1979).
Pattern generation in the lobster (Panulirus) stomatogastric ganglion.
Biological Cybernetics, 33(4):223–236.

Havrankova, J., Roth, J., and Brownstein, M. (1978).
Insulin receptors are widely distributed in the central nervous system of the rat.
Nature, 272(5656):827–9.

Heinzel, H. G. (1988a).
Gastric mill activity in the lobster. I. Spontaneous modes of chewing.
Journal of neurophysiology, 59(2):528–50.

Heinzel, H. G. (1988b).
Gastric mill activity in the lobster. II. Proctolin and octopamine initiate and modulate chewing.
Journal of neurophysiology, 59(2):551–65.

Helmstaedter, M., Briggman, K. L., Turaga, S. C., Jain, V., Seung, H. S., and Denk, W. (2013).
Connectomic reconstruction of the inner plexiform layer in the mouse retina.
Nature, 500(7461):168–174.

Hobert, O. (2010).
Neurogenesis in the nematode *C. elegans*.
WormBook : the online review of C. elegans biology, pages 1–24.

Hodgkin, A. L. and Huxley, A. F. (1939).
Action Potentials Recorded from Inside a Nerve Fibre.
Nature, 144(3651):710–711.

Horn, J. P. (1992).
The integrative role of synaptic cotransmission in the bullfrog vasomotor C system: evidence for a synaptic gain hypothesis.
Canadian journal of physiology and pharmacology, 70 Suppl:S19–26.

Howard, A. D., Wang, R., Pong, S. S., Mellin, T. N., Strack, A., Guan, X. M., Zeng, Z., Williams, D. L., Feighner, S. D., Nunes, C. N., Murphy, B., Stair, J. N., Yu, H., Jiang, Q., Clements, M. K., Tan, C. P., McKee, K. K., Hreniuk, D. L., McDonald, T. P., Lynch, K. R., Evans, J. F., Austin, C. P., Caskey, C. T., Van der Ploeg, L. H., and Liu, Q. (2000).
Identification of receptors for neuromedin U and its role in feeding.
Nature, 406(July):70–74.

Hückesfeld, S., Peters, M., and Pankratz, M. J. (2016).
Central relay of bitter taste to the protocerebrum by peptidergic interneurons in the *Drosophila* brain.
Nature Communications, 7:12796.

Hückesfeld, S., Schoofs, A., Schlegel, P., Miroschnikow, A., and Pankratz, M. J. (2015).

Localization of Motor Neurons and Central Pattern Generators for Motor Patterns Underlying Feeding Behavior in *Drosophila* Larvae.
PloS one, 10(8):e0135011.

Hwang, R. Y., Zhong, L., Xu, Y., Johnson, T., Zhang, F., Deisseroth, K., and Tracey, W. D. (2007).
Nociceptive neurons protect *Drosophila* larvae from parasitoid wasps.
Current biology : CB, 17(24):2105–16.

Ikeya, T., Galic, M., Belawat, P., Nairz, K., and Hafen, E. (2002).
Nutrient-dependent expression of insulin-like peptides from neuroendocrine cells in the CNS contributes to growth regulation in *Drosophila*.
Current biology : CB, 12(15):1293–300.

Inada, K., Kohsaka, H., Takasu, E., Matsunaga, T., and Nose, A. (2011).
Optical dissection of neural circuits responsible for *Drosophila* larval locomotion with halorhodopsin.
PloS one, 6(12):e29019.

Ivanov, T. R., Le Rouzic, P., Stanley, P. J., Ling, W. Y., Parello, R., and Luckman, S. M. (2004).
Neuromedin U neurones in the rat nucleus of the tractus solitarius are catecholaminergic and respond to peripheral cholecystokinin.
Journal of Neuroendocrinology, 16(7):612–619.

Jan, Y. N. and Jan, L. Y. (1983).
Coexistence and corelease of cholinergic and peptidergic transmitters in frog sympathetic ganglia.
Federation Proceedings, 42(12):2929–2933.

Jarrell, T. A., Wang, Y., Bloniarz, A. E., Brittin, C. A., Xu, M., Thomson, J. N., Albertson, D. G., Hall, D. H., and Emmons, S. W. (2012).
The connectome of a decision-making neural network.
Science (New York, N.Y.), 337(6093):437–44.

Jenett, A., Rubin, G. M., Ngo, T.-T. B., Shepherd, D., Murphy, C., Dionne, H., Pfeiffer, B. D., Cavallaro, A., Hall, D., Jeter, J., Iyer, N., Fetter, D., Hausenfluck, J. H., Peng, H., Trautman, E. T., Svirskas, R. R., Myers, E. W., Iwinski, Z. R., Aso, Y., DePasquale, G. M., Enos, A., Hulamm, P., Lam, S. C. B., Li, H.-H., Laverty, T. R., Long, F., Qu, L., Murphy, S. D., Rokicki, K., Safford, T., Shaw, K., Simpson, J. H., Sowell, A., Tae, S., Yu, Y., and Zugates, C. T. (2012).
A GAL4-driver line resource for *Drosophila* neurobiology.
Cell reports, 2(4):991–1001.

Jiu, Y.-M., Yue, Y., Yang, S., Liu, L., Yu, J.-W., Wu, Z.-X., and Xu, T. (2010).

Insulin-like signaling pathway functions in integrative response to an olfactory and a gustatory stimuli in *C. elegans*.
Protein & cell, 1(1):75–81.

Kandel, E. R. (2001).
The molecular biology of memory storage: A dialogue between gene and synapses.
Science, 294(5544):1030–1038.

Katz, P., Grillner, S., Wilson, R., Borst, A., Greenspan, R., Buzsáki, G., Martin, K., Marder, E., Kristan, W., Friedrich, R., and Chklovskii, D. (2013).
Vertebrate versus invertebrate neural circuits.
Current Biology, 23(12):R504–R506.

Kavaliers, M. and Hirst, M. (1986).
FMRFamide: an endogenous peptide with marked inhibitory effects on opioid-induced feeding behavior.
Brain research bulletin, 17(3):403–8.

Keynes, R. D. (1989).
The role of giant axons in studies of the nerve impulse.
BioEssays : news and reviews in molecular, cellular and developmental biology, 10(2-3):90–3.

Kim, S. K. and Rulifson, E. J. (2004).
Conserved mechanisms of glucose sensing and regulation by *Drosophila* corpora cardiaca cells.
Nature, 431(7006):316–20.

Kiss, B., Szlanka, T., Zvara, Á., Žurovec, M., Sery, M., Kakaš, Š., Ramasz, B., HegedUs, Z., Lukacsovich, T., Puskás, L., Fónagy, A., and Kiss, I. (2013).
Selective elimination/RNAi silencing of FMRF-related peptides and their receptors decreases the locomotor activity in *Drosophila melanogaster*.
General and Comparative Endocrinology, 191:137–145.

Klose, M. K., Dason, J. S., Atwood, H. L., Boulianne, G. L., and Mercier, A. J. (2010).
Peptide-induced modulation of synaptic transmission and escape response in *Drosophila* requires two G-protein-coupled receptors.
The Journal of neuroscience : the official journal of the Society for Neuroscience, 30(44):14724–34.

Lee, T. and Luo, L. (1999).
Mosaic analysis with a repressible cell marker for studies of gene function in neuronal morphogenesis.
Neuron, 22(3):451–61.

Lee, W. H., Wang, G. M., Seaman, L. B., and Vannucci, S. J. (1996).
Coordinate IGF-I and IGFBP5 gene expression in perinatal rat brain after hypoxia-ischemia.
Journal of cerebral blood flow and metabolism : official journal of the International Society of Cerebral Blood Flow and Metabolism, 16(2):227–36.

Levine, D. N. (2007).
Sherrington's "The Integrative action of the nervous system": A centennial appraisal.
Journal of the Neurological Sciences, 253(1-2):1–6.

Li, Q. and Gong, Z. (2015).
Cold-sensing regulates *Drosophila* growth through insulin-producing cells.
Nature Communications, 6:10083.

Luan, H., Peabody, N. C., Vinson, C. R., and White, B. H. (2006).
Refined spatial manipulation of neuronal function by combinatorial restriction of transgene expression.
Neuron, 52(3):425–36.

Luo, J., Becnel, J., Nichols, C. D., and Nässel, D. R. (2011).
Insulin-producing cells in the brain of adult *Drosophila* are regulated by the serotonin 5-HT(1A) receptor.
Cellular and molecular life sciences : CMLS.

Lynch, K. (1980).
Stimulation-induced reduction of large dense core vesicle numbers in cholinergic motor nerve endings.
Brain Research, 194(1):249–254.

Malendowicz, L. K., Ziolkowska, A., and Rucinski, M. (2012).
Neuromedins U and S involvement in the regulation of the hypothalamo-pituitary-adrenal axis.
Frontiers in endocrinology, 3(DEC):156.

Manning, L., Heckscher, E. S., Purice, M. D., Roberts, J., Bennett, A. L., Kroll, J. R., Pollard, J. L., Strader, M. E., Lupton, J. R., Dyukareva, A. V., Doan, P. N., Bauer, D. M., Wilbur, A. N., Tanner, S., Kelly, J. J., Lai, S.-l. L., Tran, K. D., Kohwi, M., Laverty, T. R., Pearson, J. C., Crews, S. T., Rubin, G. M., and Doe, C. Q. (2012).
A Resource for Manipulating Gene Expression and Analyzing cis-Regulatory Modules in the *Drosophila* CNS.
Cell Reports, 2(4):1002–1013.

Marder, E. and Bucher, D. (2001).

Central pattern generators and the control of rhythmic movements.
Current biology : CB, 11(23):R986–96.

Marder, E. and Bucher, D. (2007).
Understanding circuit dynamics using the stomatogastric nervous system of lobsters and crabs.
Annual review of physiology, 69:291–316.

Markov, N. T., Misery, P., Falchier, A., Lamy, C., Vezoli, J., Quilodran, R., Gariel, M. A., Giroud, P., Ercsey-Ravasz, M., Pilaz, L. J., Huissoud, C., Barone, P., Dehay, C., Toroczkai, Z., Van Essen, D. C., Kennedy, H., and Knoblauch, K. (2011).
Weight consistency specifies regularities of macaque cortical networks.
Cerebral Cortex, 21(6):1254–1272.

McIntire, S. L., Jorgensen, E., Kaplan, J., and Horvitz, H. R. (1993).
The GABAergic nervous system of *C. elegans*.
Nature, 364:337–341.

Melcher, C., Bader, R., and Pankratz, M. J. (2007).
Amino acids, taste circuits, and feeding behavior in *Drosophila*: towards understanding the psychology of feeding in flies and man.
The Journal of Endocrinology, 192(3):467–72.

Melcher, C., Bader, R., Walther, S., Simakov, O., and Pankratz, M. J. (2006).
Neuromedin U and its putative *Drosophila* homolog hugin.
PLoS biology, 4(3):e68.

Melcher, C. and Pankratz, M. J. (2005).
Candidate gustatory interneurons modulating feeding behavior in the *Drosophila* brain.
PLoS Biology, 3(9):1618–1629.

Meng, X., Wahlström, G., Immonen, T., Kolmer, M., Tirronen, M., Predel, R., Kalkkinen, N., Heino, T. I., Sariola, H., and Roos, C. (2002).
The *Drosophila* hugin gene codes for myostimulatory and ecdysis-modifying neuropeptides.
Mechanisms of development, 117(1-2):5–13.

Merighi, A. (2002).
Costorage and coexistence of neuropeptides in the mammalian CNS.
Progress in neurobiology, 66(3):161–90.

Milyaev, N., Osumi-sutherland, D., Reeve, S., Burton, N., Baldock, R. A., and Armstrong, J. D. (2012).
The virtual fly brain browser and query interface.
Bioinformatics, 28(3):411–415.

Mirabeau, O. and Joly, J.-S. (2013).
Molecular evolution of peptidergic signaling systems in bilaterians.
Proceedings of the National Academy of Sciences of the United States of America, 110(22):E2028–37.

Miyamoto, T., Slone, J., Song, X., and Amrein, H. (2012).
A fructose receptor functions as a nutrient sensor in the *Drosophila* brain.
Cell, 151(5):1113–25.

Mohseni, N., McMillan, S. C., Chaudhary, R., Mok, J., and Reed, B. H. (2009).
Autophagy promotes caspase-dependent cell death during *Drosophila* development.
Autophagy, 5(3):329–38.

Mountcastle, V. B. (1997).
The columnar organization of the neocortex.
Brain, 120(4):701–722.

Mulloney, B. (1987).
The Crustacean Stomatogastric System - Neural Circuits.
In Selverston, A. I. and Moulins, M., editors, *The Crustacean Stomatogastric System*, chapter Neural Cir, page 338. Springer Berlin Heidelberg, Berlin, Heidelberg.

Mulloney, B. and Selverston, A. I. (1974).
Organization of the stomatogastric ganglion of the spiny lobster.
Journal of Comparative Physiology, 91(1):1–32.

Nässel, D. R. (2009).
Neuropeptide signaling near and far: How localized and timed is the action of neuropeptides in brain circuits?
Invertebrate Neuroscience, 9(2):57–75.

Nässel, D. R. and Wegener, C. (2011).
A comparative review of short and long neuropeptide F signaling in invertebrates: Any similarities to vertebrate neuropeptide Y signaling?
Peptides, 32(6):1335–55.

Nässel, D. R. and Winther, A. M. E. (2010).
Drosophila neuropeptides in regulation of physiology and behavior.
Progress in neurobiology, 92(1):42–104.

Nern, A., Pfeiffer, B. D., and Rubin, G. M. (2015).
Optimized tools for multicolor stochastic labeling reveal diverse stereotyped cell arrangements in the fly visual system.

Proceedings of the National Academy of Sciences of the United States of America, 112(22):E2967–E2976.

Ng, M., Roorda, R. D., Lima, S. Q., Zemelman, B. V., Morcillo, P., and Miesenböck, G. (2002).
Transmission of olfactory information between three populations of neurons in the antennal lobe of the fly.
Neuron, 36(3):463–74.

Nichols, R. (2003).
Signaling pathways and physiological functions of *Drosophila melanogaster* FMRFamide-related peptides.
Annual review of entomology, 48(1):485–503.

Nitabach, M. N., Wu, Y., Sheeba, V., Lemon, W. C., Strumbos, J., Zelensky, P. K., White, B. H., and Holmes, T. C. (2006).
Electrical hyperexcitation of lateral ventral pacemaker neurons desynchronizes downstream circadian oscillators in the fly circadian circuit and induces multiple behavioral periods.
The Journal of neuroscience : the official journal of the Society for Neuroscience, 26(2):479–89.

Novak, C. M., Zhang, M., and Levine, J. A. (2007).
Sensitivity of the hypothalamic paraventricular nucleus to the locomotor-activating effects of neuromedin U in obesity.
Brain Research, 1169(1):57–68.

Nusbaum, M. P., Blitz, D. M., Swensen, A. M., Wood, D., and Marder, E. (2001).
The roles of co-transmission in neural network modulation.
Trends in Neurosciences, 24(3):146–154.

Oh, S. W., Harris, J. A., Ng, L., Winslow, B., Cain, N., Mihalas, S., Wang, Q., Lau, C., Kuan, L., Henry, A. M., Mortrud, M. T., Ouellette, B., Nguyen, T. N., Sorensen, S. A., Slaughterbeck, C. R., Wakeman, W., Li, Y., Feng, D., Ho, A., Nicholas, E., Hirokawa, K. E., Bohn, P., Joines, K. M., Peng, H., Hawrylycz, M. J., Phillips, J. W., Hohmann, J. G., Wohnoutka, P., Gerfen, C. R., Koch, C., Bernard, A., Dang, C., Jones, A. R., and Zeng, H. (2014).
A mesoscale connectome of the mouse brain.
Nature, 508(7495):207–214.

Ohki, K., Chung, S., Ch'ng, Y. H., Kara, P., and Reid, R. C. (2005).
Functional imaging with cellular resolution reveals precise micro-architecture in visual cortex.
Nature, 433(7026):597–603.

Ohyama, T., Schneider-Mizell, C. M., Fetter, R. D., Aleman, J. V., Franconville, R., Rivera-Alba, M., Mensh, B. D., Branson, K. M., Simpson, J. H., Truman, J. W., Cardona, A., and Zlatic, M. (2015).

A multilevel multimodal circuit enhances action selection in *Drosophila*.
Nature, 520(7549):633–9.

Park, D., Veenstra, J. A., Park, J. H., and Taghert, P. H. (2008).
Mapping Peptidergic Cells in *Drosophila*: Where DIMM Fits In.
PLoS ONE, 3(3):e1896.

Park, Y., Kim, Y.-J., and Adams, M. E. (2002).
Identification of G protein-coupled receptors for *Drosophila* PRXamide peptides, CCAP, corazonin, and AKH supports a theory of ligand-receptor coevolution.
Proceedings of the National Academy of Sciences of the United States of America, 99(17):11423–8.

Pereira, L., Kratsios, P., Serrano-Saiz, E., Sheftel, H., Mayo, A. E., Hall, D. H., White, J. G., LeBoeuf, B., Garcia, L. R., Alon, U., and Hobert, O. (2015).
A cellular and regulatory map of the cholinergic nervous system of C.elegans.
eLife, 4(December):1–46.

Peters, M. (2013).
Funktionelle neuroanatomische Analyse eines nahrungsabhängigen Schaltkreises in Drosophila melanogaster.
Dissertation, Rheinische Friedrich-Wilhelms-Universitaet Bonn.

Prokop, A. and Meinertzhagen, I. A. (2006).
Development and structure of synaptic contacts in *Drosophila*.
Seminars in Cell and Developmental Biology, 17(1):20–30.

Pulver, S. R., Pashkovski, S. L., Hornstein, N. J., Garrity, P. a., and Griffith, L. C. (2009).
Temporal dynamics of neuronal activation by Channelrhodopsin-2 and TRPA1 determine behavioral output in *Drosophila* larvae.
Journal of neurophysiology, 101(6):3075–88.

Rajan, A. and Perrimon, N. (2012).
Drosophila cytokine unpaired 2 regulates physiological homeostasis by remotely controlling insulin secretion.
Cell, 151(1):123–37.

Rohrbough, J. and Broadie, K. (2002).
Electrophysiological analysis of synaptic transmission in central neurons of *Drosophila* larvae.
Journal of Neurophysiology, 88(2):847–60.

Root, C. M., Ko, K. I., Jafari, A., and Wang, J. W. (2011).
Presynaptic facilitation by neuropeptide signaling mediates odor-driven food search.

Cell, 145(1):133–44.

Rorden, C. and Karnath, H.-O. (2004).
Using human brain lesions to infer function: a relic from a past era in the fMRI age?
Nature reviews. Neuroscience, 5(10):813–9.

Rosenkilde, C., Cazzamali, G., Williamson, M., Hauser, F., Søndergaard, L., DeLotto, R., and Grimmelikhuijzen, C. J. P. (2003).
Molecular cloning, functional expression, and gene silencing of two *Drosophila* receptors for the *Drosophila* neuropeptide pyrokinin-2.
Biochemical and Biophysical Research Communications, 309(2):485–494.

Rulifson, E. J., Kim, S. K., and Nusse, R. (2002).
Ablation of insulin-producing neurons in flies: growth and diabetic phenotypes.
Science (New York, N.Y.), 296(5570):1118–20.

Saalfeld, S., Cardona, A., Hartenstein, V., and Tomancak, P. (2009).
CATMAID: collaborative annotation toolkit for massive amounts of image data.
Bioinformatics (Oxford, England), 25(15):1984–6.

Salio, C., Lossi, L., Ferrini, F., and Merighi, A. (2006).
Neuropeptides as synaptic transmitters.
Cell and Tissue Research, 326(2):583–598.

Sámano, C., Zetina, M. E., Marín, M. A., Cifuentes, F., and Morales, M. A. (2006).
Choline acetyl transferase and neuropeptide immunoreactivities are colocalized in somata, but preferentially localized in distinct axon fibers and boutons of cat sympathetic preganglionic neurons.
Synapse (New York, N.Y.), 60(4):295–306.

Scannell, J. W., Burns, G. A., Hilgetag, C. C., O'Neil, M. A., and Young, M. P. (1999).
The connectional organization of the cortico-thalamic system of the cat.
Cerebral cortex (New York, N.Y. : 1991), 9(3):277–99.

Schindelin, J., Arganda-Carreras, I., Frise, E., Kaynig, V., Longair, M., Pietzsch, T., Preibisch, S., Rueden, C., Saalfeld, S., Schmid, B., Tinevez, J.-Y., White, D. J., Hartenstein, V., Eliceiri, K., Tomancak, P., and Cardona, A. (2012).
Fiji: an open-source platform for biological-image analysis.
Nature methods, 9(7):676–82.

Schlegel, P., Texada, M. J., Miroschnikow, A., Schoofs, A., Hückesfeld, S., Peters, M., Schneider-Mizell, C. M., Lacin, H., Li, F., Fetter, R. D., Truman, J. W., Cardona, A., and Pankratz, M. J. (2016).

Synaptic transmission parallels neuromodulation in a central food-intake circuit.
eLife, 5.

Schneider, C. A., Rasband, W. S., and Eliceiri, K. W. (2012).
NIH Image to ImageJ: 25 years of image analysis.
Nature Methods, 9(7):671–675.

Schneider-Mizell, C. M., Gerhard, S., Longair, M., Kazimiers, T., Li, F., Zwart, M. F., Champion, A., Midgley, F. M., Fetter, R. D., Saalfeld, S., and Cardona, A. (2016).
Quantitative neuroanatomy for connectomics in *Drosophila*.
eLife, 5:e12059.

Schoofs, A., Hückesfeld, S., Schlegel, P., Miroschnikow, A., Peters, M., Zeymer, M., Spieß, R., Chiang, A. S., and Pankratz, M. J. (2014a).
Selection of Motor Programs for Suppressing Food Intake and Inducing Locomotion in the *Drosophila* Brain.
PLoS Biology, 12(6):e1001893.

Schoofs, A., Hückesfeld, S., Surendran, S., and Pankratz, M. J. (2014b).
Serotonergic pathways in the *Drosophila* larval enteric nervous system.
Journal of Insect Physiology, 69:118–125.

Schoofs, A., Niederegger, S., van Ooyen, A., Heinzel, H.-G., and Spieß, R. (2010).
The brain can eat: establishing the existence of a central pattern generator for feeding in third instar larvae of Drosophila virilis and *Drosophila melanogaster*.
Journal of insect physiology, 56(7):695–705.

Schwartz, M. W., Guyenet, S. J., and Cirulli, V. (2010).
The hypothalamus and ß-cell connection in the gene-targeting era.
Diabetes, 59(12):2991–3.

Schwartz, M. W., Woods, S. C., Porte, D., Seeley, R. J., and Baskin, D. G. (2000).
Central nervous system control of food intake.
Nature, 404(6778):661–71.

Siegmund, T. and Korge, G. (2001).
Innervation of the ring gland of *Drosophila melanogaster*.
The Journal of comparative neurology, 431(4):481–91.

Sloper, J. J. (1972).
Gap junctions between dendrites in the primate neocortex.
Brain Research, 44(2):641–646.

Söderberg, J. a. E., Carlsson, M. a., and Nässel, D. R. (2012).
Insulin-Producing Cells in the *Drosophila* Brain also Express Satiety-Inducing Cholecystokinin-Like Peptide, Drosulfakinin.
Frontiers in endocrinology, 3(August):109.

Sporns, O. (2014).
Contributions and challenges for network models in cognitive neuroscience.
Nat Neurosci, 17(5):652–660.

Sporns, O., Tononi, G., and Kötter, R. (2005).
The human connectome: A structural description of the human brain.
PLoS computational biology, 1(4):e42.

Stylianopoulou, F., Herbert, J., Soares, M. B., and Efstratiadis, A. (1988).
Expression of the insulin-like growth factor II gene in the choroid plexus and the leptomeninges of the adult rat central nervous system.
Proceedings of the National Academy of Sciences of the United States of America, 85(1):141–5.

Sugimori, M. and Llinas, R. R. (1990).
Real-time imaging of calcium influx in mammalian cerebellar Purkinje cells in vitro.
Proceedings of the National Academy of Sciences of the United States of America, 87(July):5084–8.

Sugiyama, K., Tagawa, S., and Toda, M. (1981).
Methods for Visual Understanding of Hierarchical System Structures.
IEEE Transactions on Systems, Man and Cybernetics, 11(2):109–125.

Tardif, E. and Clarke, S. (2001).
Intrinsic connectivity of human auditory areas: a tracing study with DiI.
The European journal of neuroscience, 13(5):1045–1050.

Tessmar-Raible, K., Raible, F., Christodoulou, F., Guy, K., Rembold, M., Hausen, H., and Arendt, D. (2007).
Conserved Sensory-Neurosecretory Cell Types in Annelid and Fish Forebrain: Insights into Hypothalamus Evolution.
Cell, 129(7):1389–1400.

Thorens, B. (2011).
Brain glucose sensing and neural regulation of insulin and glucagon secretion.
Diabetes, Obesity and Metabolism, 13(SUPPL. 1):82–88.

Thorens, B. (2014).
Neural regulation of pancreatic islet cell mass and function.

Diabetes, Obesity and Metabolism, 16:87–95.

Valentino, K. L., Ocrant, I., and Rosenfeld, R. G. (1990).
Developmental expression of insulin-like growth factor-II receptor immunoreactivity in the rat central nervous system.
Endocrinology, 126(2):914–20.

van den Pol, A. N. (2012).
Neuropeptide transmission in brain circuits.
Neuron, 76(1):98–115.

Varshney, L. R., Chen, B. L., Paniagua, E., Hall, D. H., and Chklovskii, D. B. (2011).
Structural properties of the *C. elegans* neuronal network.
PLoS computational biology, 7(2):e1001066.

Vickers, M. H., Ikenasio, B. A., and Breier, B. H. (2001).
IGF-I treatment reduces hyperphagia, obesity, and hypertension in metabolic disorders induced by fetal programming.
Endocrinology, 142(9):3964–73.

Vilim, F. S., Cropper, E. C., Price, D. a., Kupfermann, I., and Weiss, K. R. (1996).
Release of peptide cotransmitters in *Aplysia*: regulation and functional implications.
The Journal of neuroscience : the official journal of the Society for Neuroscience, 16(24):8105–8114.

Vogelstein, J. T., Park, Y., Ohyama, T., Kerr, R. A., Truman, J. W., Priebe, C. E., and Zlatic, M. (2014).
Discovery of Brainwide Neural-Behavioral Maps via Multiscale Unsupervised Structure Learning.
Science, 344(6182):386–392.

Vosshall, L. B. and Stocker, R. F. (2007).
Molecular architecture of smell and taste in *Drosophila*.
Annual review of neuroscience, 30:505–33.

Wang, J. W., Wong, A. M., Flores, J., Vosshall, L. B., and Axel, R. (2003).
Two-photon calcium imaging reveals an odor-evoked map of activity in the fly brain.
Cell, 112(2):271–82.

Ward, J. H. (1963).
Hierarchical grouping to optimize an objective function.
Journal of the American Statistical Association, 58(301):236–244.

Weiss, K. R., Brezina, V., Cropper, E. C., Heierhorst, J., Hooper, S. L., Probst, W. C., Rosen, S. C., Vilim, F. S., and Kupfermann, I. (1993).
Physiology and biochemistry of peptidergic cotransmission in *Aplysia*.
Journal of physiology, Paris, 87(3):141–51.

White, J. G., Southgate, E., Thomson, J. N., and Brenner, S. (1976).
The structure of the ventral nerve cord of *C. elegans*.
Philosophical transactions of the Royal Society of London. Series B, Biological sciences, 275(938):327–48.

White, J. G., Southgate, E., Thomson, J. N., and Brenner, S. (1986).
The structure of the nervous system of the nematode *C. elegans*.
Philosophical transactions of the Royal Society of London. Series B, Biological sciences, 314(1165):1–340.

Wiley, R. G., Spencer, C., and Pysh, J. J. (1987).
Time course and frequency dependence of synaptic vesicle depletion and recovery in electrically stimulated sympathetic ganglia.
Journal of Neurocytology, 16(3):359–372.

Woods, S. C., Lotter, E. C., McKay, L. D., and Porte, D. (1979).
Chronic intracerebroventricular infusion of insulin reduces food intake and body weight of baboons.
Nature, 282(5738):503–505.

Wren, a. M., Small, C. J., Abbott, C. R., Jethwa, P. H., Kennedy, A. R., Murphy, K. G., Stanley, S. A., Zollner, A. N., Ghatei, M. A., and Bloom, S. R. (2002).
Hypothalamic actions of neuromedin U.
Endocrinology, 143(11):4227–34.

Wu, Q. and Brown, M. R. (2006).
Signaling and function of insulin-like peptides in insects.
Annual review of entomology, 51(1):1–24.

Wu, Q., Zhao, Z., and Shen, P. (2005).
Regulation of aversion to noxious food by *Drosophila* neuropeptide Y- and insulin-like systems.
Nature Neuroscience, 8(10):1350–5.

Yapici, N., Cohn, R., Schusterreiter, C., Ruta, V., and Vosshall, L. B. (2016).
A Taste Circuit that Regulates Ingestion by Integrating Food and Hunger Signals.
Cell, 165(3):715–729.

Yoon, H., Enquist, L. W., and Dulac, C. (2005).
Olfactory inputs to hypothalamic neurons controlling reproduction and fertility.
Cell, 123(4):669–682.

Young, M. P. (1993).
The organization of neural systems in the primate cerebral cortex.
Proceedings. Biological sciences / The Royal Society, 252(1333):13–8.

Zhang, W., Ge, W., and Wang, Z. (2007).
A toolbox for light control of *Drosophila* behaviors through Channelrhodopsin 2-mediated photoactivation of targeted neurons.
The European journal of neuroscience, 26(9):2405–16.

Zhou, F., Mahler, S., and Toivonen, H. (2009).
Review of network abstraction techniques.
Workshop on Explorative Analytics of Information Networks at ECML PKDD 2009, page 50.

Zingg, B., Hintiryan, H., Gou, L., Song, M. Y., Bay, M., Bienkowski, M. S., Foster, N. N., Yamashita, S., Bowman, I., Toga, A. W., and Dong, H. W. (2014).
Neural networks of the mouse neocortex.
Cell, 156(5):1096–1111.

Zupanc, G. K. (1996).
Peptidergic transmission: from morphological correlates to functional implications.
Micron (Oxford, England : 1993), 27(1):35–91.

Zwart, M. F., Pulver, S. R., Truman, J. W., Fushiki, A., Fetter, R. D., Cardona, A., and Landgraf, M. (2016).
Selective Inhibition Mediates the Sequential Recruitment of Motor Pools.
Neuron, 91(4):944.

Erklärung

Hiermit erkläre ich, Philipp Schlegel, an Eides statt, dass ich die vorliegende Doktorarbeit mit dem Titel "Connectomic Analysis of a Peptidergic Circuit in *Drosophila*" selbständig verfasst habe, dass ich sie zuvor an keiner anderen Hochschule und in keinem anderen Studiengang eingereicht habe und keine anderen als die angegebenen Quellen und Hilfsmittel benutzt habe. Die Stellen der Arbeit, die dem Wortlaut oder dem Sinne nach anderen Werken entnommen wurden, sind unter Angabe der Quelle kenntlich gemacht. Teile der in dieser Doktorarbeit präsentierten Ergebnisse sind bereits in Schlegel et al. [2016] veröffentlicht worden. Dies wird an den entsprechenden Stellen vermerkt.

Unterschrift: ..... Datum: .....